ABSTRACT

NANOFILTRATION WITH ORGANIC SOLVENTS AND ITS POSSIBLE APPLICATIONS TO ORGANIC SYNTHESES

by
José Antonio Whu

Experimental results on the nanofiltration (NF) separation behavior of three different solvent-compatible membranes are presented for three organic solutes of molecular weights 351, 826 and 1355 in methanol; the manufacturer-specified molecular weight cut-offs (MWCO) of the membranes are 250, 400 and 700. Membranes were primarily tested at 440 psig, at different concentrations of the solutes in methanol; the effect of varying the applied pressure was also briefly explored. The solvent permeation flux and the solute rejection were time dependent for an extended initial period; the membranes had to be compacted to achieve steady-state results. Furthermore, the manufacturer-specified MWCO was found to be an insufficient indicator of the separation capabilities of the membranes.

Organic syntheses which involve species of diverse molecular weights and dimensions, such as those found in the pharmaceutical industry, could benefit from the availability of solvent-compatible NF membranes. A mathematical model was developed to illustrate the effects of external coupling of the operation of a batch/semibatch reactor with a NF unit. A hypothetical reaction system consisting of two parallel reactions was considered. Numerical simulations of the governing equations with realistic parameters, showed that the reaction conversion, selectivity and final product concentration could be improved considerably via this external reactor-membrane separator coupling.

NANOFILTRATION WITH ORGANIC SOLVENTS AND ITS POSSIBLE APPLICATIONS TO ORGANIC SYNTHESES

by
José Antonio Whu

A Thesis
Submitted to the Faculty of
New Jersey Institute of Technology
in Partial Fulfillment of the Requirements for the Degree of
Master of Science in Chemical Engineering

Department of Chemical Engineering,
Chemistry and Environmental Science

August 1998

APPROVAL PAGE

NANOFILTRATION WITH ORGANIC SOLVENTS AND ITS POSSIBLE APPLICATIONS TO ORGANIC SYNTHESES

José Antonio Whu

Dr. Kamalesh K. Sirkar, Thesis Advisor — Date
Distinguished Professor of Chemical Engineering, Chemistry and Environmental Science, NJIT

Dr. Basil C. Baltzis, Thesis Advisor — Date
Professor of Chemical Engineering, Chemistry and Environmental Science, NJIT

Dr. Robert G. Luo, Committee Member — Date
Assistant Professor of Chemical Engineering, Chemistry and Environmental Science, NJIT

BIOGRAPHICAL SKETCH

Author: José Antonio Whu

Degree: Master of Science in Chemical Engineering

Date: August 1998

Undergraduate and Graduate Education:

- Master of Science in Chemical Engineering,
  New Jersey Institute of Technology, Newark, NJ, 1998

- Bachelor of Science in Chemical Engineering
  National University of Engineering, Lima, Perú, 1984

Major: Chemical Engineering

Presentations and Publications:

Whu, J. A., Baltzis, B. C. and Sirkar, K. K. "Nanofiltration with Organic Solvents and its Possible Applications to Organic Syntheses." *Tenth Annual North American Membrane Society Meeting*. Cleveland, OH, May 18, 1998.

To my mother

ACKNOWLEDGMENT

The author is glad to express his indebtedness to Professors Kamalesh K. Sirkar and Basil C. Baltzis for their continuous advice during this study. Special thanks to Professor Robert G. Luo for serving as Member of the Committee.

Funding for this project was provided by the Emission Reduction Research Center and Membrane Separations Program at New Jersey Institute of Technology, which is greatly appreciated.

The author also expresses his gratitude to the current and former members of the Membrane Separations Laboratory and especially to Judy Kapp and Dr. Uttam Shanbhag, for their suggestions and support.

TABLE OF CONTENTS

TABLE OF CONTENTS
(Continued)

TABLE OF CONTENTS
(Continued)

TABLE OF CONTENTS
(Continued)

LIST OF TABLES

LIST OF TABLES
(Continued)

LIST OF FIGURES

LIST OF FIGURES
(Continued)

LIST OF FIGURES
(Continued)

LIST OF FIGURES
(Continued)

Figure **Page**

LIST OF SYMBOLS

A : concentration of species A / initial concentration of species A in the reactor ($A = C_A / C_{A0}$), dimensionless

AA : $= A$, used in Appendix C, dimensionless

A_k : lumped parameters of the Finely Porous Model (k = 1, 2, 3), defined in equations (4.3), (4.4) and (4.5), respectively

A_m : total membrane area, m^2

A_{m0} : membrane module area, m^2

b : combined frictional coefficient, defined in equation (2.14), dimensionless

B : concentration of species B / initial concentration of species A in the reactor ($B = C_B / C_{A0}$), dimensionless

BB : $= B$, used in Appendix C, dimensionless

C : concentration of species C / initial concentration of species A in the reactor ($C = C_C / C_{A0}$), dimensionless

CC : $= C$, used in Appendix C, dimensionless

C_{A0} : initial concentration of species A in the reactor, mol L^{-1}

C_i : concentration of species i, mol L^{-1}; concentration in the reactor, mol L^{-1} (Chapter 5 and Appendix C)

$C_i|_{drum}$: concentration of species i in the drum, mol L^{-1}

D : concentration of species D / initial concentration of species A in the reactor ($D = C_D / C_{A0}$), dimensionless; diffusion coefficient for large pores, $m^2\ s^{-1}$

DD : $= D$, used in Appendix C, dimensionless

D_e : effective diffusion coefficient for small pores, defined in equation (2.15), $m^2\ s^{-1}$

E : concentration of species E / initial concentration of species A in the reactor ($E = C_E / C_{A0}$), dimensionless

LIST OF SYMBOLS
(Continued)

EE : $= E$, used in Appendix C, dimensionless

f : friction coefficient

F : Faraday constant, C/equiv-g

F_m : frictional force (mole basis), defined in equation (2.11)

F_v : frictional force (pore volume basis), defined in equation (2.4)

J_i : local molar flux of removal of species *i* through the NF membrane, mol $(m^2\ s)^{-1}$

J_s : solvent flux through the NF membrane, L $(m^2\ s)^{-1}$

k_1 : specific reaction rate constant for forward reaction (5.1), L $mol^{-1}\ s^{-1}$

k_{-1} : specific reaction rate constant for backward reaction (5.1), L $mol^{-1}\ s^{-1}$

k_2 : specific reaction rate constant for reaction (5.2), L $mol^{-1}\ s^{-1}$

k' : partition coefficient (high-pressure side), defined in equation (2.18), dimensionless

k'' : partition coefficient (low-pressure side), defined in equation (2.19), dimensionless

K_{eq} : thermodynamic equilibrium constant, dimensionless

L_i : molar rate of addition of species *i* from the drum into the reactor, mol s^{-1}

L_p : permeability of the membrane, L $(m^2\ s)^{-1}$ / psi m^{-1}

L_p' : apparent permeability of the membrane, defined in equation (2.7)

L_v : volumetric rate of addition of solvent from the drum into the reactor, L s^{-1}

m_i : mobility of the solute i in the solvent, defined in equation (2.13)

M_i : molality of the solution, mol L^{-1} (solvent)

LIST OF SYMBOLS
(Continued)

MW : molecular weight, g mol^{-1}

MWCO : molecular weight cut-off, defined in section 1.1

N_{avog} : Avogadro's Number

NF : nanofiltration

N_i : number of moles of species *i* in the reactor, mol

P : pressure, psig

r_i : characteristic solute radius, nm

$-r_{jA}$: rate of consumption of species A by reaction *j* (= 1, 2), mol L^{-1} s^{-1}

r_p : hydrodynamic pore radius, nm

R : gas constant

R_i : observed fractional rejection of solute *i* by the NF membrane, dimensionless

RO : reverse osmosis

S_C : selectivity with respect to species C, dimensionless

t : reaction time, s

T : absolute temperature, K

u : permeation velocity in the membrane pore, m s^{-1}

UF : ultrafiltration

v : reaction mixture volume / initial reaction mixture volume ($v = V/V_0$), dimensionless

V : reaction mixture volume, L

V_i : solute molal volume at normal boiling point, cm^3 mol^{-1}

: initial reaction mixture volume, L

: axis perpendicular to the membrane surface

: conversion of species A in reaction (5.1), dimensionless

: conversion of species A in reaction (5.2), dimensionless

: valence of the ion

k letters

: defined in equation (5.20), dimensionless

: defined in equation (5.20), dimensionless

: defined in equation (5.20), dimensionless

: activity coefficient of the ion in the interphase, dimensionless

: difference between the feed and permeate phases

: membrane thickness, m

: membrane porosity, dimensionless

: viscosity of the solution inside the pore, g m^{-1} s^{-1}

: initial number of moles of species *i* / initial number of moles of species A in the reactor ($\theta_i = C_{i0}/C_{A0}$) , dimensionless

: ratio of solute radius to pore radius (for cylindrical pores), defined in equation (2.24), dimensionless

: wavelength of maximum absorbance, nm

: chemical potencial of species *i*

ν_{ij} : stoichiometric coefficient of species *i* for the reaction *j*, dimensionless

π : osmotic pressure, psi

σ_i : reflection coefficient of species *i*, dimensionless

τ : reaction time, defined in equation (5.19), dimensionless; tortuosity

Φ : steric partition coefficient, defined in equation (2.23), dimensionless

ψ : electric potential in the axial direction, V

$\Delta\psi_D$: Donnan Potential, V

Subscripts

c : convection

d : diffusion

e : electric field

i : species *i*

j : reaction number

m : membrane

0 : initial value, parameter basic value, basic membrane module

p : permeate

r : retentate

s : solvent

Superscripts

$'$	:	high-pressure side of the membrane
$''$	:	low-pressure side of the membrane
o	:	external solution

CHAPTER 1

INTRODUCTION

1.1 General

Separation processes play an important role in many major industries. These processes include a large variety of applications ranging from analytical techniques using small quantities of materials to large-scale separations, involving product and unused raw material recovery for further enrichment, concentration and purification.

In the pharmaceutical industry, separation needs frequently involve synthetic organic processes. Because of the chemical and physical properties of the active components and intermediate products, having molecular weights in the range of 300 to 1000, most reactions are heterogeneous (Paul and Rosas, 1990). The selection of a separation process depends on several factors. Of particular importance is the thermal instability of the valuable products, which may preclude the use of standard unit operations, such as distillation, during downstream processing. Instead, less conventional processes involving, among others, chromatographic methods and membrane-based separation processes, could be used to advantage. Other factors to be considered are: initial and final concentration levels; chemical nature, stability and solubility of the constituents; technological maturity of the process (reliability, durability and availability of commercial units in the processing rate required); equipment cleaning; isolation and containment requirements; costs and so on. Most often, the separation goals cannot be achieved with a single process, but with a judicious combination of different technologies.

Membrane-based separation processes exhibit many attributes that have made them attractive to the pharmaceutical industry. Membrane separations are generally carried out at room temperature and are therefore suitable for processing labile compounds. Besides, they do not add extraneous components and the waste products they generate are the unwanted compounds from the feed streams. Furthermore, they are relatively modest in their energy consumption (Meares, 1976). Commercial units are compact and modular, so they can easily satisfy the processing rate required.

In general, membrane separation processes allow selective transfer of one or more constituents of a mixture between two bulk phases. A semipermeable membrane acts as a barrier. As a result, the feed phase is depleted of the more permeable species, while the receiving phase is enriched in these. The driving forces for these separations arise from a gradient of chemical potential (due to a pressure gradient or concentration gradient) or electrical potential (Ho and Sirkar, 1992). Most common membrane processes comprise 1. gas/gas systems (gas permeation, e.g. nitrogen-enrichment of air, separation of organic vapors from industrial gas streams); 2. liquid/vapor systems (pervaporation, e.g. organic dehydration, removal of volatile organic compounds from waste water) and 3. a broad range of applications in liquid/liquid systems, depending on the nature of the membrane and the driving force (pressure: reverse osmosis, nanofiltration, ultrafiltration, microfiltration; concentration: dialysis, emulsion liquid membrane, etc.; an electrical potential difference: electrodialysis).

Nanofiltration (NF) is a relatively novel membrane separation process. No generally accepted definition of it is available and it is commonly classified as a process intermediate

between reverse osmosis (RO) and ultrafiltration (UF) (Eriksson, 1988; Bowen et al., 1997). Although the driving force for the separation of solutes in the liquid phase is, in all three processes (RO, UF and NF), the pressure difference across the membrane, there are significant differences in their applications and operating range. It has been suggested (Soltanieh and Gill, 1981; Eriksson, 1988; Raman et al., 1994, Bowen et al., 1997) that these processes may be defined using one or a combination of the following criteria: molecular weight cut-off (MWCO), which is the molecular weight of the smallest compound, taken as typical or model, that is rejected by the membrane at least up to 95% and is a relative measure of the rejected solute dimensions; membrane pore size; transport mechanisms through the membrane and operating pressure range. To establish a relative framework in which NF membranes can be discussed, it is interesting therefore to review briefly the application ranges of RO and UF.

Traditional applications of RO are the desalination of seawater and brackish water and the concentration of fruit juices. More recently, it has been extensively used in the treatment of wastewater from industrial and municipal sources. Small inorganic ionic solutes such as those present in seawater (e.g. sodium, potassium, calcium, magnesium, chloride, sulfate, bicarbonate) and wastewater (components like zinc, chromium, copper and arsenic), and organic solutes (e.g. benzene, phenol, methylene chloride, etc.) from industrial wastewaters as well as sugars from fruit juices, can be separated by this technique. Solute radii can be as small as 0.2 nm (for ions such as sodium and chloride) or as large as about 0.5 nm (for sucrose). RO membranes are considered to be essentially nonporous. A classical description of solute rejection in nonporous membranes is the one by the Solution-Diffusion

Model (Lonsdale et al., 1965). Solvent and solute dissolve into the membrane at the high pressure solution-membrane interphase, then they diffuse independently (uncoupled flow) through the membrane and are desorbed at the low pressure solution-membrane interphase. Species concentrations on the membrane interphases are assumed to be in equilibrium with those in the solution they are in contact with. Separation results because the solvent and solute diffusion rates are different. Many additional models have been proposed to account for diffusive and convective contributions of the membrane nonidealities and the solute/membrane interaction (Soltanieh and Gill, 1981). Operating pressures are generally above 600 psig (4.1 MPa), although pressures as high as 1520 psig (10.5 MPa) and as low as 100 psig (0.7 MPa) have been reported (e.g. surface water treatment is performed at the indicated lower limit pressure) (Fu, 1994). The osmotic pressure of the solutions and the operating costs play a determining role in the selection of the operating pressure.

Established UF applications involve the separation of biomolecules in the food industry such as milk concentration and whey fractionation of proteins, the concentration of pharmaceutical products such as proteins and the separation of enzymes after a bioconversion (Meindersma and Kuczynski, 1995). The range of the size of the molecules is very large; in the lower limit, UF can be used to separate solutes as small as lactose with a molecular size of less than 1.0 nm (MWCO: 300); in the upper limit, UF can involve large proteins or polymers of a characteristic molecular size of up to 20 nm (MWCO: 200000). UF of molecules of a molecular weight of 500000 or more has also been reported (Meares, 1976). The pore size of UF membranes is not uniform; a wide or a narrow pore size distribution results from the process used in manufacturing the membranes. Mean pore size is in the

range of 1 to 100 nm. It is usually accepted that separation is due to a sieving process. The simplest transport mechanism is represented by a purely convective model known as Viscous Flow Model (Muldowney and Punzi, 1988). This model assumes the existence of membrane pores through which solvent passes in viscous flow conveying solute with it (coupled flow). Separation occurs if the solute concentration in the pore liquid differs from that in the solution on the high-pressure side. Operating pressures are usually in the range of 30 to 150 psig (0.2 to 1 MPa).

Early descriptions of NF membranes (referred to as low-pressure RO, loose RO, ultra-osmosis or charged RO/UF), stressed the fact that these membranes share some properties of the RO and UF membranes (Tsuru et al., 1991, Raman et al., 1994). For example, RO membranes reject efficiently small ionic solutes (e.g. NaCl, $MgSO_4$) and sugars (sucrose), whereas UF membranes let them pass through. Combining properties from both, NF membranes reject divalent ions ($MgSO_4$) and sugars, but their retention of monovalent salts (e.g. NaCl) is considerably lower. Therefore, NF membranes were originally applied to softening water, by using them to remove calcium and magnesium salts. Current applications of these membranes include: cleaning up of groundwater contaminated with natural organic matter and disinfection by-products, with particular emphasis placed on the removal of trihalomethanes precursors (Amy et al., 1990; Blau, 1992; Fu, 1994; Jacangelo, 1995); treatment of wastewater in metalworking, pulp and paper mills, textile production, mining operations (Afonso et al., 1992; Awadalla et al., 1994); desalting of whey production (Raman et al., 1994), etc. More recently, use of NF membranes was explored in connection with organic coenzyme-dependent synthesis of polyols such as mannitol and xylitol, used widely

as sweeteners in the food industry; the coenzyme, with a molecular weight of about 700, was retained with a NF membrane (Nidetzky et al., 1996).

The application range of NF separation processes has been restricted so far to aqueous solutions. However, the emergence of new solvent-compatible membranes, such as those considered in this study, promise to open NF processing to organic solvent-based systems. Provided with a pore size of about 1 nm, NF membranes stand in the upper limit of the solute dimensions which are rejected by RO and, at the same time, in the lower limit for UF techniques to be applied. This intermediate pore size allows NF membranes to retain solutes with a molecular weight between, say, 250 and 700, more efficiently than their counterparts, and, as a result, NF membranes can be of particular importance in the pharmaceutical industry. Operating pressures are moderate, somewhere between 150 and 600 psig (1.0 to 4.1 MPa).

Mechanisms to describe the transport of solvent and solute through NF membranes consider that while large, neutral molecules undergo separation through sieving (like in UF), small charged solutes would be rejected mainly due to electrostatic interaction between the ions and the often-negatively-charged membrane (Bowen et al., 1997). These unique properties of combining a sieving process based on molecular size and electrostatic repulsion could be exploited in non-aqueous solvent-based systems having relatively high dielectric constants, such as methanol. The dielectric constant or relative permittivity of methanol @ 298 K is 32.6, compared to 78.5 for water and 2.2 for cyclohexane (Popovych and Tomkins, 1981; Atkins, 1994), at the same temperature. This implies that electrolytes remain dissociated into ions in methanol solutions, but not in cyclohexane.

Added versatility provided by the solvent-compatible NF membranes open new uses in systems involving species of diverse molecular weights and dimensions. Potential applications in organic syntheses include downstream concentration and purification steps as well as the external coupling of a reactor with a membrane separator to enhance the performance of the synthesis.

1.2 Scope of the Thesis

This thesis has two distinct parts:

1) The experimental results of the NF membrane separation behavior of selected organic solutes dissolved in methanol, at different operating conditions, and
2) Modeling of the effects of the external coupling of a semibatch/batch reactor with a NF membrane separator, with results from numerical studies.

Selected membranes were specifically recommended by a manufacturer for use with organic solvents, over a broad range of pH, at room temperature. The manufacturer-specified MWCO of the membranes were 250, 400 and 700, which allowed for the testing of organic solutes of different molecular weights (MW) and hence, dimensions. Methanol was selected as the solvent due to its extensive use in pharmaceutical syntheses, good solubility of many organic solutes at high concentrations and easy availability. In addition to their solubility in methanol, solutes were selected using the following basis: molecular weights and dimensions (in order to show how efficient the separation would be for a given pair of membrane and solute), molecular configuration (preferably a globular or spherical arrangement), safe handling without restrictions from governmental agencies, analytical

methods for monitoring and cost. Experiments were performed with three solutes: safranin O (MW 351), brilliant blue R (MW 826) and vitamin B_{12} (MW 1355), under different conditions of concentration, pressure and stirring.

The MW of target compounds in many organic syntheses in the pharmaceutical industry is in the range of 300 to 1000. The potential benefits of using solvent-compatible NF membranes to separate the valuable products from the smaller MW products and residual reactants present in the reaction mixture were assessed using a mathematical model for a hypothetical reaction system consisting of two parallel reactions. The model developed allows for determination of the progress of the reactions with time for different operation protocols (batch reactor, semibatch reactor, uncoupled of or coupled to a NF membrane separator) and conditions (reaction and equilibrium constants, rate of addition, membrane area, solvent flux through the membrane, solute rejection, etc.), by using appropriate parameter values. Numerical modeling results provide a better understanding of the effect of coupling a reactor with a membrane separator and may be used in predicting the overall performance of more complex reaction systems, provided that basic kinetic data are available.

CHAPTER 2

THEORETICAL CONSIDERATIONS

Separation through NF membranes is considered to be the combined result of a sieving process and electrostatic interaction between the membrane and the solute. For large, neutral molecules, the predominant mechanism is based on steric or sieving effects, extensively studied in connection with UF membranes. However, the fact that NF membranes also reject small charged ions indicates the importance of including electrostatic interactions between the ions and the often-negatively-charged membranes in any proposed mechanism.

In the published literature it is commonly assumed that NF membranes consist of bundles of capillary tubes. No complete theory is, however, currently available to explain the performance of the membranes. Although there is still controversy on the applicability of macroscopic models of hydrodynamics and charge interaction used for larger pores to describe the permeate flux and the solute transport through pores of nanometer dimensions, these models are widely used in the absence of alternative ones.

In this chapter, the expressions for the Viscous Flow Model characteristic of highly porous membranes are presented only as a limiting case. The equations for a more realistic model, accounting for the hindered diffusion through pores which are not much larger than the molecular dimensions of the solutes and commonly known as the Finely Porous Model (Merten, 1966) are also presented. This model was proposed originally to describe RO membranes with a pore size too small to permit unrestricted flow of solute molecules and is particularly suitable for NF membranes.

2.1 Permeate Flux through NF Membranes

In highly porous membranes, the permeate flux, J_s, is generally estimated using the following expression:

$$J_s = \frac{L_p}{\tau\ \delta} (\Delta P - \Delta \pi) \qquad (2.1)$$

where L_p is the permeability of the membrane, δ is the membrane thickness, τ is the tortuosity of the membrane (hence, the product $\tau\delta$ is the effective membrane thickness), ΔP is the difference of applied pressure across the membrane and $\Delta\pi$ is the osmotic pressure difference between the feed and permeate phases.

The Hagen-Poiseuille equation is usually considered to correlate the permeability and the pore radius for fully developed velocity inside the pore (Bowen et al., 1997). This choice is supported by other investigators as well (Sarrade et al., 1996), as it provides a suitable model to explain permeability variations in NF membranes. Thus, assuming cylindrical pores:

$$L_p = \frac{\epsilon\ r_p^{\,2}}{8\ \eta} \qquad (2.2)$$

where ϵ is the porosity of the membrane, r_p is the hydrodynamic pore radius and η is the viscosity of the solution inside the pore.

Equations (2.1) and (2.2) are simple to apply but they provide a limited picture of the interaction between solutes and membrane pore walls. This interaction can be expressed via

the Finely Porous Model which includes a term accounting for the frictional forces acting on the pore fluid. The frictional force term, F_v, must be added to the pressure gradient to get the total force acting on a unit volume of pore fluid,

$$J_s = -L_p \left(\frac{dP}{dx} + F_v \right) \tag{2.3}$$

where x is the direction perpendicular to the membrane surface.

The frictional force, F_v, can be calculated as:

$$F_v = - \frac{f_{im} J_i}{\epsilon} \tag{2.4}$$

where f_{im} is the friction coefficient between the solute i and the membrane and J_i is the solute flux. Since $J_i = J_s C_{ip}$ (C_{ip} being the permeate solute concentration), equation (2.3) can be integrated over the effective membrane thickness $\tau\delta$ to give:

$$J_s = L_p \left[\frac{1}{1 + \frac{L_p f_{im} C_{ip}}{\epsilon}} \right] \frac{(\Delta P - \Delta\pi)}{\tau\delta} \tag{2.5}$$

or

$$J_s = L_p' \frac{(\Delta P - \Delta\pi)}{\tau\delta} \tag{2.6}$$

where L_p' is the apparent permeability defined as

$$L_p' = L_p \left| \frac{1}{1 + \frac{L_p f_{im} C_{ip}}{\epsilon}} \right| \tag{2.7}$$

L'_p is, in general, smaller than the permeability, L_p, estimated for highly porous membranes. The correction factor, in brackets, is less than the unity and will decrease with an increasing frictional factor, a higher concentration in the permeate or a lower porosity of the membrane. When the interaction between the solute and the membrane, f_{im}, is negligible, L'_p is at its maximum and $L'_p = L_p$. The Hagen-Poiseuille equation provides the connection between the permeability, L_p, and the pore radius via equation (2.2) given earlier.

2.2 Transport of Solute through NF Membranes

The transport flux of solute, J_i, can be expressed via the Nernst-Planck equation as the sum of the transport fluxes due to diffusion, convection and electric field gradient, as follows:

$$J_i = J_{i,d} + J_{i,c} + J_{i,e} \tag{2.8}$$

The specific form of each term in the equation above will be presented later.

2.2.1 Transport of Uncharged Solutes

For uncharged solutes, $J_{i,e} = 0$ and equation (2.8) is simplified as follows:

$$J_i = J_{i,d} + J_{i,c} \tag{2.9}$$

The Finely Porous Model (Merten, 1966; Soltanieh and Gill, 1981) considers the existence of a frictional force acting on the solute due to its interaction with the pore wall, which opposes the Fickian diffusion. The result of this hindered diffusion is to increase the drag on the solute. The diffusive term can be written as:

$$J_{i,\,d} = m_i\, C_{im} \left[- \left(\frac{\partial \mu_i}{\partial C_{im}} \right)_{P,T} \frac{dC_{im}}{dx} + F_m \right] \tag{2.10}$$

where m_i is the mobility of the solute in the solvent, C_{im} is the solute concentration within the membrane; μ_i is the chemical potential of species i and F_m is the per mole of solute frictional force resulting from the solute interaction with the membrane,

$$F_m = - \frac{f_{im}\, J_i}{C_{im}} \tag{2.11}$$

F_m is similar to F_v defined by equation (2.4) but differs in the calculation basis of the frictional force. F_v is based on the unit volume of pore fluid while F_m is based on the mole of solute.

To derive a useful expression for $J_{i,\,d}$, some simplifications are needed. For dilute solutions,

$$\left(\frac{\partial \mu_i}{\partial C_{im}} \right)_{P,T} = \frac{R\ T}{C_{im}} \tag{2.12}$$

Furthermore, the following definitions were adopted (Soltanieh and Gill, 1981): m_i is the inverse of the friction coefficient between the solute i and the solvent s,

$$m_i = \frac{1}{f_{is}} \tag{2.13}$$

b is a combined frictional coefficient,

$$b = 1 + \frac{f_{im}}{f_{is}} \tag{2.14}$$

D_e and D are the effective diffusion coefficient for small pores and the diffusion coefficient for large pores, respectively,

$$D_e = \frac{R\ T}{f_{is}} \left(\frac{1}{b} \right) = \frac{D}{b} \tag{2.15}$$

On the other hand, the convective term can be written as

$$J_{i,\,c} = u\ C_{im} = \frac{J_s\ C_{im}}{\epsilon} \tag{2.16}$$

where u is the permeation velocity in the membrane pore.

Using Equations (2.10) to (2.15) to describe $J_{i,\,d}$, and (2.16) for $J_{i,\,c}$, Equation (2.9) reduces to:

$$J_i = \frac{C_{im}}{f_{is}} \left[- \frac{R\ T}{C_{im}} \frac{\mathrm{d}C_{im}}{\mathrm{d}x} - \frac{f_{im}\ J_i}{C_{im}} \right] + \frac{J_s\ C_{im}}{\epsilon} \tag{2.17}$$

This expression can be further rearranged to:

$$J_i = - D_e \frac{\mathrm{d}C_{im}}{\mathrm{d}x} + \frac{J_s\ C_{im}}{b\ \epsilon} \tag{2.18}$$

Before solving this equation, it is interesting to contrast it with the expression that can be derived from the Viscous Flow or Highly Porous Model. The first term, which is the diffusive contribution, is much smaller in the Finely Porous Model, because the effective diffusion coefficient, D_e, defined by the expression (2.15) is smaller than that for large pores, D, by the factor $1/b$. Similarly, the second term which is the convective contribution is also reduced by the factor $1/b$.

Equation (2.18) can be integrated subject to the following boundary condition:

at $x = 0$ (i.e., at the high pressure side or retentate side),

$$C_{im}(0) = k' C_{ir} \tag{2.19}$$

where k' is a solute partition coefficient and C_{ir} is the solute concentration in the retentate side.

Integration of equation (2.18) when (2.19) is used, and J_i, J_s, D_e and b are assumed constant with $J_i = J_s C_{ip}$ leads to:

$$C_{im}(x) = C_{ip}\, b \left[1 - exp\left(\frac{J_s\, x}{b\, \epsilon\, D_e} \right) \right] + k' C_{ir}\, exp\left(\frac{J_s\, x}{b\, \epsilon\, D_e} \right) \tag{2.20}$$

At $x = \tau\delta$ (i.e., at the low pressure side), one can write

$$C_{im}(\tau\delta) = k'' C_{ip} \tag{2.21}$$

where k'' is a solute partition coefficient and C_{ip} is the solute concentration in the permeate side.

Evaluating (2.20) at $x = \tau\delta$ and using (2.21) one gets:

$$\frac{C_{ip}}{C_{ir}} = \frac{k' \exp\left(\frac{J_s \tau \delta}{b \epsilon D_e}\right)}{k'' - b\epsilon + b\epsilon \exp\left(\frac{J_s \tau \delta}{b \epsilon D_e}\right)} \tag{2.22}$$

In terms of the fractional solute rejection R,

$$R = 1 - \frac{C_{ip}}{C_{ir}} \tag{2.23}$$

equation (2.22) can be rewritten as:

$$\left(\frac{1}{1 - R}\right) = \left(\frac{b\epsilon}{k'}\right) - \left(\frac{b\epsilon - k''}{k'}\right) \exp\left[-\frac{J_s \left(\frac{\tau \delta}{\epsilon}\right)}{b D_e}\right] \tag{2.24}$$

In general, the values of k' and k'' are different. For the limiting case of purely steric interactions between the solute and the pore wall (Deen, 1987), k' and k'' are equal to Φ, the steric partition coefficient, defined as:

$$\Phi = (1 - \lambda)^2 \tag{2.25}$$

For cylindrical pores, λ is the ratio of solute radius (r_i) to pore radius (r_p):

$$\lambda = \frac{r_i}{r_p} \tag{2.26}$$

Finally, an interesting simple result of the steric exclusion of solutes from membrane pores, applicable for dilute solutions of neutral solutes is given by equation (2.27), where σ_o is the osmotic reflection coefficient, which is the limiting value of the rejection R (Deen, 1987; Aimar et al., 1990):

$$\sigma_o = (1 - \Phi)^2 \tag{2.27}$$

2.2.2 Transport of Charged Solutes

When the solutes involved are charged, none of the three terms of the Nernst-Planck equation (2.8) is equal to zero. In NF separations, there are no external electric fields gradients; any gradient that exists within the membrane is the result of the transport processes themselves (Merten, 1966).

The expressions for the diffusive and convective contributions are the same as those presented in Section 2.2.1.

The electric field term can be written as follows:

$$J_{i,e} = - \frac{z_i C_{im}}{R T} F \frac{d\psi}{dx} \tag{2.28}$$

where ψ represents the electric potential in the axial direction, x; z_i is the valence of the ion and F is the Faraday constant.

The conditions of electroneutrality in the external solution and in the membrane are described by the following expressions (Bowen et al., 1997):

$$\sum_{i=1}^{n} z_i C_i^{\circ} = 0 \tag{2.29}$$

$$\sum_{i=1}^{n} z_i C_{im} = - X \tag{2.30}$$

where C_i° is the concentration of ion i in the external solution and X is the effective volumetric membrane charge density. Additionally, since there is no current inside the membrane:

$$\sum_{i=1}^{n} F (z_i J_i) = 0 \tag{2.31}$$

The concentration at the interface can be determined with the following expression (Bowen et al., 1997) which combines Donnan and steric effects:

$$\frac{\gamma_{im} C_{im}}{\gamma_i^o C_i^o} = \Phi \; exp \left[- \frac{z_i F}{R T} \Delta\psi_D \right] \tag{2.32}$$

where γ_i is the activity coefficient of the ion, $\Delta\psi_D$ is the Donnan Potential and Φ is the steric partitioning term, defined in equation (2.25).

No attempt has been made in this study to solve the equation for transport of charged solutes in its general form. Solutions for particular cases can be found elsewhere (Merten, 1966).

CHAPTER 3

EXPERIMENTAL

3.1 Chemicals

The following chemicals were used in the experiments: methanol (HPLC-grade), safranin O (dye content 95%) and vitamin B_{12}, cyanocobalamin (99%) (Fisher Scientific, Fair Lawn, NJ); brilliant blue R (dye content 90%) (Sigma Chemical, St. Louis, MO).

Additionally, ethanol, reagent alcohol (90%) (obtained from Fisher Scientific, Fair Lawn, NJ) was utilized in the conditioning of the membranes before the actual experiments. Furthermore, glycerol (99%) and sodium metabisulfite, ACS reagent (98.8%) (both from Sigma Chemical, St. Louis, MO) and benzalkonium chloride (from Acros Organics, Pittsburgh, PA) were used to prepare the preserving solutions for the membranes.

3.2 Membranes

The flat MPF SelRO™ nanofiltration (NF) membranes utilized in this study were manufactured by Membrane Products Kiryat Weizmann, Ltd., Rehovot, Israel. These were supplied in 21.6 x 27.9 cm (8 ½ x 11") sheets by LCI Corporation, Process Division, Charlotte, NC.

Three NF membrane types, namely MPF-44, MPF-50 and MPF-60 were used. According to the manufacturer, these membranes are stable in most organic solvents, such as alcohols, ketones, esters, alkyl halides, alkanes, etc., at room temperature and over a wide range of pH values. Their use is, however, not recommended for extremely polar solvents

like dimethylsulfoxide (DMSO) or dimethylformamide, among others. Table 3.1 summarizes some properties of these membranes and their application range (Kiryat Weizmann, 1996). For example, MPF-44 has a manufacturer-specified molecular weight cut-off (MWCO) of 250, i.e., a fractional rejection of at least 0.95 for species of molecular weight of 250 or higher and might be used in either aqueous solutions or organic solvents.

Table 3.1 Properties of the NF Membranes Utilized in this Study

Type	MWCO	pH range	Features and chemical stability
MPF-44	250	2-10	Hydrophilic, aqueous/organic solutions
MPF-50	700	4-10	Hydrophobic, organic solutions
MPF-60	400	2-10	Hydrophobic, organic solutions

Membranes were supplied soaked in a preserving solution, the composition of which depended on the type of membrane. Membranes of type MPF-44 and MPF-50 were preserved in a solution of 0.1% sodium metabisulfite and 10% glycerin; MPF-60 membranes were soaked in a solution of 20% glycerin and 0.7% benzalkonium chloride. The active side of the membrane was shiny and smooth, and should be in contact with the test solution. The substrate side was dull.

3.3 Experimental Setup

A schematic of the laboratory setup utilized for the experiments is shown in Figure 3.1. Separation tests were performed in a pressure cell (model 56414 SEPA® ST) obtained from Osmonics, Minnetonka, MN. A schematic of the cell is shown in Figure 3.2. The cell

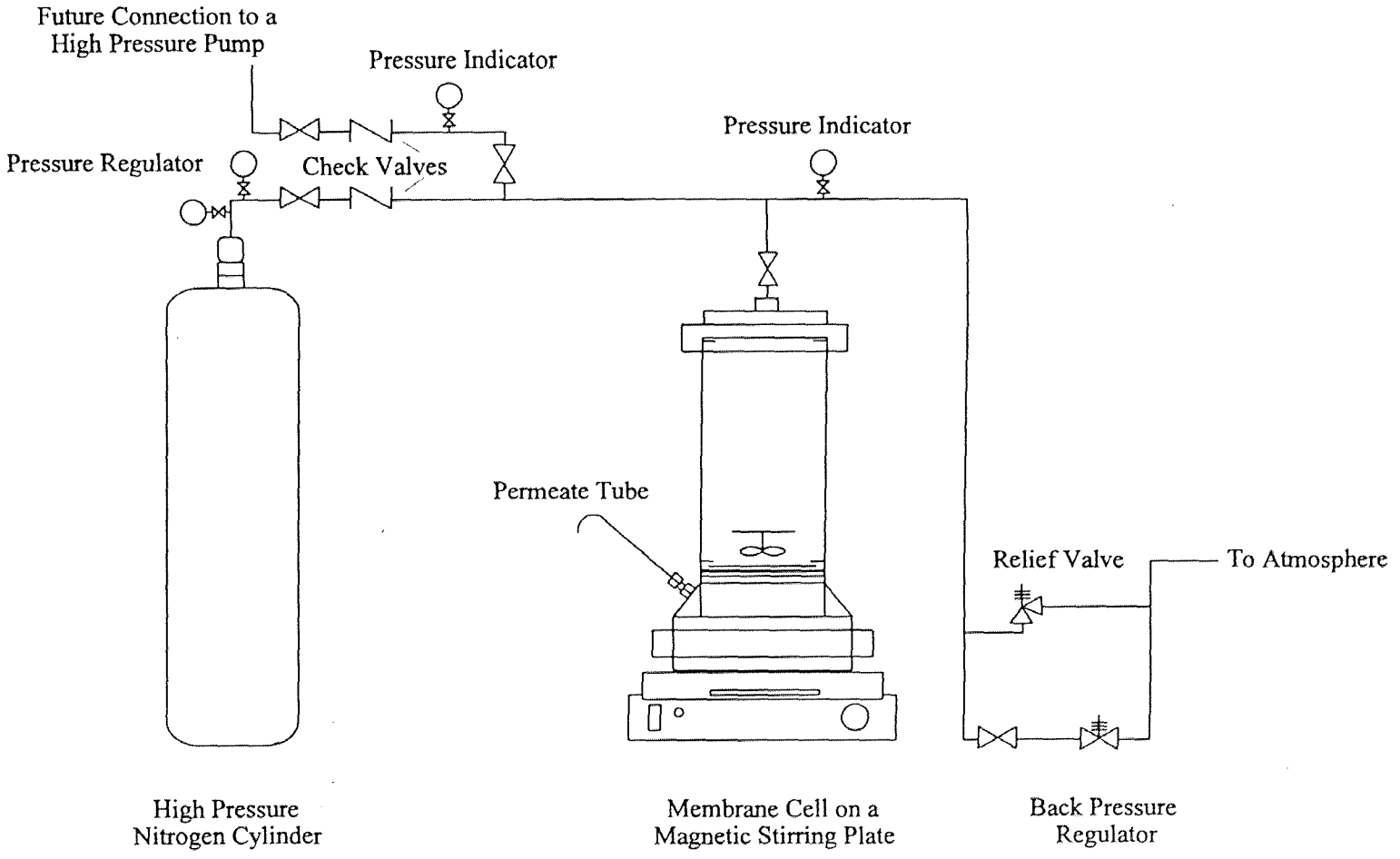

Figure 3.1 Schematic Diagram of the Laboratory Setup

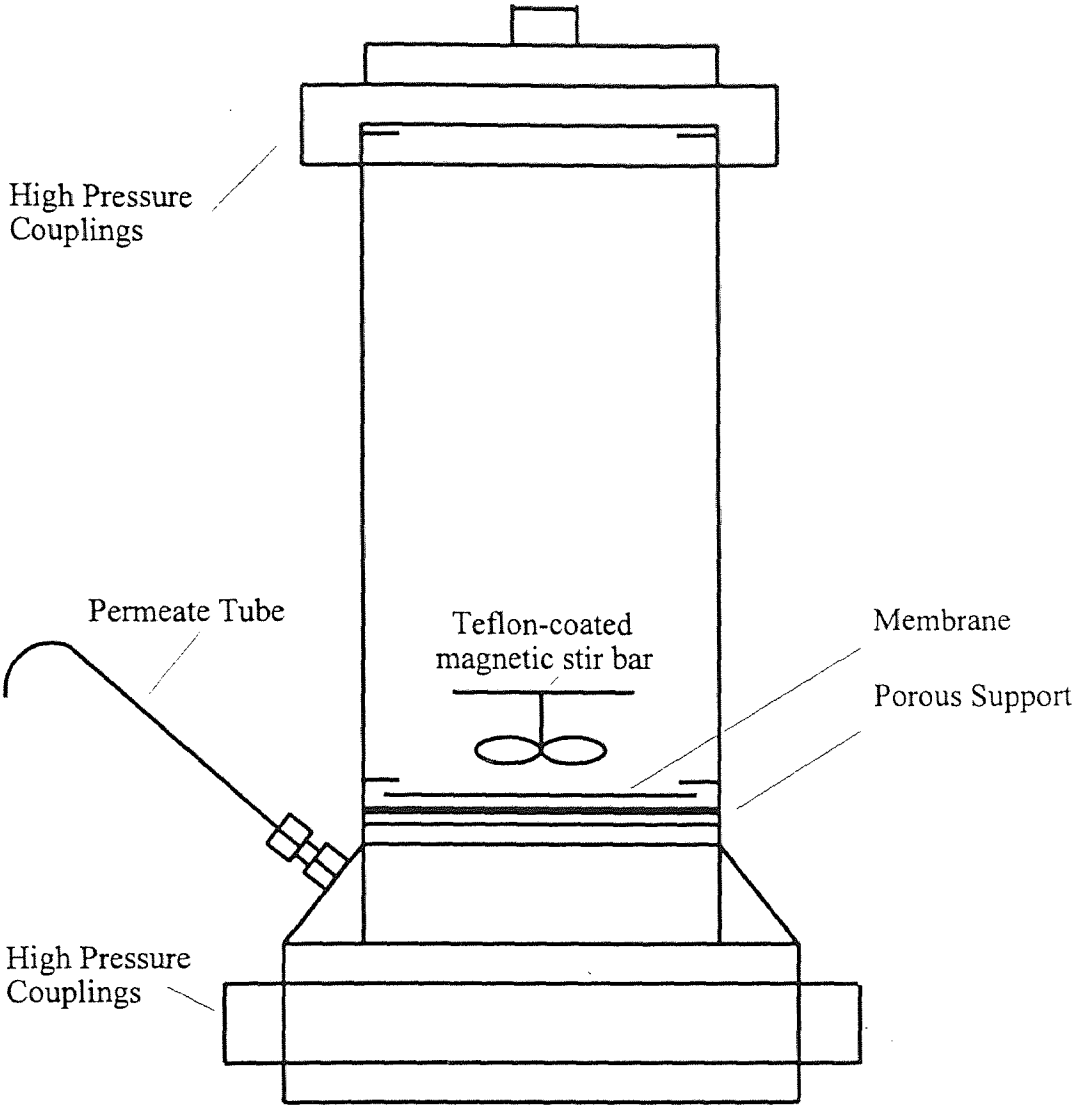

Figure 3.2 Schematic Diagram of the Pressure Cell

consisted of a 300 cm^3, 316 stainless steel cylindrical body provided with high pressure-resistant couplings (up to 1000 psig). A flat, round-cut membrane having a diameter of 4.9 cm and an effective (exposed or active) membrane area of 15.2 cm^2 was placed on top of a porous stainless steel support disk. The 0.16 cm (1/16") thick, 20 μm porous support disk was provided by the manufacturer along with the pressure cell. The hold-up volume underneath the porous support was 1 cm^3. Stirring was provided by means of a teflon-coated magnetic stir bar mechanism supported on a rim in the internal wall of the cell body. The permeate tube consisted of a 5 cm long, 1/8" diameter, stainless steel, removable tube, bent at its end to facilitate permeate collection. The design of the permeate tube was custom-made. The original, 14 cm long, 1/8" diameter, stainless steel tube was welded to the permeate orifice at the tapered base of the cell and was replaced with a Swagelock® 1/8" female pipe connector for a safer operation and easier cleaning. Wetted sealing parts, such as O-rings and gaskets were made of ethylene propylene (EP) to ensure resistance to methanol. A 1/4" diameter inlet tube was provided at the top of the cell. The pressure cell was placed on a variable-speed stirring plate.

Feed solution pressurization was provided by compressed nitrogen (extra dry) and the pressure was controlled by a single stage stainless steel pressure regulator, both from Matheson Gas Products, East Rutherford, NJ. A pressure gauge, attached to the inlet line, allowed convenient readings of the system pressure.

The setup was also provided with connections for a high pressure pump which, in the future, would add versatility to the system, by allowing it to be used as a flow cell, coupled to reacting or non-reacting systems or for solvent exchange studies. Check valves,

ball valves, a back pressure regulator (with a delivery pressure range of 50-700 psig, from Matheson Gas Products, East Rutherford, NJ) and an externally adjustable relief valve (set manually at 470 psig, from R. S. Crum, Mountainside, NJ), completed the laboratory setup. The tubing was 1/4" seamless stainless steel 316 (McMaster-Carr, New Brunswick, NJ). All wetted sealing parts in the valves were made of ethylene propylene (EP).

3.4 Experimental Procedure

The first step involved conditioning of the membrane. A pre-cut piece was rinsed thoroughly by immersion in deionized water overnight to remove the preserving solution. Then, the membrane was activated by flushing it with ethanol at 440 psig for about 60-80 minutes, long enough to collect at least a permeate of 10 cm^3. In order to prevent performance loss, conditioned membranes were kept soaked in ethanol.

3.4.1 Tests with Pure Solvents

Preliminary tests with pure methanol were carried out with the three membranes. Additional tests with deionized water were performed only with the hydrophilic membrane MPF-44.

A conditioned membrane sample was loaded in the pressure cell. Subsequently, 250 cm^3 of the test solvent was poured into the cell body and the tightly-closed cell was pressurized with nitrogen to a given test pressure. A summary of the test run conditions is given in Table 3.2. Permeate samples were collected in graduated cylinders to measure the permeation rate. Duration of the tests depended on the membrane type and applied pressure.

Table 3.2 Summary of the Test Run Conditions with Pure Solvent

Membrane Type	Solvent	Applied Pressure (psig)
MPF-44	Water	200, 440
	Methanol	200, 440
MPF-50	Methanol	440
MPF-60	Methanol	200, 440

Upon completion of the test, the pressure source was turned off and the system was depressurized to atmospheric pressure. This step was done slowly for safety purposes, especially when using methanol, in order to avoid sudden decompression of the volatile solvent, and to affect as little as possible the compression of the membrane sample. Pressure release was attained using the back pressure regulator, at an average rate of not more than 30 psi/min, i.e., it took at least 15 minutes to release the pressure when the system was operated at 440 psig. Information on the permeate flux dependence on time and pressure was obtained after repeated cycles of pressurization, testing and depressurization. Used membranes were kept soaked in ethanol at atmospheric pressure for further tests.

3.4.2 Tests with Solutions

Actual separation tests with solutions of the selected solutes were conducted in a similar way as for the pure solvents. Differences in the experimental procedure are given in detail below.

A test solution was prepared by dissolving, in methanol, a known amount of the solute in a 250 cm^3 flask; its concentration was determined spectrophotometrically (see

Section 3.5 for details on the concentration analysis) after appropriate dilution of 2 cm^3 of the solution in methanol. The average of the absolute value of the difference between the concentration determined spectrophotometrically and gravimetrically, was less than 0.5%.

After loading a conditioned membrane sample in the pressure cell, 248 cm^3 of the test solution was poured into the cell body. The cell was pressurized with nitrogen to a given test pressure, and the stirring plate was operated accordingly. Permeate samples were collected in graduated cylinders at regular intervals to measure the permeation rate and for subsequent analysis of their concentration, after appropriate dilution. Most of the membrane samples were tested for about 16 hours, in two 8-hour runs, in different days. During a typical 8-hour run and depending on the membrane type and test run conditions, 12 to 24 samples were collected. In order to do a consistent comparison of the initial performance of the membranes, the initial sample (sample 1) was collected after the first 10 minutes of permeation beginning with the first drop of permeate. Afterwards, sampling was done approximately every 30 minutes. By knowing the permeate solute concentration and the collected volume of permeate, a mass balance of solute in the cell (retentate) could be performed, after each sample was collected. Using this information, the percent rejection, % R, (defined by $\% R = 100 * [1 - (C_{permeate} / C_{cell})]$) was determined as a function of time. Appendix A shows spreadsheets with sample calculations of the average permeate flux and % rejection.

Experiments were done with the three membranes using methanol solutions of the following solutes: safranin O (molecular weight (MW) 351), brilliant blue R (MW 826) and vitamin B_{12} (MW 1355). Experiments employed different initial concentrations of solute in

the feed, mostly at the maximum operating pressure of 440 psig and at a constant stirring speed of about 100 rpm. Additional experiments at high initial concentrations of the feed and without any stirring were also carried out. One of the membranes (MPF-60) was tested at different operating pressures. A summary of the test run conditions is shown in Table 3.3.

Table 3.3 Summary of the Test Run Conditions with Methanol Solutions

Membrane Type	Solute	Initial Conc. Feed (wt%)	Stirring	Applied Pressure (psig)
MPF-44	Safranin O	0.01	Yes	440
	Safranin O	1.00	Yes	440
	Brilliant Blue R	0.01	Yes	440
	Brilliant Blue R	1.00	Yes	440
	Vitamin B_{12}	0.01	Yes	440
MPF-50	Safranin O	0.01	Yes	440
	Safranin O	1.00	Yes	440
	Safranin O	3.00	Yes	440
	Safranin O	3.00	No	440
	Brilliant Blue R	0.01	Yes	440
	Brilliant Blue R	1.00	Yes	440
	Vitamin B_{12}	0.01	Yes	440
	Vitamin B_{12}	1.00	Yes	440

Table 3.3 (Cont.) Summary of the Test Run Conditions with Methanol Solutions

Membrane Type	Solute	Initial Conc. Feed (wt%)	Stirring	Applied Pressure (psig)
MPF-60	Safranin O	0.01	Yes	440
	Safranin O	0.01	Yes	365
	Safranin O	0.01	Yes	295
	Safranin O	0.01	Yes	220
	Safranin O	1.00	Yes	440
	Safranin O	3.00	Yes	440
	Safranin O	3.00	No	440
	Brilliant Blue R	0.01	Yes	440
	Brilliant Blue R	0.01	Yes	365
	Brilliant Blue R	0.01	Yes	295
	Brilliant Blue R	0.01	Yes	220
	Brilliant Blue R	0.01	Yes	150
	Brilliant Blue R	1.00	Yes	440
	Vitamin B_{12}	0.01	Yes	440

Figure 3.3 compares the MW of the solutes and the manufacturer-specified MWCO of the membranes. Shaded areas depict the MW of the solutes which are expected to be rejected at least up to 95 % by the corresponding membrane. The larger the positive difference between MW and MWCO, the higher would be the rejection. Therefore, this figure suggests qualitatively how efficient the separation would be for a given pair of membrane and solute.

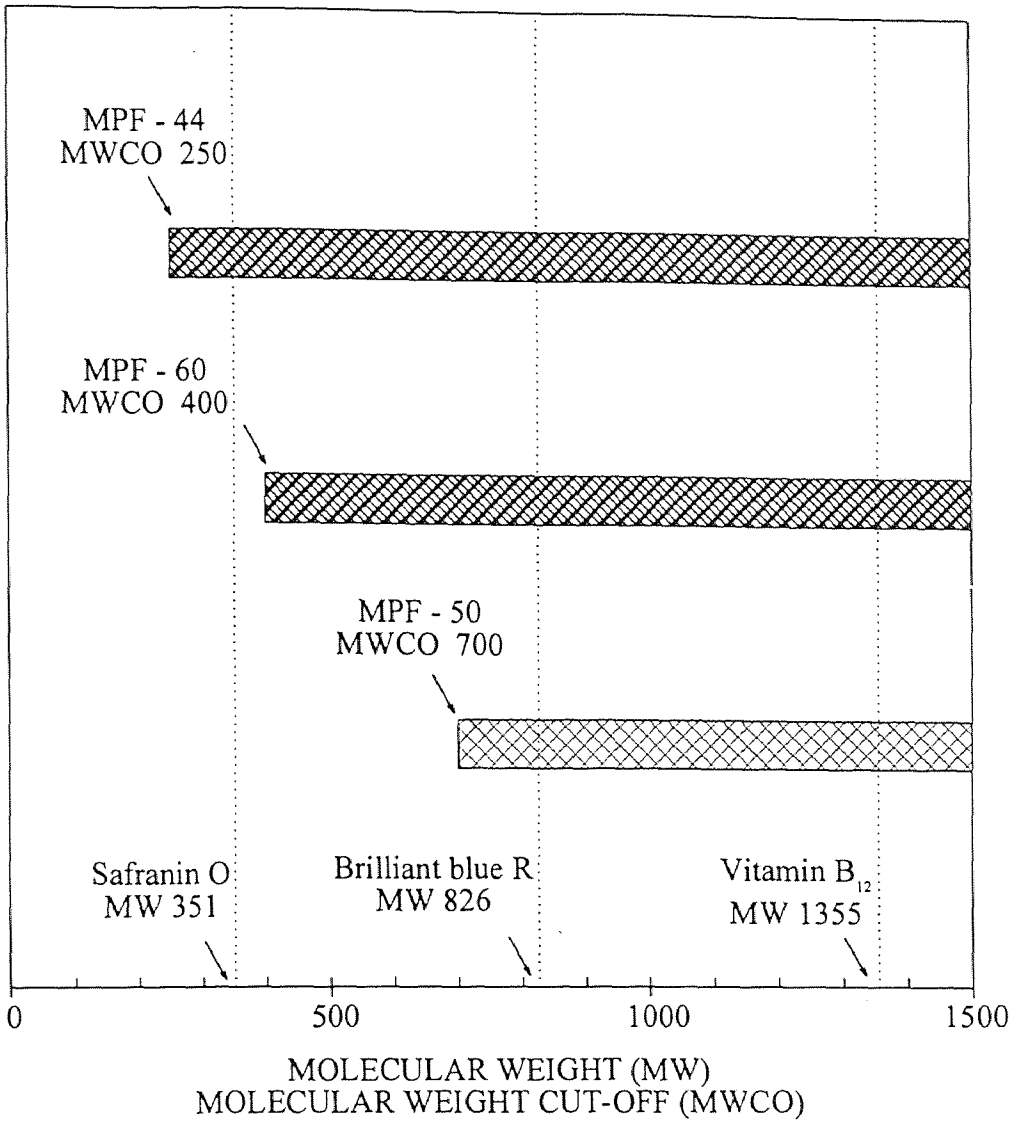

Figure 3.3 Comparison of the Molecular Weight (MW) of the Solutes and the Manufacturer-Specified Molecular Weight Cut-Off (MWCO) of the Membranes

The same caution, as indicated for the tests with pure solvents, has to be exercised upon completion of the test. Sudden decompression of the volatile methanol should be avoided for safety reasons and affecting the membrane compression as little as possible. Used membranes were stored soaked in ethanol at atmospheric pressure for further tests.

Membrane samples were typically subjected to a series of three pressurization cycles, consisting of the following steps as shown schematically in Figure 3.4: pressurization; activation or testing; depressurization. In all cases, in the first cycle, the membrane was pressurized to 440 psig for activation with ethanol for 60-80 minutes. This pressure was the same for all samples, so it did not depend on the future test run conditions. The second and third cycles were the actual test cycles. Most of the times, activation and subsequent testing of the membrane samples were performed in three consecutive days. The figure illustrates a schematic of the particular case of two 8-hour test runs at 220 psig with a MPF-60 membrane, the results of which are shown in Appendix A.

3.5 Concentration Analysis of the Test Solutions and Permeate

Concentrations of the test solutions and permeate were determined using a Double Beam UV/Vis spectrophotometer, model U-2000, from Hitachi Instruments, Danbury, CT, in the visible region. Figure 3.5 shows the wavelength scan of dilute solutions of each of the three solutes considered in this study, namely safranin O, brilliant blue R and vitamin B_{12} , in methanol @ 293 K. As the first step, blank wavelength scans with pure methanol were performed to assure that it did not exhibit extraneous impurity peaks in the spectral region of interest, that there were no resolution problems because of the solvent itself (UV cutoff

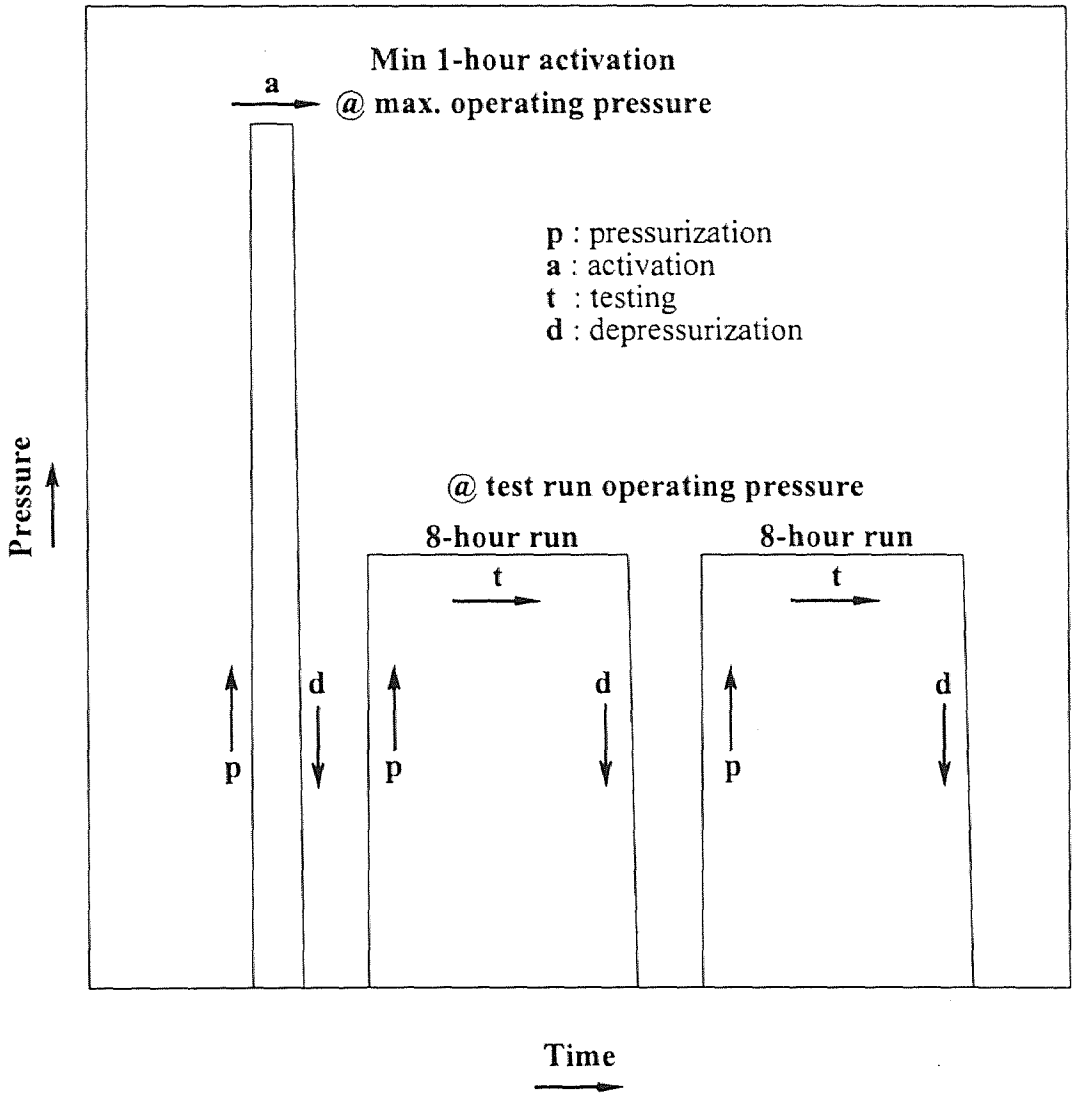

Figure 3.4 Schematic of the Pressurization Cycles of a Membrane Sample Tested in Two 8-Hour Runs at a Pressure Lower than the Maximum

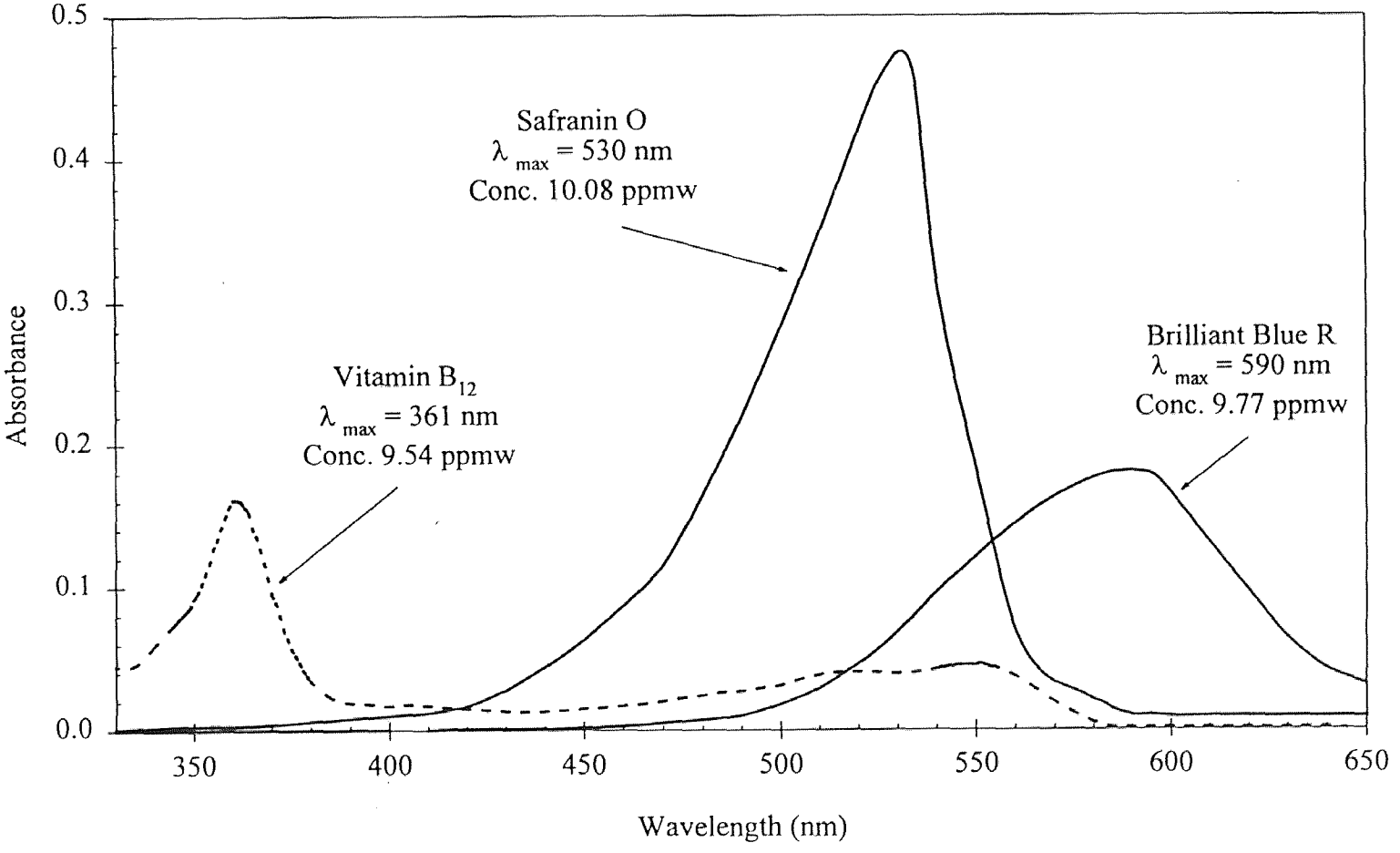

Figure 3.5 Wavelength Scan of Dilute Solutions of the Solutes Studied in Methanol @ 293 K

of methanol is 205 nm) (Willard et al., 1981), and that there were no compatibility problems with the polystyrene cuvettes (exposure of the cuvettes to methanol for periods as long as 8 hours did not affect the wavelength scans). The wavelength of maximum absorbance (λ_{max}) is listed in Table 3.4. These values match closely with those reported in the literature for aqueous solutions (Merck, 1996) and for the relative absorbance at the two peaks (361 and 551 nm) in the visible region of aqueous solutions of vitamin B_{12} (Merck, 1996; Kirk-Othmer, 1984).

Calibration curves were prepared from fresh, standard, dilute solutions of each of the solutes in methanol to relate the concentration of a solution with the absorbance measured at λ_{max}. The calibration curves for standard solutions of safranin O, brilliant blue R and vitamin B_{12} , in methanol @ 293 K are shown in Figures 3.6, 3.7 and 3.8, respectively. Actual concentration of the test solutions and permeate were determined after dilution (in some cases 1000 times) with methanol.

Table 3.4 Wavelength of Maximum Absorbance (λ_{max})

Solute	Solvent	λ_{max} (nm)
Safranin O	Methanol	530
Brilliant blue R	Methanol	590
Vitamin B_{12}	Methanol	361

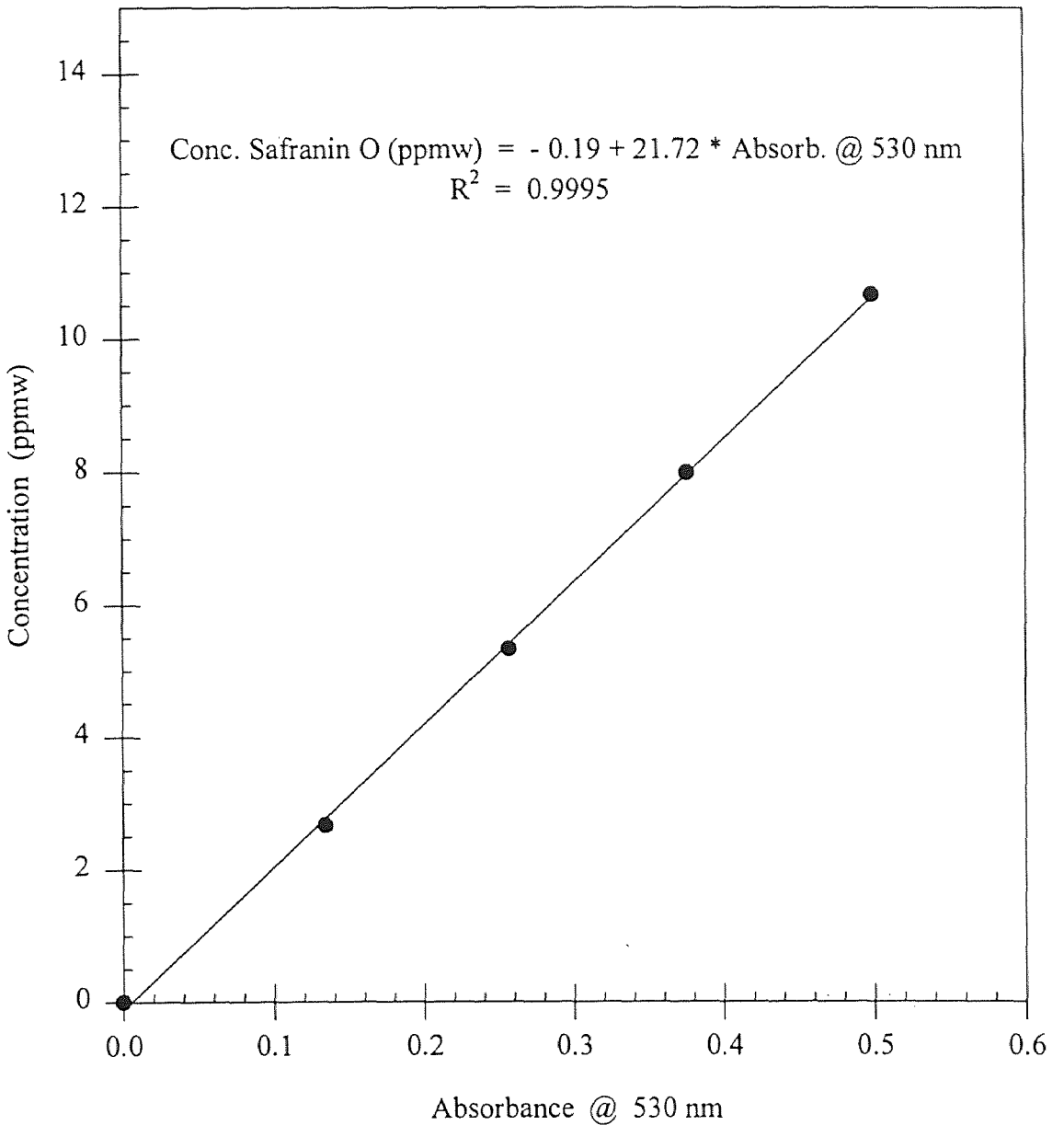

Figure 3.6 Calibration Curve for a Solution of Safranin O in Methanol @ 293 K

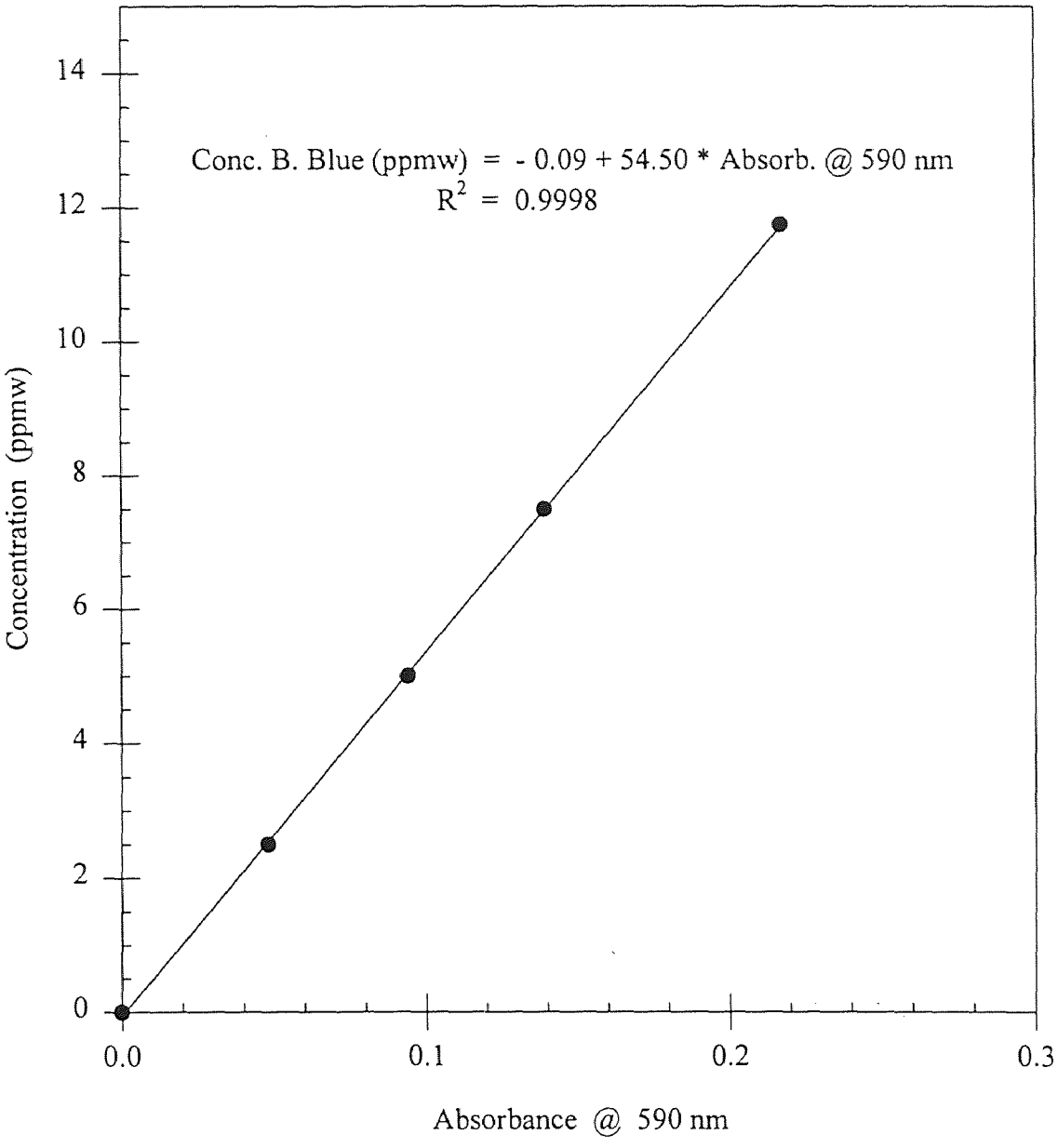

Figure 3.7 Calibration Curve for a Solution of Brilliant Blue R in Methanol @ 293 K

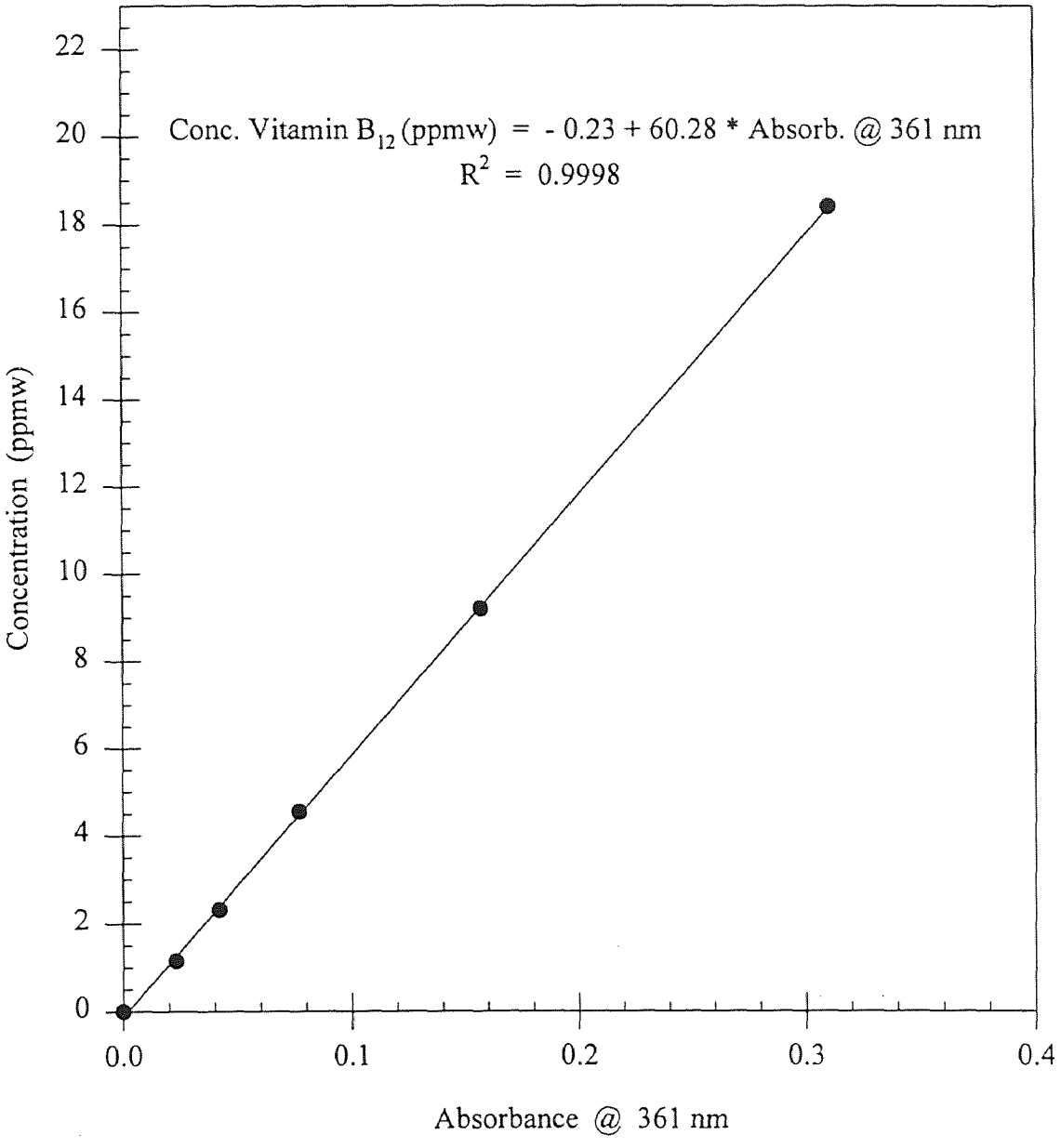

Figure 3.8 Calibration Curve for a Solution of Vitamin B_{12} in Methanol @ 293 K

CHAPTER 4

RESULTS AND DISCUSSION

The experimental results of the NF separation tests are presented and discussed in this chapter. The permeate flux of pure solvents through NF membranes is presented as a function of time for different applied pressures. The membrane performance with test solutions is shown in terms of the permeate flux and the solute rejection; results for these indicators are also time dependent. Appendix A shows sample calculations for the permeate flux and solute rejection.

4.1 Effect of Applied Pressure on the Permeate Flux of Pure Solvents

The permeate flux of a pure solvent for a given membrane is a function of the applied pressure. Dependence of the permeate flux through a MPF-44 membrane is shown as a function of time in Figure 4.1 for deionized water and in Figure 4.2 for methanol.

In general, membrane samples were tested several times at a given test pressure. Results from these consecutive tests show that the permeate flux was at its highest at the initial period and it declined as the test progressed. In the subsequent test with the same membrane sample and applied pressure, the initial permeate flux was higher than the final value attained in the previous test; afterwards, it followed a similar declining trend.

This behavior suggests that the membrane was compacted during the test. Because of the compaction, the membrane pores were shrunk, the pore size, r_p, became smaller and the permeate flux declined accordingly. Compaction and its effect on the permeate flux

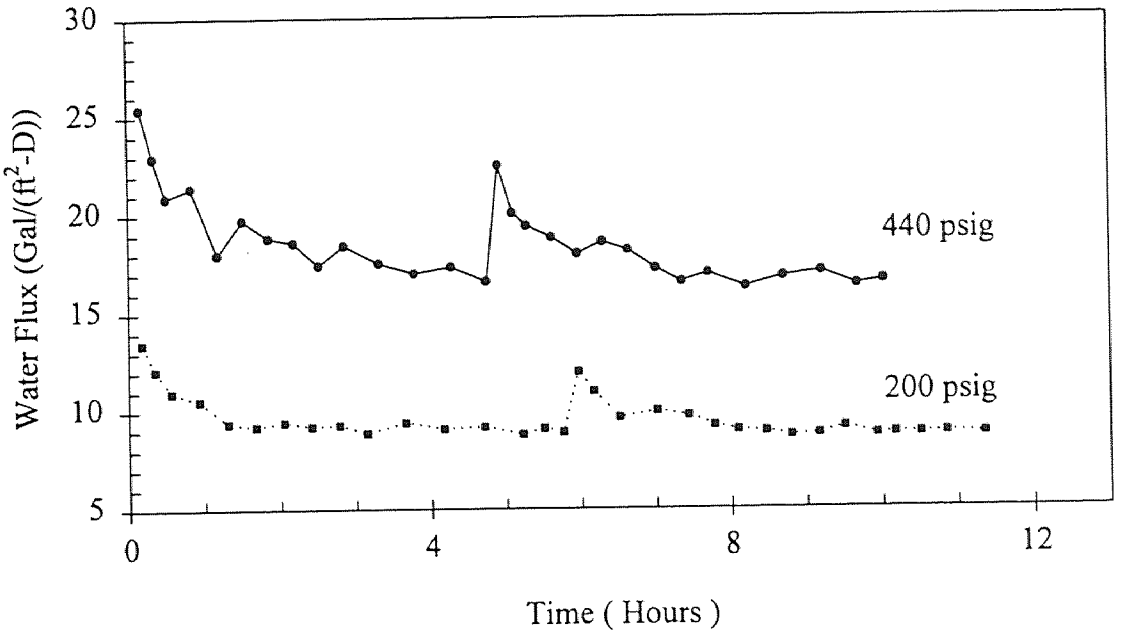

Figure 4.1 Effect of Applied Pressure on Water Flux as a Function of Time for a MPF-44 Membrane. Conditions: Pure Water Feed

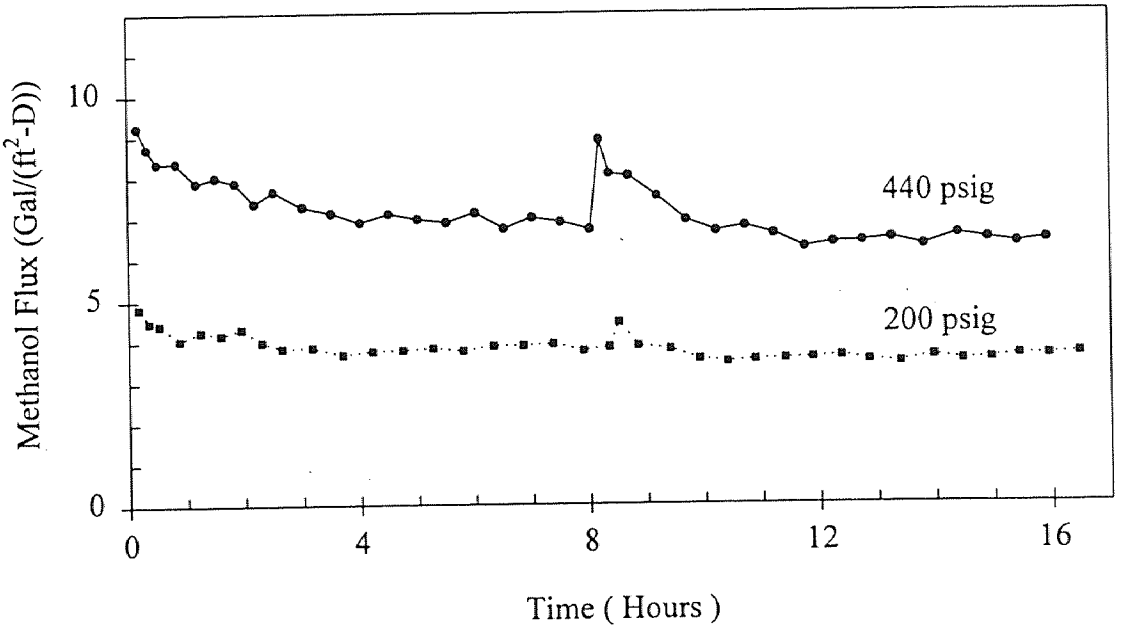

Figure 4.2 Effect of Applied Pressure on Methanol Flux as a Function of Time for a MPF-44 Membrane. Conditions: Pure Methanol Feed

would last as long as the membrane was under pressure. Once the pressure was released (upon completion of the test), the deformation of the pores due to the compaction process was not permanent or irreversible. Compaction also reduced the membrane thickness, which according to equation (2.1) would lead to an increase of the permeate flux. However, the effect of a smaller pore size on the reduction of the permeate flux seems to be predominant as the permeability depends on r_p^2, as indicated in equation (2.2).

In subsequent tests, the permeate flux increased initially to some extent, due to the partial reversibility of the membrane deformation. The compaction continued until the membrane reached a state in which no further permeate flux reduction occurred. This final permeate flux was attained after 10 to 12 hours of testing. For example, the methanol flux through a MPF-44 membrane and an applied pressure of 440 psig went down from an initial value of 9.24 Gal/(ft^2-D) (measured in the first 10 minutes of permeate collection) to 6.72 Gal/(ft^2-D) after the first 8-hour run. In a second run with the same membrane sample, the initial permeate flux was 8.90 Gal/(ft^2-D) and it declined again, reaching a steady state value of 6.40 Gal/(ft^2-D) after about 12 hours of total running time. The long-term slow flux decline, if any, was not determined.

Results using methanol for membranes MPF-50 (Figure 4.3) and MPF-60 (Figure 4.4) exhibit a higher permeate flux, but a partial reversibility of the membrane and declining trend with time similar to that found for MPF-44. MPF-50 is the loosest of the three membranes and hence, it exhibited the highest permeate flux changes and steady state values. Table 4.1 summarizes some of the results from the pure solvent permeation flux measurements.

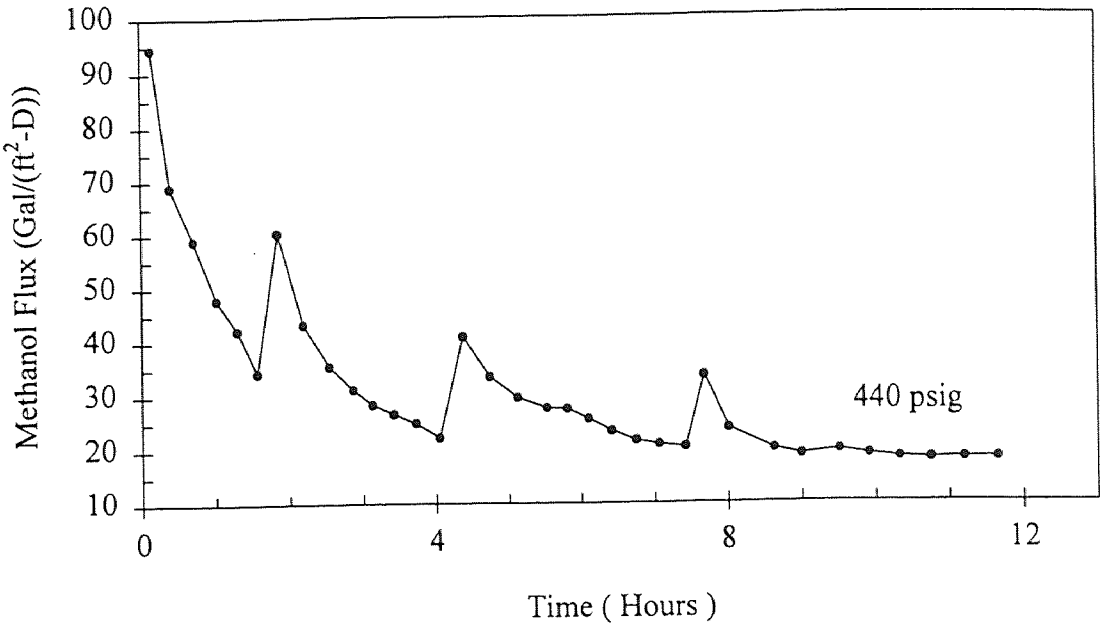

Figure 4.3 Methanol Flux as a Function of Time for a MPF-50 Membrane. Conditions: Pure Methanol Feed

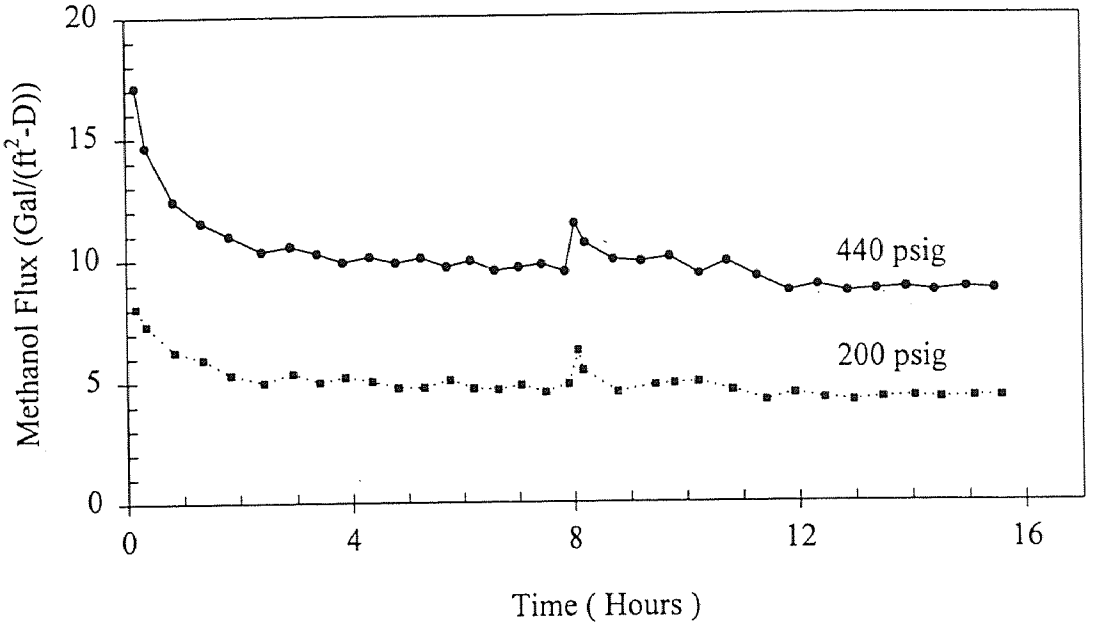

Figure 4.4 Effect of Applied Pressure on Methanol Flux as a Function of Time for a MPF-60 Membrane. Conditions: Pure Methanol Feed

Table 4.1 Pure Solvent Permeation Flux for Different Membranes and Applied Pressures

Membrane MPF-	Solvent	Applied Pressure (psig)	Permeation Flux (Gal/ft^2-D))			
			First Run		Second Run	
			Initial	Final	Initial	Final
44	Water	440	25.41	16.61	22.50	16.59
44	Water	200	13.48	8.91	12.00	8.79
44	Methanol	440	9.24	6.72	8.90	6.43
44	Methanol	200	4.83	3.85	4.45	3.66
50	Methanol	440	94.50	34.23	60.28	22.25
60	Methanol	440	17.11	9.50	11.45	8.71
60	Methanol	200	8.07	4.89	6.28	4.33

4.2 Permeate Flux and Solute Rejection for Dilute Solutions of Different Solutes at the Maximum Operating Pressure

Membranes were tested using methanol solutions. The permeate fluxes of the membranes using dilute solutions of about 0.01 wt% at the maximum operating pressure of 440 psig were slightly lower than those for pure solvent; the rejection depended strongly on the membrane type. Stirring speed was kept constant at about 100 rpm.

Permeate flux variation with time followed a trend quite similar to that previously discussed for pure solvent tests. A final steady-state value was reached after 10 to 12 hours of testing.

Solute rejection was initially at its lowest value and it increased with time as the membrane was compacted and the pore size became smaller. The partial reversibility of the

membrane, after the pressure was released, allowed the membrane sample to regain to some extent its original characteristics. This was evident as the initial values of the solute rejection in a second run were lower than the final value attained in the first run. As the test run progressed, the solute rejection reached a final, steady-state value after about 12 hours of total running time.

Performance behavior for longer run periods is not known. Only MPF-60 was tested with brilliant blue R for 24 hours, with no significant changes in the performance.

4.2.1 MPF-44 Membrane

A summary of the performance of the MPF-44 membrane with dilute solutions is shown in Table 4.2. Figure 4.5 illustrates the permeate flux and solute rejection behavior as a function of time for a MPF-44 membrane and methanol solutions having an initial concentration of 0.01 wt% of three different solutes, safranin O, brilliant blue R and vitamin B_{12}. Tests were conducted at a constant applied pressure of 440 psig.

Permeate flux declined with time. The ratio of the initial to the steady-state value was approximately constant and equal to 1.5. Final permeate fluxes were reached after 12 hours and were slightly lower than those for pure methanol at the same applied pressure (Figure 4.2). Furthermore, final permeate fluxes using different solutes were quite similar. Examination of equation (2.6) indicates that the permeate flux depends on the pressure difference (ΔP - $\Delta\pi$) and the apparent permeability L'_p; their contributions will be briefly discussed below.

Table 4.2 Performance of a MPF-44 Membrane for Different Solutes. Conditions: Initial Conc. in the Feed Cell = 0.01 wt % in Methanol; P = 440 psig; Stirring

Solute	Permeate flux (Gal/(ft^2-D))		% Rejection (2)
	Initial (1)	Steady-State	
Safranin O	9.95	6.11	67.6
Brilliant blue R	8.79	5.70	94.8
Vitamin B_{12}	9.05	6.47	98.8
No solute (3)	9.24	6.40	-----

Notes: (1) Initial 10 minutes of permeate collection in the first run.
(2) Steady-state values.
(3) Pure methanol.

Osmotic pressure of a solution with concentrations less than 0.2 M, can be estimated using the Van't Hoff law of osmotic pressure (Nabetani et al., 1992; Atkins, 1994):

$$\pi = M_i R T \tag{4.1}$$

where M_i is the molality of the solution, R is the gas constant and T the absolute temperature. The concentration in the feed side increased during the run because the batch operation mode leads to a buildup of solute inside the cell. Concentrations in the feed side were in the range of 0.01 to 0.06 wt%. In this concentration range, the osmotic pressure of the solutions, calculated using equation (4.1), was less than 1 psi. Even if there is concentration polarization, it can be concluded that there was no significant effect of osmotic pressure on the net pressure gradient and hence on the permeate flux.

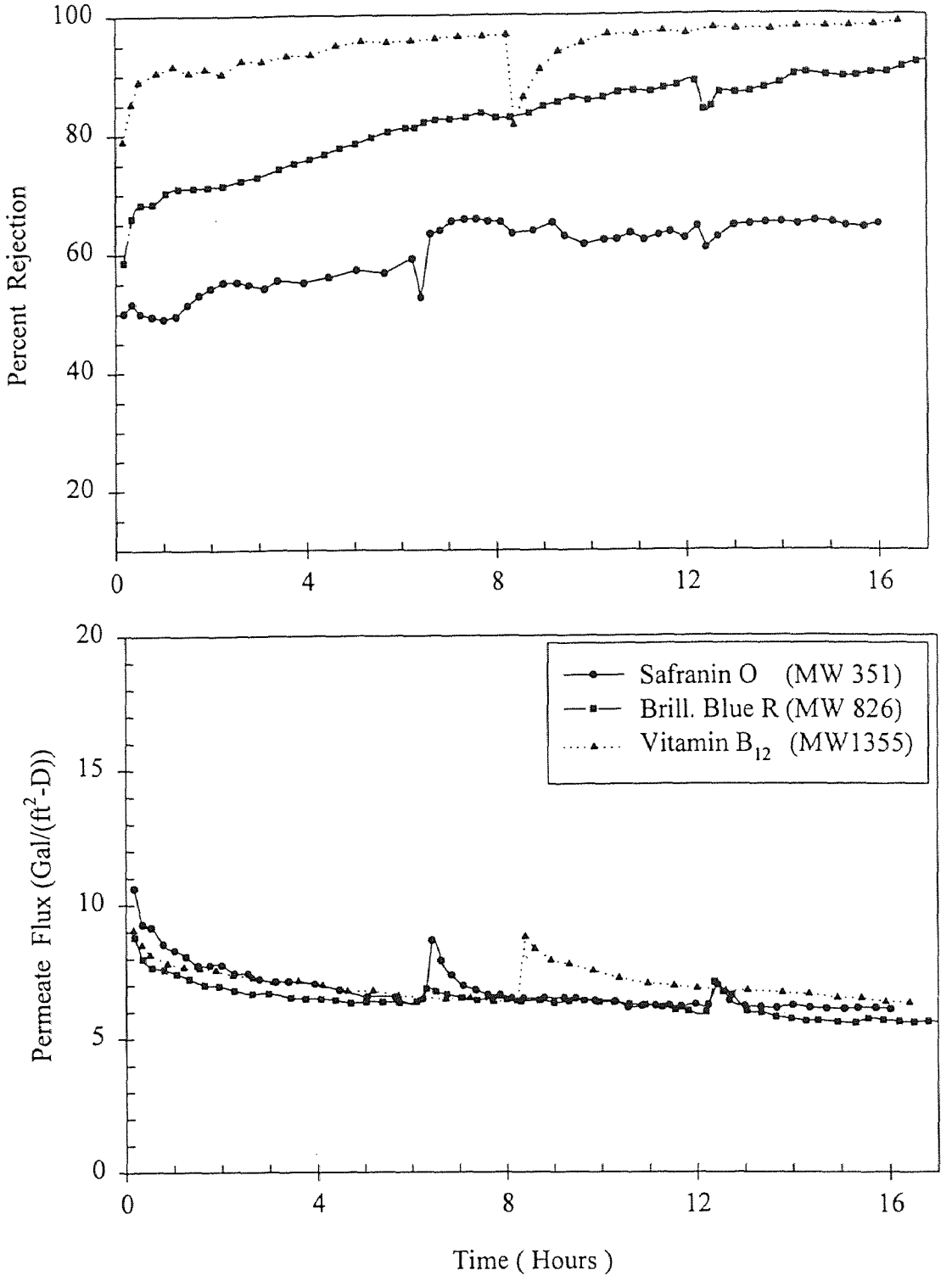

Figure 4.5 Permeate Flux and Solute Rejection of Different Solutes as a Function of Time for a MPF-44 Membrane. Conditions: Initial Conc. in the Feed = 0.01 wt% in Methanol; Applied Pressure = 440 psig; Stirring

On the other hand, the apparent permeability is lower than the permeability for pure methanol because of the frictional forces introduced with the solute that oppose the flux. Experimental results show that this reduction effect on the permeate flux was small, as long as very dilute solutions were involved.

Rejection depended strongly on the solute. Initial values of the rejection were at least 50% for safranin O and 78% for vitamin B_{12} . As the test run progressed, rejection increased slowly. Final values of the rejection showed that, at a concentration level of 0.01 wt%, safranin O was rejected in 68%, while brilliant blue R reached 95% and vitamin B_{12} was almost completely rejected, up to 99%.

Qualitatively, there was agreement between the molecular dimensions and the observed solute rejection, i.e. the larger the solute, the higher the rejection. But from the point of view of the manufacturer-specified MWCO (MWCO 250 for MPF-44), the rejection of safranin O (MW 351) was low. This anomaly can be explained through the consideration of the molecular structure of safranin O, which exhibits a partially shielded positive charge. The negatively-charged MPF-44 membrane (Levenstein et al., 1996) would interact with this ion and allow its passage through the membrane pores to a higher extent than it would for uncharged solutes of similar MW and dimensions. On the other hand, the rejection of brilliant blue R (MW 826) was lower than expected, since its MW is more than three times the manufacturer-specified MWCO and it was not rejected completely. Appendix B shows the molecular structures of the solutes used in this study along with estimated values of the molecular dimensions.

4.2.2 MPF-50 Membrane

The experimental results of the permeate flux and solute rejection as a function of time for a MPF-50 membrane are shown in Figure 4.6. This figure illustrates the case of methanol solutions of an initial concentration of 0.01 wt% of three solutes, safranin O, brilliant blue R and vitamin B_{12}, at an applied pressure of 440 psig.

As in the case for the MPF-44 membrane, the final permeate fluxes were slightly lower than those for pure methanol (Figure 4.3), but there was no significant difference when the solute was changed. Considerations related to the minimal influence of the osmotic pressure in dilute solutions on the reduction of the permeate flux were also valid here. MPF-50 is the loosest of the three membranes (largest pore size) studied and this characteristic accounts for the remarkable fluctuations in the permeate flux due to the partial reversibility of the membrane compaction and the considerable reduction observed. From Table 4.3, the ratio of the initial to the steady-state value was approximately 4.9.

With respect to the solute rejection, safranin O was not rejected at all, while the rejection of vitamin B_{12} was 89%. There is no available information of whether MPF-50 is charged or not.

4.2.3 MPF-60 Membrane

The experimental results of the permeate flux and solute rejection as a function of time using a MPF-60 membrane are shown in Figure 4.7. These results were obtained with dilute solutions (0.01 wt%) at an applied pressure of 440 psig.

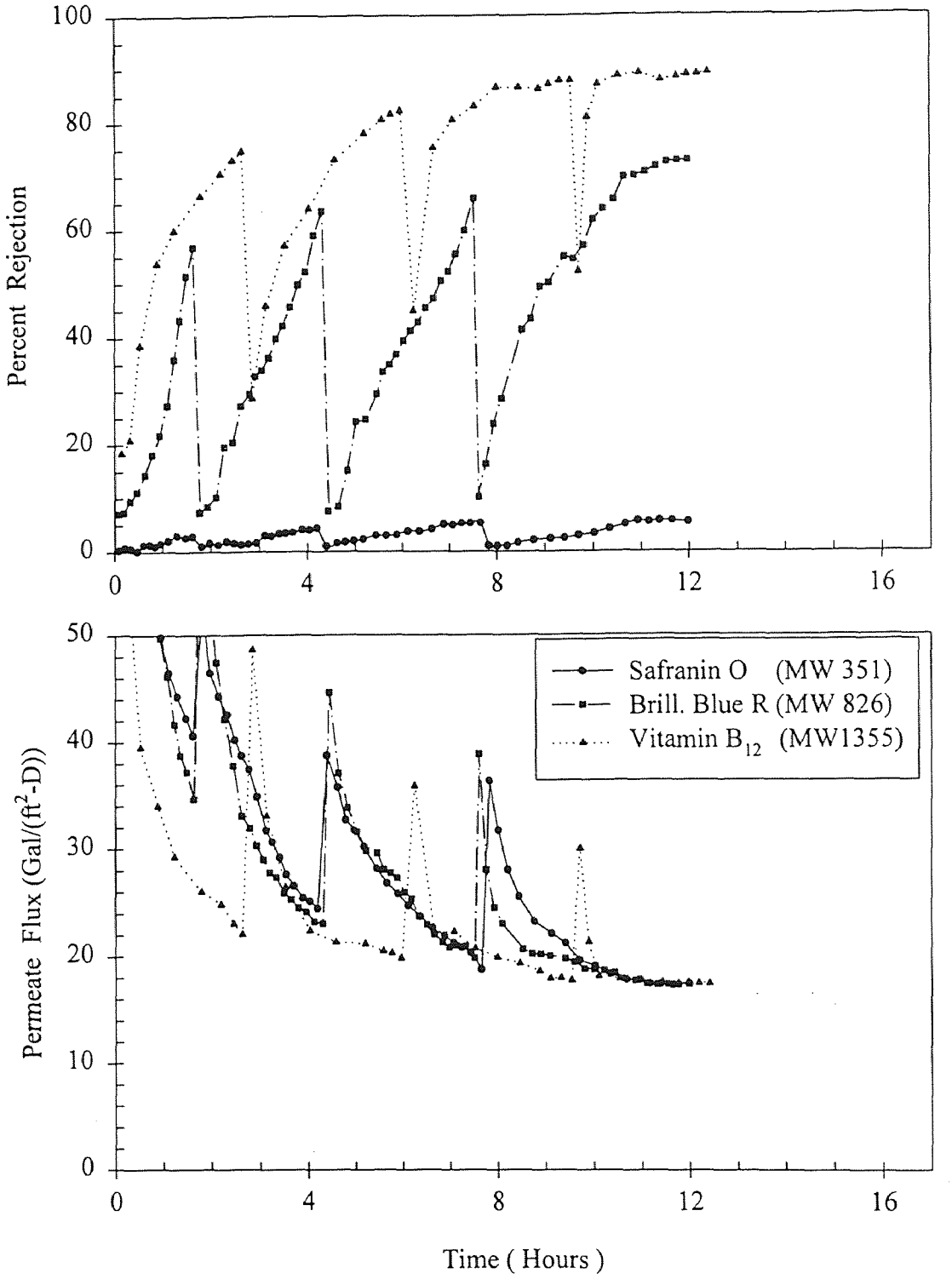

Figure 4.6 Permeate Flux and Solute Rejection of Different Solutes as a Function of Time for a MPF-50 Membrane. Conditions: Initial Conc. in the Feed = 0.01 wt% in Methanol; Applied Pressure = 440 psig; Stirring

Table 4.3 Performance of a MPF-50 Membrane for Different Solutes. Conditions: Initial Conc. in the Feed Cell = 0.01 wt % in Methanol; P = 440 psig; Stirring

Solute	Permeate flux (Gal/(ft^2-D))		% Rejection (2)
	Initial (1)	Steady-State	
Safranin O	92.49	17.60	5.6
Brilliant blue R	87.71	17.41	73.8
Vitamin B_{12}	71.93	17.50	89.0
No solute (3)	94.50	18.05	-----

Notes: (1) Initial 10 minutes of permeate collection in the first run.
(2) Steady-state values.
(3) Pure methanol.

From Table 4.4, the final permeate flux declined 1.9 times from its initial value. The final permeate flux values were between those for MPF-44 and MPF-50, and were quite similar to those previously shown for pure methanol at the same applied pressure (Figure 4.4).

The initial solute rejection achieved with MPF-60 was low, but it increased very fast as the test progressed. Final values were similar to that of MPF-44 in the cases of brilliant blue R and vitamin B_{12} . Moreover, the rejection of safranin O was somewhat higher (87% vs. 68%) even though the pore size of MPF-60 is supposed to be larger (from the MWCO information). This suggests that the sieving mechanism, based solely on steric effects, is insufficient to describe the separation of safranin O and that electrostatic effects have to be taken into account as was discussed in Section 4.2.1. Information on whether MPF-60 is charged or not is not available; experimental results suggest that either it is not charged or

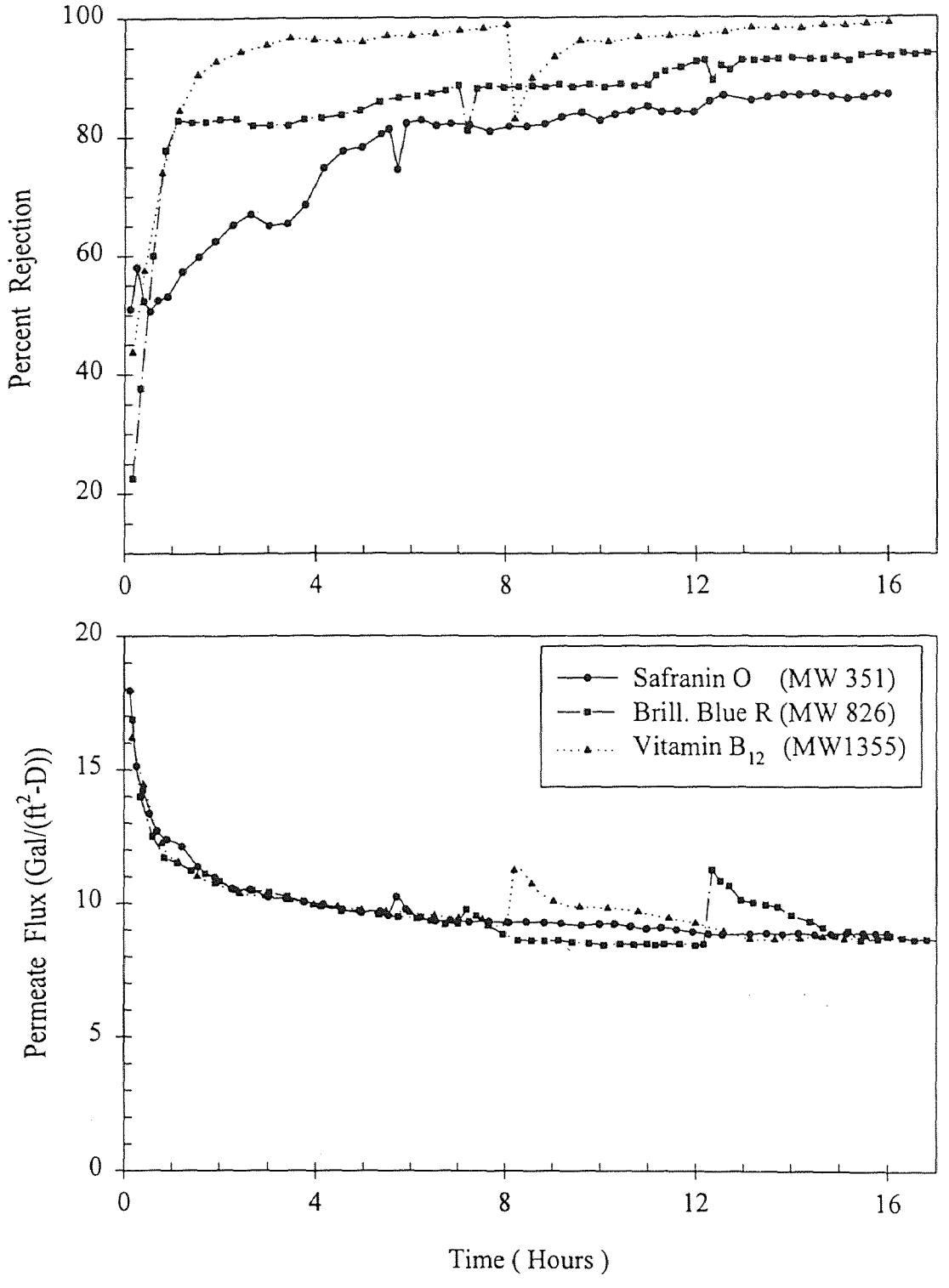

Figure 4.7 Permeate Flux and Solute Rejection of Different Solutes as a Function of Time for a MPF-60 Membrane. Conditions: Initial Conc. in the Feed = 0.01 wt% in Methanol; Applied Pressure = 440 psig; Stirring

the membrane charge density, X, of equation (2.28) is very low in comparison to that of MPF-44.

Tests with brilliant blue R were run for up to 24 hours to explore long-term effects. No significant changes were observed in the permeate flux and solute rejection, although longer tests would be necessary to confirm these results.

Table 4.4 Performance of a MPF-60 Membrane for Different Solutes. Conditions: Initial Conc. in the Feed Cell = 0.01 wt % in Methanol; P = 440 psig; Stirring

Solute	Permeate flux (Gal/(ft^2-D))		% Rejection (2)
	Initial (1)	Steady-State	
Safranin O	17.62	8.86	86.9
Brilliant blue R	15.04	8.64	93.8
Vitamin B_{12}	16.19	8.68	99.0
No solute (3)	17.11	8.70	-----

Notes: (1) Initial 10 minutes of permeate collection in the first run.
(2) Steady-state values.
(3) Pure methanol.

4.3 Permeate Flux and Solute Rejection of Concentrated Solutions of Different Solutes at the Maximum Operating Pressure

Membranes were tested using concentrated methanol solutions of about 1.0 wt% at the maximum operating pressure of 440 psig. When compared with the results for dilute solutions of Section 4.2, there was a considerable decrease in the permeate flux through all the three membranes and an increase in the solute rejection. Stirring speed was constant (about 100 rpm).

4.3.1 MPF-44 Membrane

The experimental results of the permeate flux and solute rejection as a function of time are shown in Figure 4.8 for an initial concentration of 1.0 wt% in the feed at an applied pressure of 440 psig. Two solutes, namely safranin O and brilliant blue, were tested in methanol solutions.

Permeate flux variation with time followed the trend observed for dilute solutions. Final values of the permeate flux were, however, about 60% lower (see Table 4.5). The average ratio of the initial to final values of the permeate flux was 3.1, much higher than the ratio of 1.5 for dilute solutions, suggesting that other factors in addition to the membrane compaction influenced the permeate flux reduction.

Due to build up of solute in the cell, concentrations in the feed side were in the range of 1.0 to 2.0 wt%. The effect of a higher osmotic pressure at this concentration range on the reduction of the permeate flux was estimated using Van't Hoff equation (4.1) (valid for concentrations up to 0.2 M, equivalent to a methanol solution of about 8.0 wt% of safranin O). For example, the calculated osmotic pressure of a 2.0 wt% solution of safranin O in methanol is about 16 psi. This was the maximum value of the osmotic pressure difference, $\Delta\pi_{max}$ = 16 psi, assuming that very little solute was present in the permeate. Since the difference of applied pressure across the membrane was ΔP = 440 psi, the net pressure gradient, given by $\Delta P - \Delta\pi$, was reduced in only 4%, when compared to the case of dilute solutions in Section 4.2. Using equation (2.6), osmotic pressure effects would explain only a 4% reduction of the permeate flux. Even if concentration polarization would increase $\Delta\pi_{max}$ two or three times, the permeate flux reduction is much more.

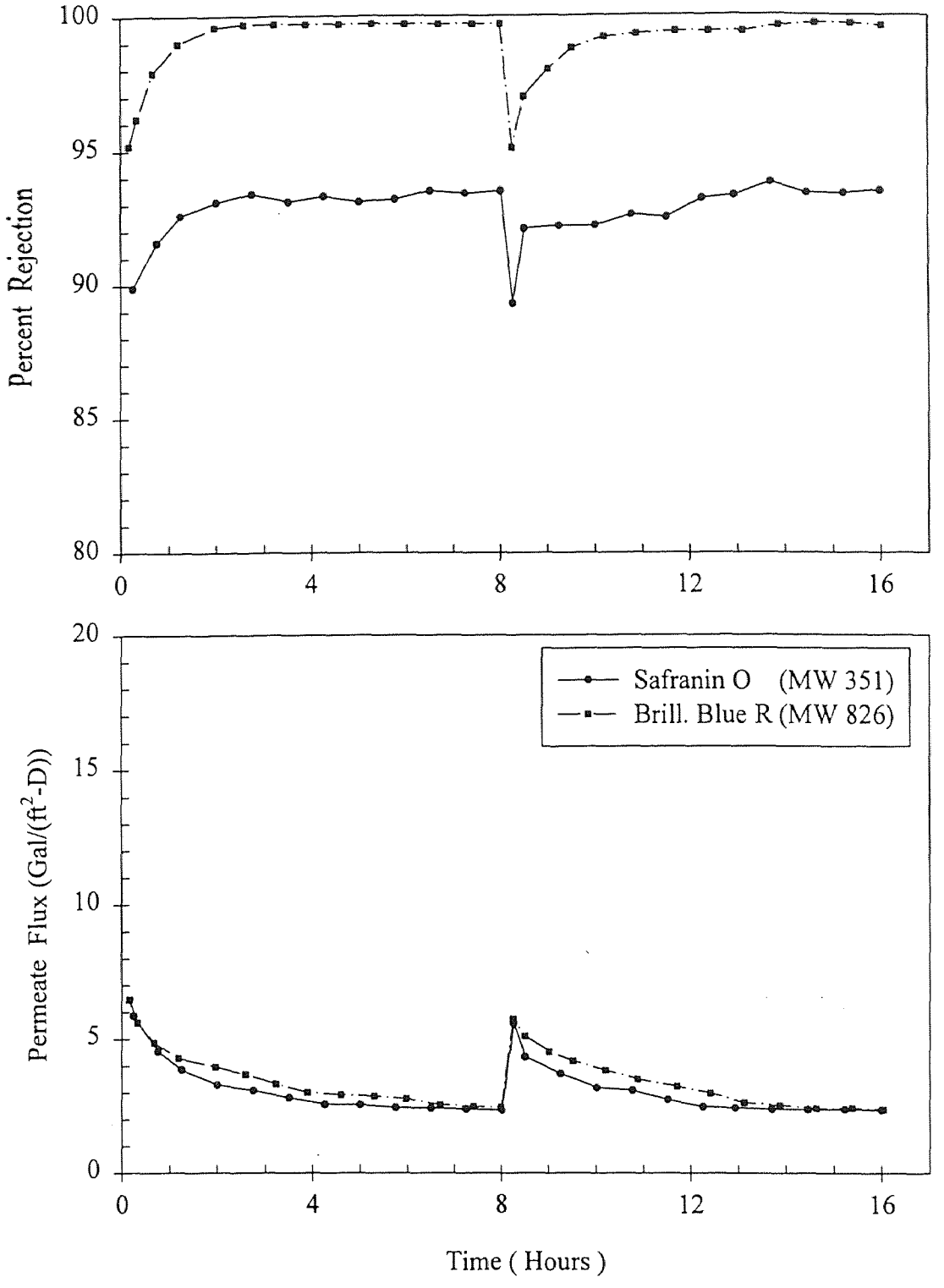

Figure 4.8 Permeate Flux and Solute Rejection of Different Solutes as a Function of Time for a MPF-44 Membrane. Conditions: Initial Conc. in the Feed = 1.0 wt% in Methanol; Applied Pressure = 440 psig; Stirring

Table 4.5 Performance of a MPF-44 Membrane for Different Solutes. Conditions: Initial Conc. in the Feed Cell = 1.0 wt % in Methanol; P = 440 psig; Stirring

Solute	Permeate flux (Gal/(ft^2-D))		% Rejection (2)
	Initial (1)	Steady-State	
Safranin O	5.87	2.38	93.5
Brilliant blue R	6.47	2.40	99.7

Notes: (1) Initial 10 minutes of permeate collection in the first run.
(2) Steady-state values.

Further explanation of the drastic reduction of the permeate flux is to be sought in the crowding effect of a concentrated solution on the active side of the membrane. It is shown in Appendix B that the solute dimensions are of the same order of magnitude as the membrane pores. Therefore, some solute molecules could block the pore openings; additionally solute molecules present/trapped inside the pores will create an extra resistance to the flow. On the other hand, the adsorption of the solute in the pores might be of considerable importance especially for safranin O; used membrane samples retain small amounts of safranin O, even after being rinsed several times with pure methanol.

Solute rejection was higher than for dilute solutions. Crowding effect and pore blocking contributed to the rejection of the membrane for a particular solute. Safranin O was rejected up to 93%, while the rejection of brilliant blue R was almost complete.

4.3.2 MPF-50 Membrane

The experimental results of the permeate flux and solute rejection as a function of time for a MPF-50 membrane are shown in Figure 4.9. The initial concentration of methanol solutions of the three solutes, safranin O, brilliant blue R and vitamin B_{12}, was 1.0 wt%. The applied pressure was 440 psig.

Permeate flux declined with time. The trend was similar to that for dilute solutions, but final values of the permeate flux were about 77% lower (see Table 4.6). Explanation for this drastic reduction can be found again in a combination of multiple factors. As in the case for MPF-44 membrane, it is estimated that the most important factor was the crowding and blocking of the pores because of the solute molecules, followed by the effect of the compaction of the membrane on the pore size. Of less importance was the influence of the osmotic pressure, as was indicated in Section 4.3.1.

With respect to the solute rejection, there was no rejection of safranin O and the rejection of brilliant blue R increased from 74% for dilute solutions to about 90%.

4.3.3 MPF-60 Membrane

Results for a MPF-60 membrane and solutions of two solutes, safranin O and brilliant blue R, are summarized in Table 4.7. Permeate flux was reduced to lower values compared to the case for dilute solutions. Final values of the permeate flux were about 64% lower and the average ratio of the initial to final values of the permeate flux was 2.9, much higher than the ratio of 1.9 for dilute solutions. Considerations discussed previously in Sections 4.3.1 and 4.3.2 to explain the reduction of the permeate flux for the other two membranes are also valid

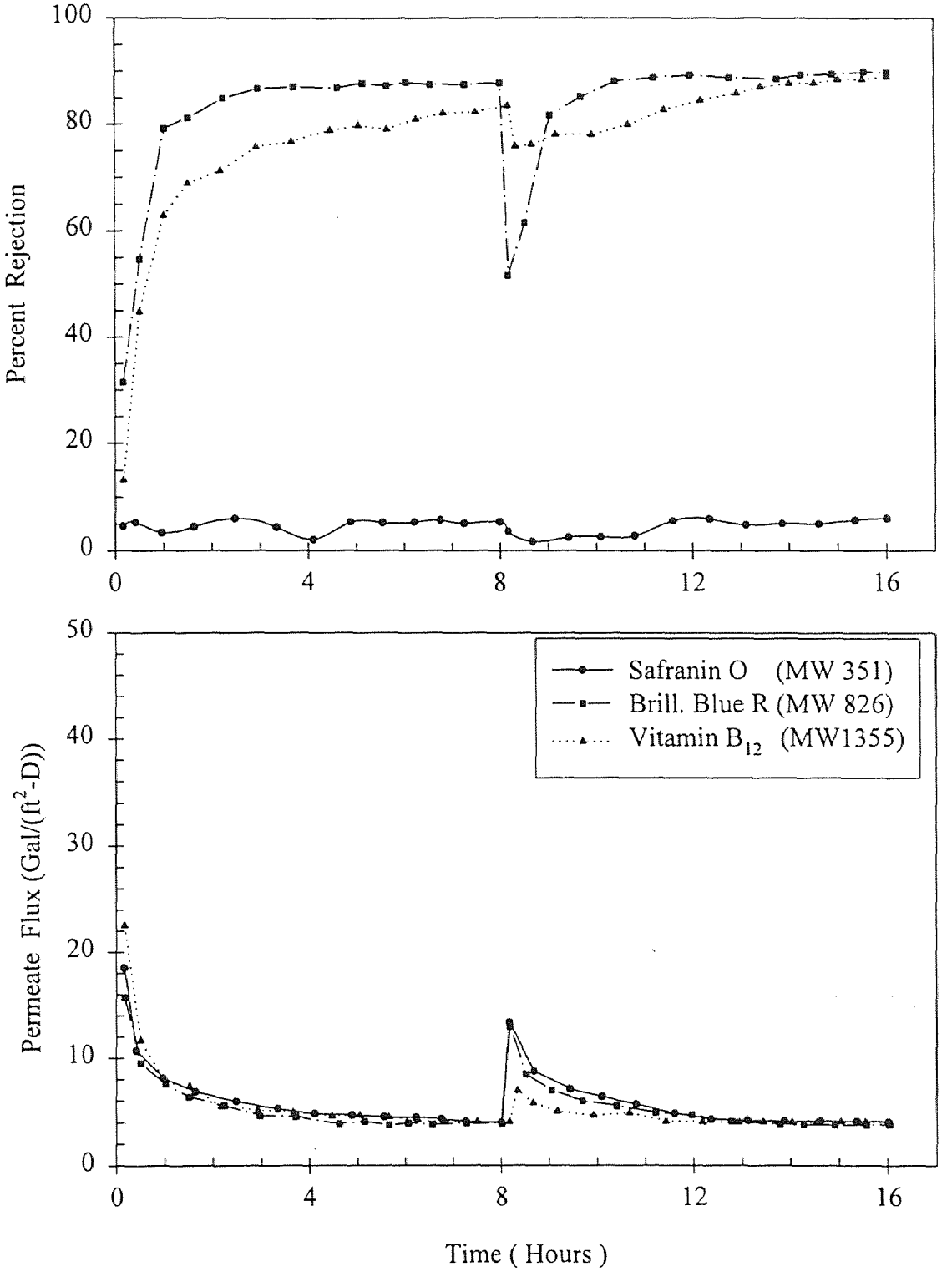

Figure 4.9 Permeate Flux and Solute Rejection of Different Solutes as a Function of Time for a MPF-50 Membrane. Conditions: Initial Conc. in the Feed = 1.0 wt% in Methanol; Applied Pressure = 440 psig; Stirring

for MPF-60 membrane. Solute rejection increase can also be explained as being due to the simultaneous crowding and blocking of the membrane pores due to the solute molecules. The variations of the performance indicators with time are shown in Figure 4.10.

Table 4.6 Performance of a MPF-50 Membrane for Different Solutes. Conditions: Initial Conc. in the Feed Cell = 1.0 wt % in Methanol; P = 440 psig; Stirring

Solute	Permeate flux (Gal/(ft^2-D))		% Rejection (2)
	Initial (1)	Steady-State	
Safranin O	18.51	4.16	6.0
Brilliant blue R	15.75	3.80	89.9
Vitamin B_{12}	22.50	4.04	88.5

Notes: (1) Initial 10 minutes of permeate collection in the first run.
(2) Steady-state values.
(3) Pure methanol.

Table 4.7 Performance of a MPF-60 Membrane for Different Solutes. Conditions: Initial Conc. in the Feed Cell = 1.0 wt % in Methanol; P = 440 psig; Stirring

Solute	Permeate flux (Gal/(ft^2-D))		% Rejection (2)
	Initial (1)	Steady-State	
Safranin O	9.30	3.28	93.7
Brilliant blue R	9.05	3.04	98.8

Notes: (1) Initial 10 minutes of permeate collection in the first run.
(2) Steady-state values.

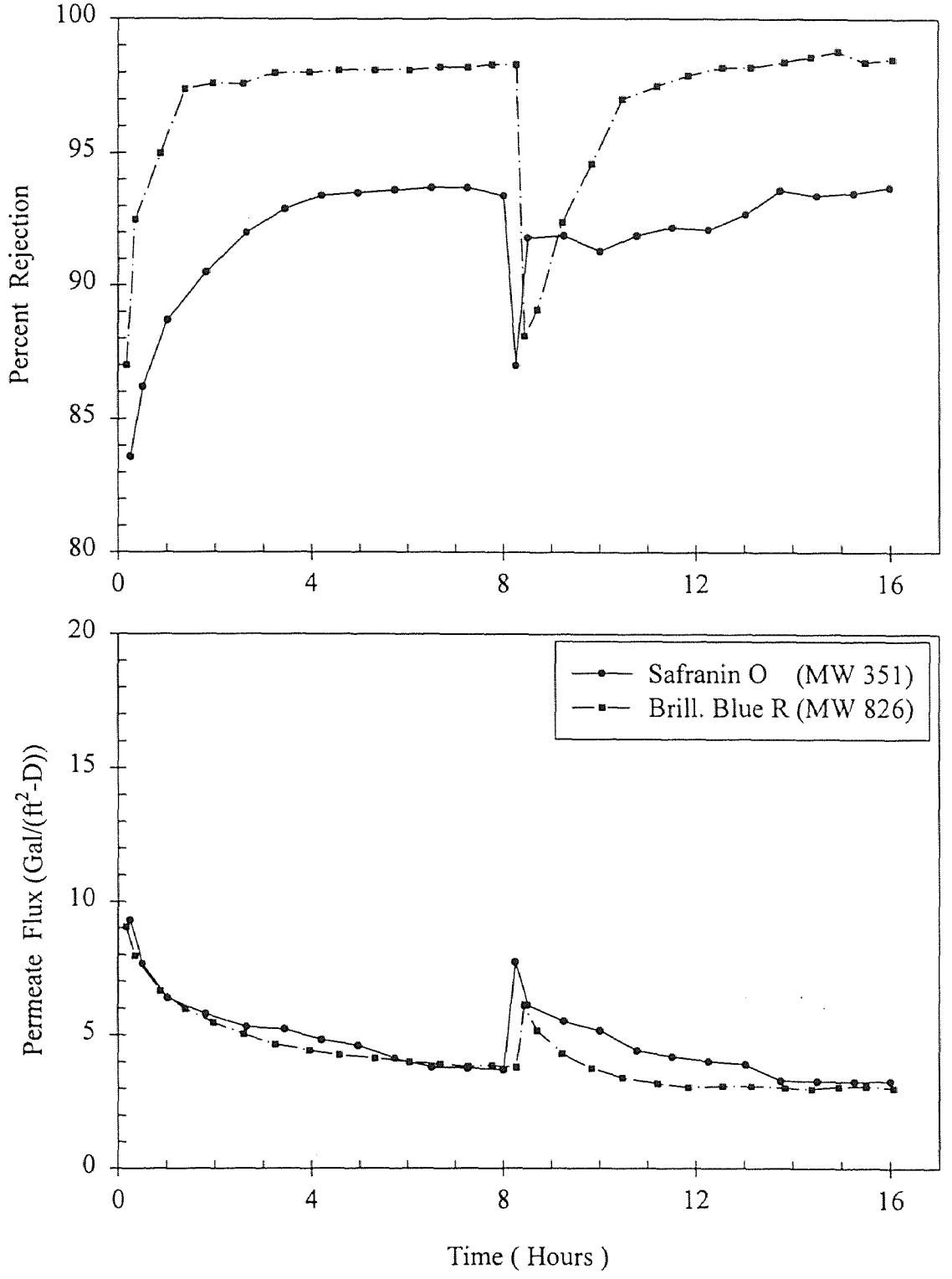

Figure 4.10 Permeate Flux and Solute Rejection of Different Solutes as a Function of Time for a MPF-60 Membrane. Conditions: Initial Conc. in the Feed = 1.0 wt% in Methanol; Applied Pressure = 440 psig; Stirring

4.4 Effect of Concentration and Stirring on Permeate Flux and Solute Rejection of Solutions of Safranin O at the Maximum Operating Pressure

The combined effect of increasing the concentration of the test solution to values higher than 1.0 wt% studied in Section 4.3, and the suppression of the stirring in the cell is briefly examined in this Section for MPF-50 and MPF-60 membranes and methanol solutions of safranin O. The initial concentration of the feed solution was 3.0 wt% and two separate membrane samples were tested with and without stirring. Stirring speed was kept constant at about 100 rpm. As expected, permeate fluxes were extremely low. On the other hand, the effects on the solute rejection depended on the membrane type.

4.4.1 MPF-50 Membrane

Figure 4.11 illustrates the variations with time of the permeate flux and solute rejection for the tests using a 3.0 wt% solution of safranin O, with and without stirring in the pressure cell. For the sake of comparison, the results previously discussed for an initial concentration in the feed of 0.01 wt% and 1.0 wt% are also presented in the same figure. Table 4.8 summarizes the results.

The final permeate flux was inversely proportional to the initial concentration in the feed. For tests with 3.0 wt%, the final values for both stirred and unstirred cases were about the same. However, in the absence of stirring, the initial permeate flux dropped significantly. For the unstirred cell, a gel-like layer was visible on the membrane upon completion of the test. The rapid decline of the permeate flux in this case would suggest that the gel started forming immediately after the test run began, offering an additional resistance to flow across the membrane.

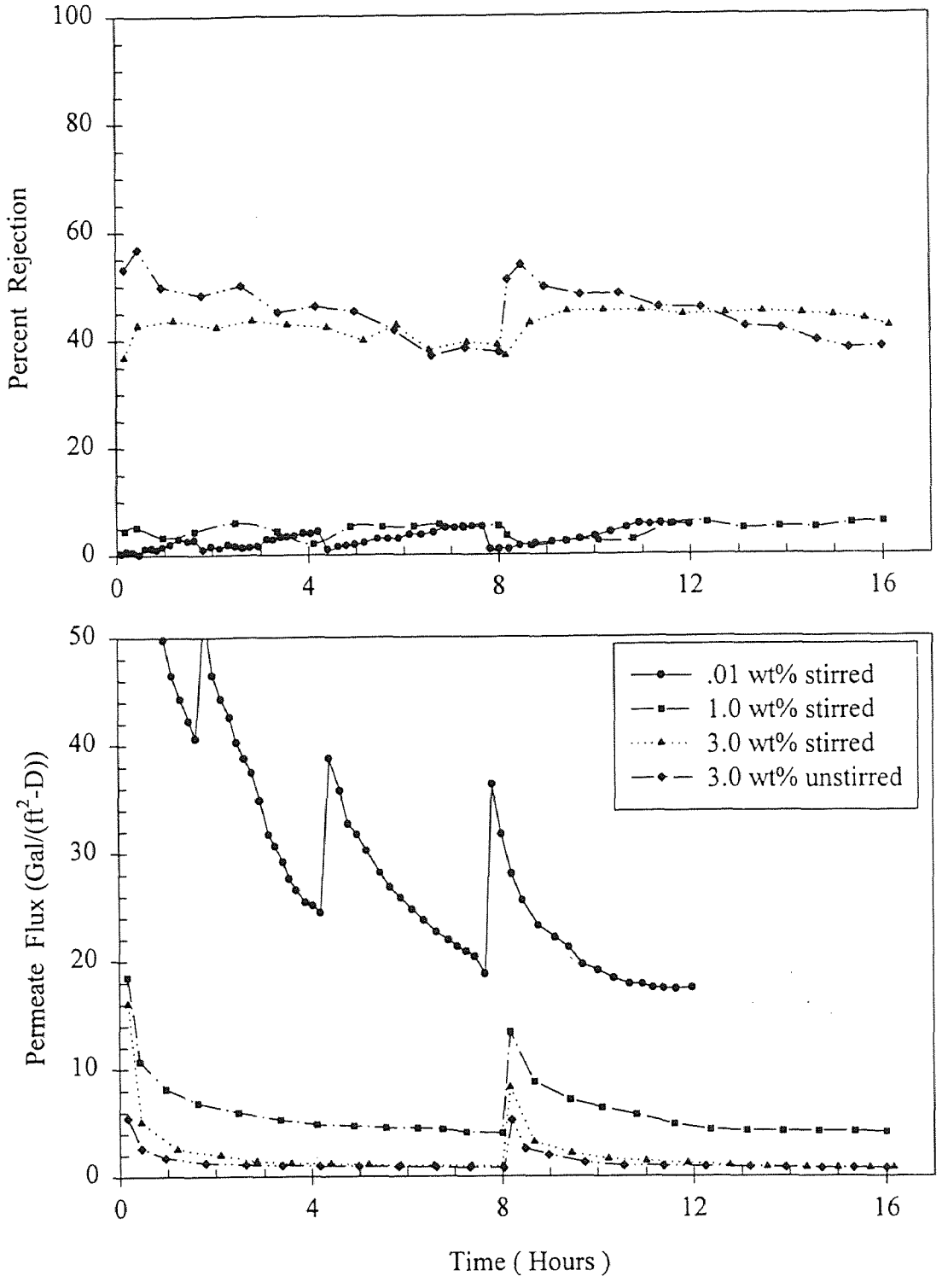

Figure 4.11 Effect of Concentration and Stirring on the Permeate Flux and Solute Rejection as a Function of Time for a MPF-50 Membrane. Conditions: Solute = Safranin O; Solvent = Methanol; Applied Pressure = 440 psig

Table 4.8 Performance of a MPF-50 Membrane for Different Initial Concentrations and Stirring Conditions: Solute = Safranin O; Solvent = Methanol; P = 440 psig

Initial Conc. Feed (wt %)	Stirring	Permeate flux (Gal/(ft^2-D))		% Rejection(2)
		Initial (1)	Steady-State	
0.01	Yes	92.49	17.60	5.6
1.0	Yes	18.51	4.16	6.0
3.0	Yes	16.05	0.79	44.9
3.0	No	5.49	0.76	53.8 (3)

Notes: (1) Initial 10 minutes of permeate collection in the first run.
(2) Steady-state values.
(3) Observed rejection reached a maximum (indicated), then decreased steadily.

The effect of the osmotic pressure was not negligible especially for the unstirred cell, although it was not as important as the combined effect of the gel formation, blocking of the pores and pore size reduction because of the compaction. Even though the average concentration in the bulk, external solution inside the cell did not change so much during the test (for practical purposes it can be assumed that it was 3.0 wt% because of the low permeate fluxes and hence, low solute fluxes involved), there were localized points on the membrane surface where the concentration was very high. Assuming an 8.0 wt% solution of safranin O in methanol immediately above the membrane surface and a typical 1.5 wt% in the permeate (an observed rejection R $\approx$ 0.5), the estimated osmotic pressure difference $\Delta\pi$ was 65 psi - 12 psi = 53 psi. This would reduce the permeate flux by about 12%.

At concentration levels of safranin O of 1.0 wt% or less, no rejection was observed with MPF-50 membrane. However, at 3.0 wt% with stirring, the final solute rejection

reached 45%. In the absence of stirring, the observed rejection reached a maximum of 54% and then it decreased steadily. These results suggest that the concentration inside the cell had exceeded a value above which the safranin O molecules would start precipitating on the membrane, blocking the pores, and contributing with an additional resistance to the reduction of solvent and solute transport.

4.4.2 MPF-60 Membrane

Figure 4.12 illustrates the variation of the experimental results with time of the tests performed with a 3.0 wt% solution of safranin O, with and without stirring in the pressure cell. Table 4.9 summarizes some of the results.

The permeate fluxes for the tests with 3.0 wt% were much lower than those for dilute solutions. As was pointed out for the MPF-50 membrane, in the absence of stirring, the initial permeate flux dropped significantly for the same initial concentration. For the unstirred cell, a gel layer was also observed on the membrane upon completion of the test. The formation of this gel would explain the low permeate fluxes observed from the beginning of the run. Considerations about the effect of the osmotic pressure are also valid for this membrane.

In comparison to more dilute feed solutions, the solute rejection was slightly lower when the initial concentration in the feed was 3.0 wt% and the cell was stirred; the final solute rejection reached 84%. In the absence of stirring, the observed rejection reached a maximum of 72% and then it decreased steadily; some precipitate was observed on the membrane surface which contributed an additional resistance leading to a further reduction of the permeate flux.

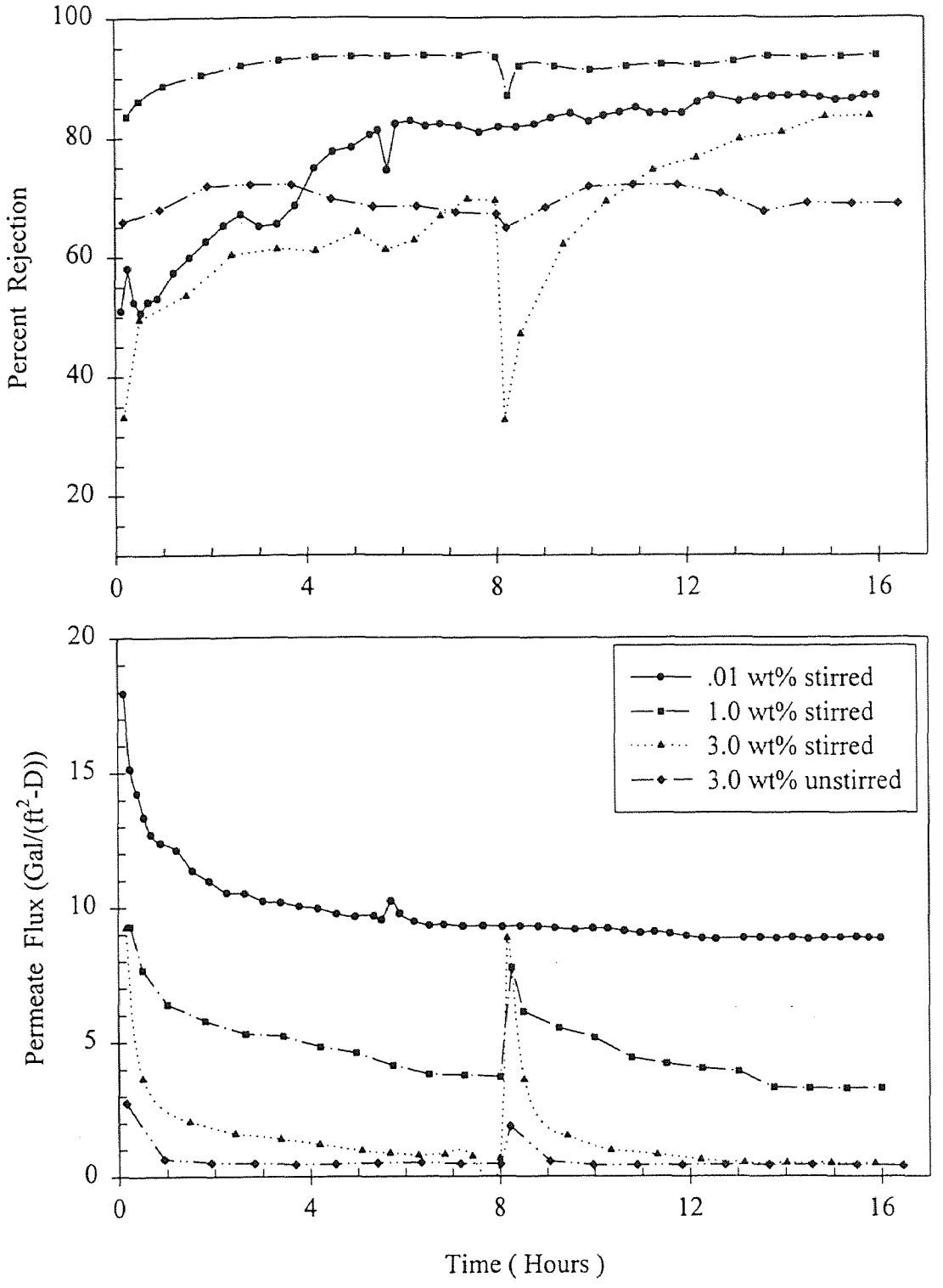

Figure 4.12 Effect of Concentration and Stirring on the Permeate Flux and Solute Rejection as a Function of Time for a MPF-60 Membrane. Conditions: Solute = Safranin O; Solvent = Methanol; Applied Pressure = 440 psig

Table 4.9 Performance of a MPF-60 Membrane for Different Initial Concentrations and Stirring Conditions: Solute = Safranin O; Solvent = Methanol; P = 440 psig

Initial Conc. Feed (wt %)	Stirring	Permeate flux (Gal/(ft^2-D))		% Rejection(2)
		Initial (1)	Steady-State	
0.01	Yes	17.62	8.86	86.9
1.0	Yes	9.30	3.28	93.7
3.0	Yes	9.24	0.48	83.5
3.0	No	2.76	0.40	72.1 (3)

Notes: (1) Initial 10 minutes of permeate collection in the first run.
(2) Steady-state values.
(3) Observed rejection reached a maximum (indicated), then decreased steadily.

4.5 Effect of Applied Pressure on the Permeate Flux and Solute Rejection of Dilute Solutions using MPF-60 Membrane

Previous sections have addressed the effect of concentration and stirring on the permeate flux and solute rejection of different membrane types at the maximum operating pressure. In this section, the effect of changing the applied pressure is explored to determine its influence on the performance of a given membrane, MPF-60, for dilute solutions of safranin O and brilliant blue R. Stirring speed was kept constant in all the tests.

The major emphasis in this section is not on the analysis of the transient performance of the membrane, but on the correlation of the final or steady-state values of the permeate flux and solute rejection with the applied pressure difference, ΔP. Final values of the permeate flux were found to be directly proportional to ΔP. Osmotic pressure differences were estimated to be negligible, $\Delta\pi \approx 0$, because of the dilute solutions involved. An

interesting feature of the results is that the plot of the final permeate flux (or permeate velocity) and the final solute rejection suggested an exponential relationship of the type encountered in the nonlinear Finely Porous Model (Merten 1966), originally proposed for RO membranes with small pores.

4.5.1 Safranin O

Table 4.10 summarizes some of the results of the permeate flux and solute rejection at four different applied pressures for a MPF-60 membrane and methanol solutions of safranin O. The initial concentration in the feed was approximately 0.01 wt%. Figure 4.13 illustrates the variations with time. It can be observed that for each operating pressure, both the permeate flux and the solute rejection reached their steady-state value after about 12 hours. These final values increased with the applied pressure.

Table 4.10 Performance of a MPF-60 Membrane for Different Applied Pressures. Conditions: Solute = Safranin O; Initial Conc. in the Feed Cell = 0.01 wt % in Methanol; Stirring

Applied pressure (psig)	Permeate flux (Gal/(ft^2-D))		% Rejection (2)
	Initial (1)	Steady-State	
440	17.62	8.86	86.9
365	13.95	7.55	74.1
295	11.68	7.10	71.9
220	9.53	5.72	45.0

Notes: (1) Initial 10 minutes of permeate collection in the first run.
(2) Steady-state values.

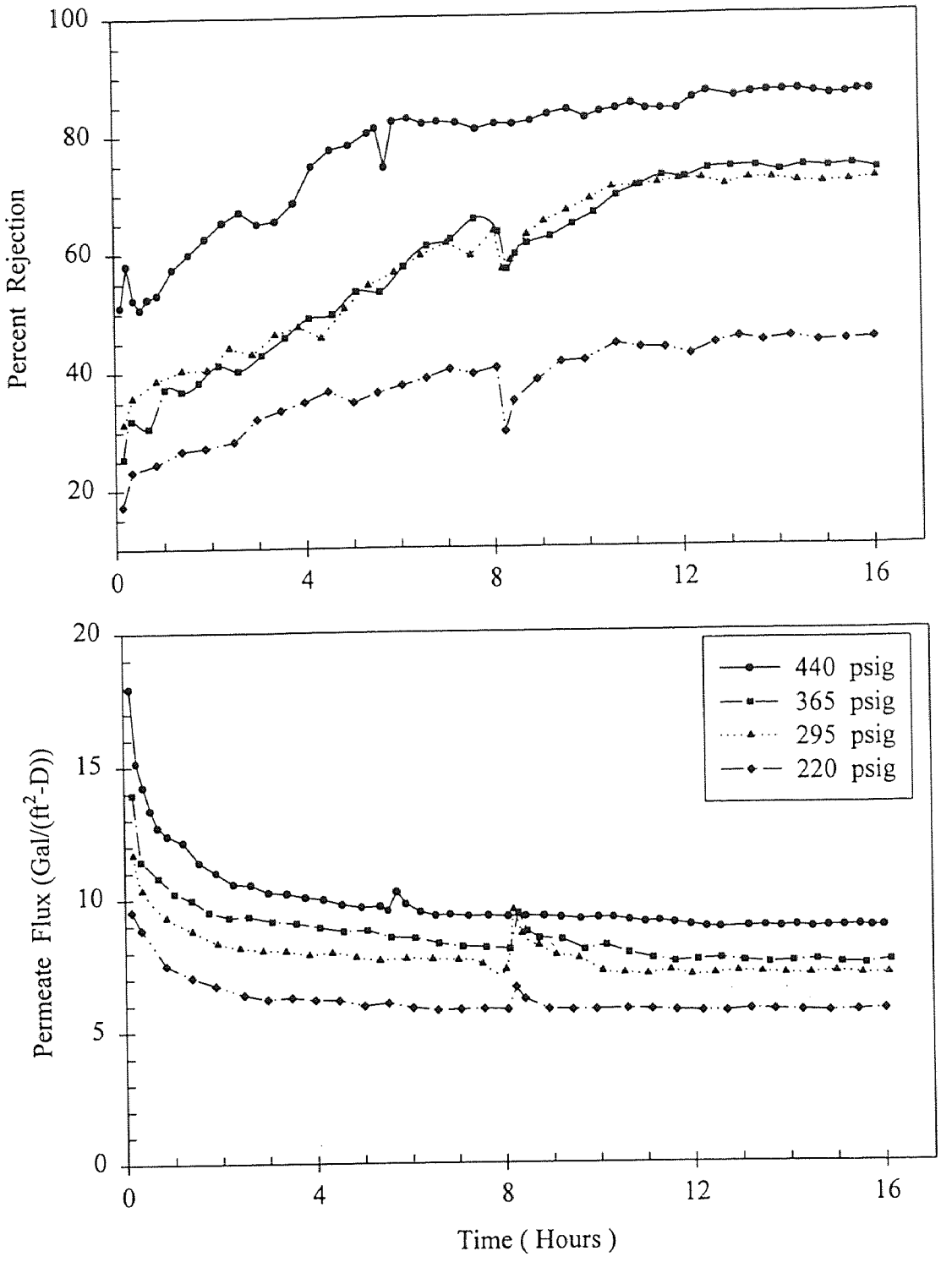

Figure 4.13 Effect of Applied Pressure on the Permeate Flux and Solute Rejection as a Function of Time for a MPF-60 Membrane. Conditions: Solute = Safranin O; Initial Conc. in the Feed = 0.01 wt % in Methanol; Stirring

4.5.2 Brilliant Blue R

A summary of the results of the permeate flux and solute rejection for a MPF-60 membrane at five different applied pressures is shown in Table 4.11. The initial concentration in the feed was 0.01 wt%. Figure 4.14 illustrates the variations with time. The steady-state values of the permeate flux and solute rejection were reached after about 12 hours and were a function of the applied pressure. Detailed calculations of the permeate flux and solute rejection for 220 psig are presented in Appendix A.

Table 4.11 Performance of a MPF-60 Membrane for Different Applied Pressures. Conditions: Solute = Brilliant Blue R; Initial Conc. in the Feed Cell = 0.01 wt % in Methanol; Stirring

Applied pressure (psig)	Permeate flux (Gal/(ft^2-D))		% Rejection (2)
	Initial (1)	Steady-State	
440	15.04	8.64	93.8
365	14.04	7.81	92.4
295	11.59	6.80	90.4
220	9.41	5.38	82.6
150	6.57	4.18	54.0

Notes: (1) Initial 10 minutes of permeate collection in the first run.
(2) Steady-state values.

4.5.3 Steady-State Values

Final or steady-state values of the performance indicators provided a rather useful insight on the application range of the membranes. The final values of the permeate flux and solute

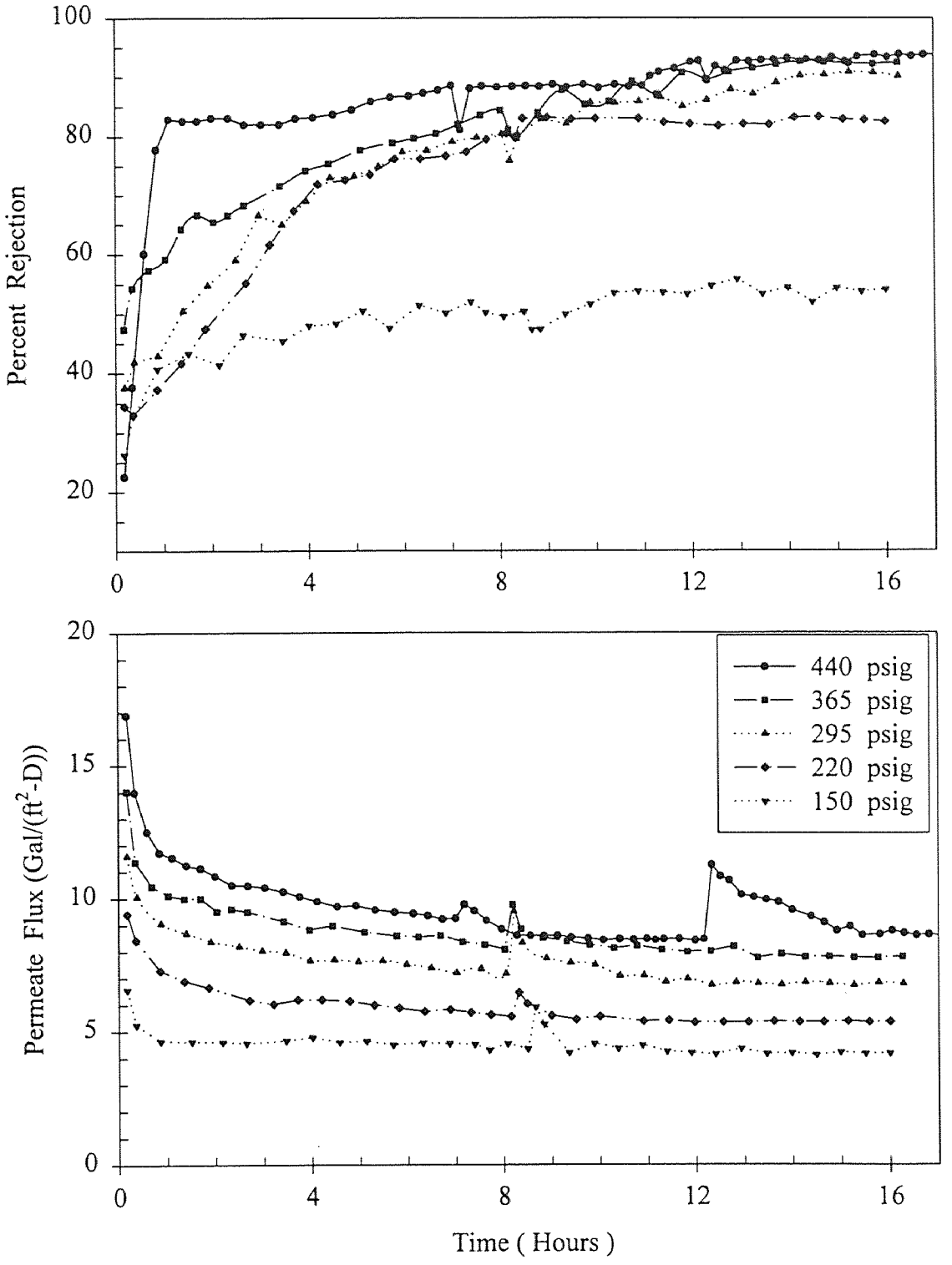

Figure 4.14 Effect of Applied Pressure on the Permeate Flux and Solute Rejection as a Function of Time for a MPF-60 Membrane. Conditions: Solute = Brilliant Blue R; Initial Conc. in the Feed = 0.01 wt % in Methanol; Stirring

fractional rejection were both found to increase with the applied pressure (as can be seen in Figure 4.15) for the cases presented in Sections 4.5.1 and 4.5.2.

The final permeate flux was found to be directly proportional to the difference of the applied pressure, ΔP. At this concentration level (0.01 wt%), an approximately linear relationship was followed by both safranin O and brilliant blue R solutions, with only minor differences. The final solute rejection and ΔP had a nonlinear relationship; at high pressures, the effect of an increment in the pressure on the solute rejection became smaller.

A plot of the final permeate flux (or permeate velocity) and the final solute rejection, in Figure 4.16, shows the strong exponential relationship between these two indicators. The applicability of the Finely Porous Model for uncharged solutes, described in section 2.2.1, was tested with the two sets of data.

Equation (2.24) can be rewritten as:

$$\left(\frac{1}{1 - R} \right) = A_1 - A_2 \, exp \left[- A_3 \, J_s \right] \tag{4.2}$$

where the lumped parameters are,

$$A_1 = \left(\frac{b \, \epsilon}{k'} \right) \tag{4.3}$$

$$A_2 = \left(\frac{b \, \epsilon - k''}{k'} \right) \tag{4.4}$$

$$A_3 = \frac{\left(\frac{\tau \, \delta}{\epsilon} \right)}{b \, D_e} \tag{4.5}$$

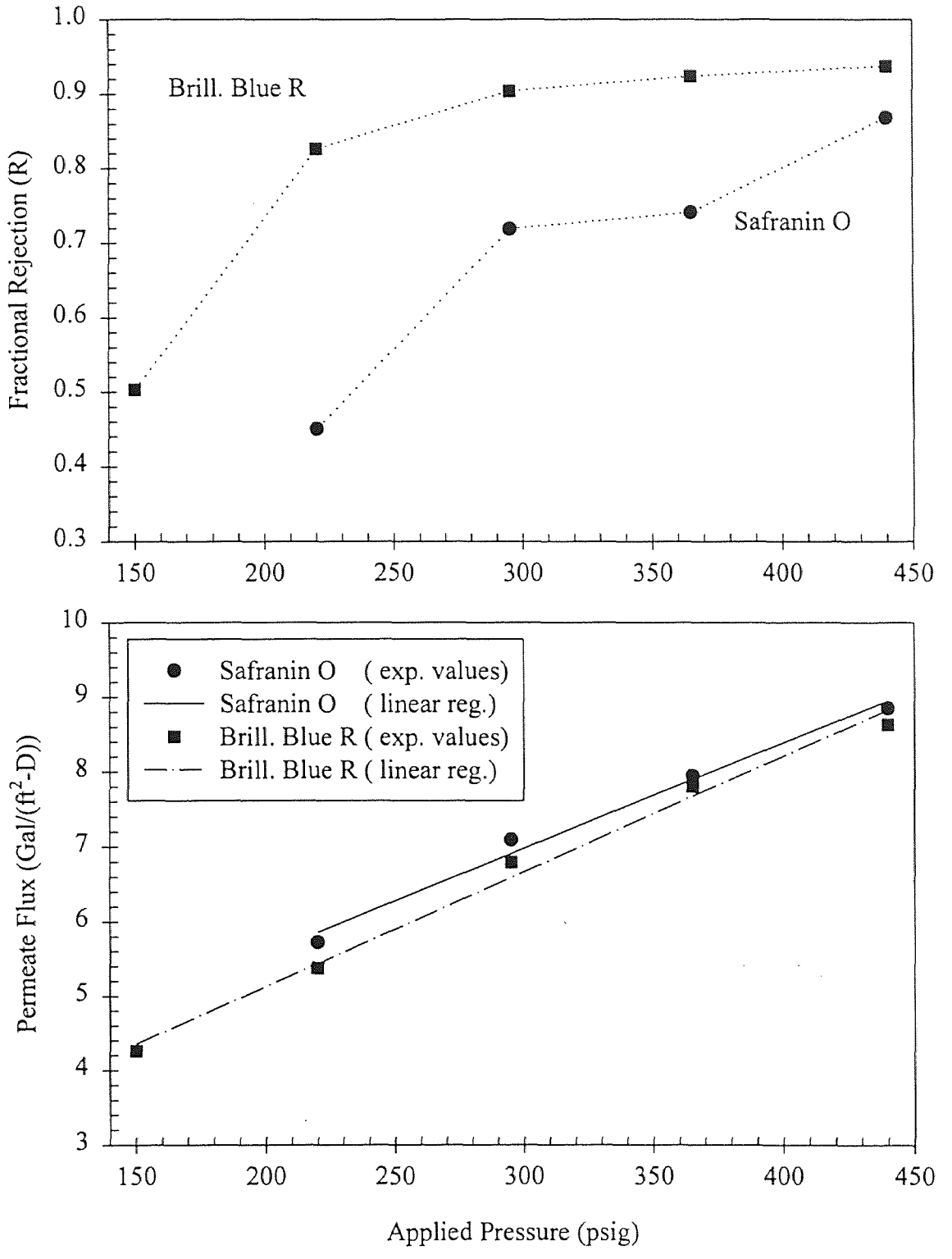

Figure 4.10 Effect of the Applied Pressure on the Ultimate Values of the Permeate Flux and Fractional Rejection for a MPF- 60 Membrane. Conditions: Initial Conc. of Solute in the Feed = 0.01 wt % in Methanol.

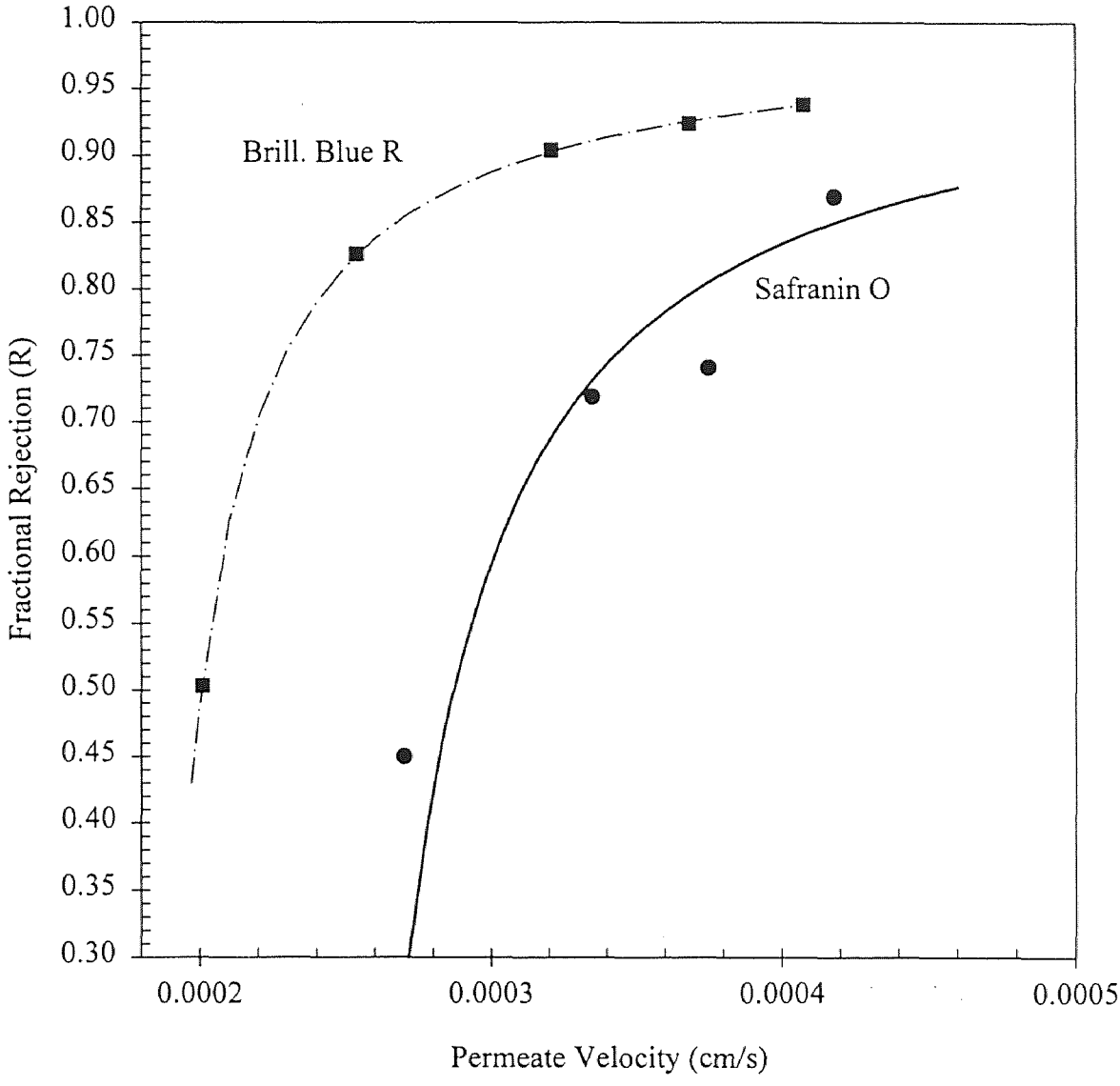

Figure 4.11 Relation between the Ultimate Values of the Fractional Rejection and the Permeate Velocity for a MPF- 60 Membrane. Conditions: Initial Conc. of Solute in the Feed = 0.01 wt % in Methanol

Experimental results of the final permeate velocity and final solute fractional rejection were correlated with equation (4.2) using the nonlinear curve fitter in SigmaPlot® 2.0 based on the Marquardt-Levenberg algorithm. Two parameter constraints were fixed $A_1 > 0$ and $A_3 > 0$. Permeate velocities were obtained from the final permeate flux data using a conversion factor of 0.4716 $\frac{\text{cm s}^{-1}}{\text{Gal ft}^{-2}\text{D}^{-1}}$. Data are provided in Tables 4.10 and 4.11. The calculated parameters A_1, A_2 and A_3 are listed in Table 4.12 and the fitted curves using the Finely Porous Model are plotted as continuous lines in Figure 4.16.

Table 4.12 Calculated Parameters of the Finely Porous Model of Equation (4.2) for MPF-60 Membrane (1) (2)

Solute	A_1	A_2	A_3
Safranin O	96.4	105.5	385.5
Brilliant blue R	160.6	173.3	444.1

Notes: (1) Initial concentration in the feed = 0.01 wt% in methanol.
(2) Final permeate velocity in cm s^{-1}.

It is worth mentioning that the calculated parameter values are preliminary, as their determination require more experimental data. Besides, the effect of the membrane charge on charged solutes was not considered here and a proper model would be needed to check the effect.

From the analysis of the absolute values of the lumped parameters, A_1 should be slightly larger than A_2 , and this was not found in either case. However, the difference between these two values was not larger than 9%.

On the other hand, the comparison of the set of parameters for safranin O and brilliant blue R gave consistent results. Since brilliant blue R is a larger molecule than safranin O (see Appendix B), the combined frictional coefficient, b, defined in equation (2.14), for a given membrane, is expected to be larger for brilliant blue R. Therefore their values of A_1 and A_2 are consistently larger. For the comparison of the value of A_3 for the two solutes, it is necessary to take into account the product bD_e. From equation (2.15) this product is simply the diffusion coefficient D for large pores, which is inversely proportional to the molecule size (Reid et al., 1977). Hence the diffusion coefficient for brilliant blue R is smaller and A_3 is consistently larger.

CHAPTER 5

MATHEMATICAL MODEL FOR A SEMIBATCH / BATCH REACTOR COUPLED EXTERNALLY WITH A NF MEMBRANE SEPARATOR

Separation potential of NF membranes is not restricted to non-reacting systems of the type studied experimentally. The benefits of coupling externally a reactor with a NF membrane separator were numerically explored during the course of this thesis and the results are presented in this chapter. The study is based on a reaction system consisting of two parallel reactions. The following aspects were of specific interest: conversion and selectivity in the production of the target compound, conversion in equilibrium-limited reactions, deleterious side reactions, concentration and separation of the target compound from other species and reduction of reaction time. A mathematical model that describes the dependence of the concentration of each species and the reaction volume on time was developed and solved numerically for a particular assumed kinetics scheme and different operating conditions.

5.1 Reaction System

The reaction system considered involves the production of a valuable product C via the following reversible reaction:

$$A + B \underset{k_{-1}}{\overset{k_1}{\rightleftharpoons}} C + D \qquad (5.1)$$

It is also assumed that the byproduct D consumes reactant A to produce an undesired product, E, via the following irreversible reaction:

$$A + D \xrightarrow{k_2} E \qquad (5.2)$$

Of the five species that form the reaction mixture described by reactions (5.1) and (5.2), three, namely A, C and E, are assumed to be large molecules with MW in the range of, say, 400 to 600, whereas species B and D are much smaller with MW of, say, 50 to 100. Species A is considered to be the limiting reactant and C is the target product. Synthesis is assumed to take place in a solvent of low molecular weight, such as methanol, in which all five species are completely soluble and miscible.

5.2 Reactor and NF Membrane Separator Arrangement

The process is assumed to take place in a unit the schematic of which is shown in Figure 5.1. A reactor vessel, provided with a jacket to control the temperature of the reaction, is initially charged with a solution of reactants A and B. The vessel is provided with connections to a drum, containing a solution of B in the same solvent, and from which the solution can be continuously fed.

A part of the reaction mass is continuously withdrawn, cooled in a heat exchanger and passed over a NF membrane separator under pressure. The membrane unit is operated in a crossflow mode, i.e., the feed flows parallel to the membrane while the permeate has a

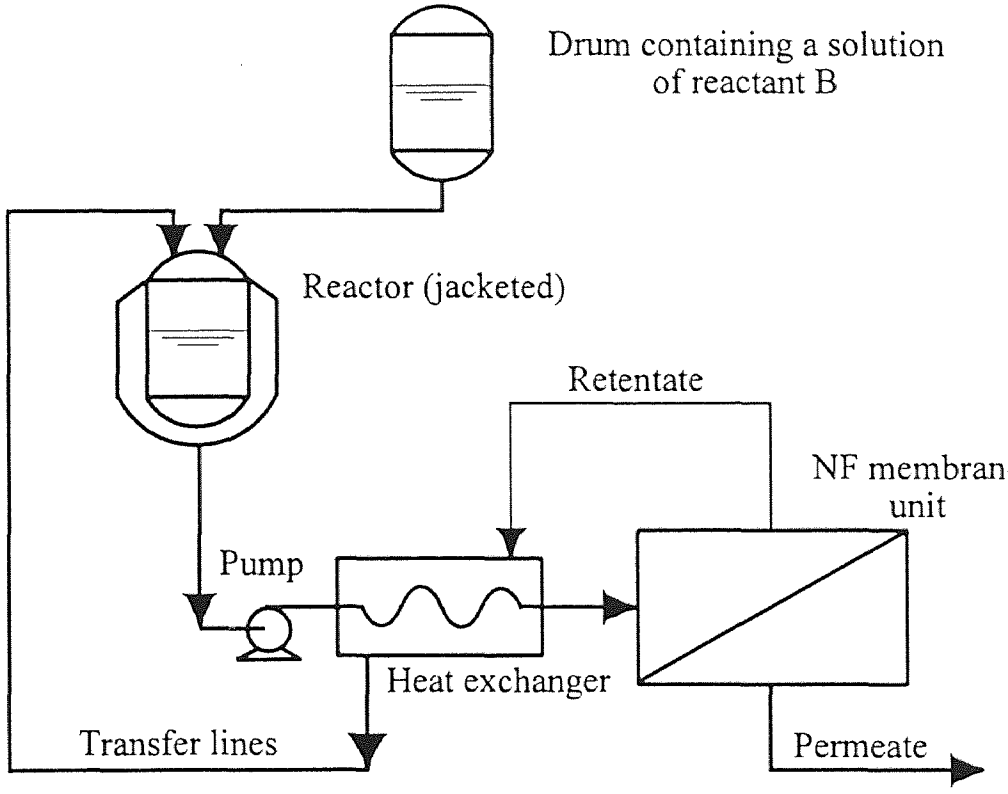

Figure 5.1 Schematic Representation of the Coupling of a Semibatch Reactor with a Nanofiltration (NF) Membrane Unit

transverse flow direction (as opposed to the dead-end operation of the experimental setup, where the whole feed is forced to pass through the membrane).

Two streams exit the membrane unit: the retentate or the concentrate, containing the species which are retained or rejected by the membrane, and the permeate, which is the portion of the feed passing through the membrane. The retentate is returned to the reactor vessel after being reheated countercurrently in the above-mentioned heat exchanger, the latter being used then for the dual purpose of cooling the stream to and heating the stream from the membrane unit. The permeate is processed in downstream separation stages.

5.3 Mathematical Model

5.3.1 Model Assumptions

The mathematical model is based on the following assumptions:

1. Reactions (5.1) and (5.2) occur only in the reactor. There is no reaction in the transfer lines, in the heat exchanger, or the NF unit, because of the low residence time and/or lower temperature.
2. The NF membrane and its properties are unaffected by either the solvent or any of the species in reactions (5.1) and (5.2).
3. The observed rejections are constant in the concentration ranges encountered in the reaction mixture.
4. The solvent flux through the NF membrane is constant, i.e. the membrane has been preconditioned (compacted).
5. The local molar flux of the solute does not vary along the membrane length.

6. Fluxes through the NF membrane are low and mixing is efficient in the unit, so that no concentration polarization occurs.
7. No fouling is assumed to occur on the membrane.
8. The density of the reaction mixture is constant.

5.3.2 Model Equations

A molar balance on any species *i* in the reaction mixture is described by the general equation:

$$\frac{dN_i}{dt} = L_i - \int_0^{A_m} J_i \, dA_m + V \sum_{j=1}^{2} \nu_{ij} \, (-r_{jA}) \tag{5.3}$$

Here, N_i is the total number of moles of species *i* in the reactor at time *t*, L_i is the rate at which species *i* is being added to the reactor, J_i is the local molar flux of removal of species *i* through the NF membrane of area A_m, V is the reaction mixture volume, ν_{ij} is the stoichiometric coefficient of species *i* vis-a-vis reaction *j* and $-r_{jA}$ is the rate of consumption of species A by reaction *j* (represented by subscripts 1 and 2, for reactions (5.1) and (5.2), respectively).

If reactions (5.1) and (5.2) are elementary, the reaction rates with respect to the limiting reactant A are the following:

$$-r_{1A} = k_1 C_A C_B - k_{-1} C_C C_D = k_1 \left[C_A C_B - \frac{1}{K_{eq}} C_C C_D \right] \tag{5.4}$$

where:

$$K_{eq} = \frac{k_1}{k_{-1}} \tag{5.6}$$

$$-r_{2A} = k_2 C_A C_D \tag{5.5}$$

and k_1, k_{-1} and k_2 are the specific reaction rate constants, K_{eq} is the thermodynamic equilibrium constant and C_i is the concentration of species i in the reaction mixture.

The assumption of constant solvent flux, J_s, along the membrane module, leads to the following local species flux expression in the membrane module:

$$J_i = J_s C_i (1 - R_i) \tag{5.7}$$

where R_i is the fractional rejection of solute i, defined as follows:

$$R_i = 1 - \frac{C_{ip}}{C_i} \tag{5.8}$$

C_{ip} is the concentration of species i in the permeate side of the NF unit (ideally one should use the reflection coefficient σ_i; however, that is generally unavailable).

Using assumption 5, the expression for J_i in (5.7) may be incorporated in the integral term of the general equation (5.3) for the flux of species i, rendering the following simplified expression for equation (5.3):

$$\frac{dN_i}{dt} = L_i - J_s A_m C_i (1 - R_i) + V \sum_{j=1}^{2} \nu_{ij} (-r_{jA}) \tag{5.9}$$

On the other hand, the reaction volume V at any time t can be determined using the following expression:

$$V = V_0 - \int_0^t J_s A_m \, dt + \int_0^t L_v \, dt \tag{5.10}$$

where V_0 is the initial reaction mixture volume and L_v is the volumetric rate of addition of solvent from the drum into the reaction vessel. If L_v is constant and since the solvent flux J_s has been assumed independent of time, equation (5.10) is changed to:

$$V = V_0 + (L_v - J_s A_m) t \tag{5.11}$$

from which it follows that:

$$\frac{dV}{dt} = L_v - J_s A_m \tag{5.12}$$

Additionally, by definition:

$$N_i = C_i V \tag{5.13}$$

and

$$L_i = L_v C_i|_{drum} \tag{5.14}$$

where L_i is the molar rate of addition of species i from the drum into the reactor and $C_i|_{drum}$ is the concentration of species i in the drum. However, since the drum contains a solution of species B only,

$$L_A = L_C = L_D = L_E = 0 \quad \text{and} \quad L_B = L_v\, C_B|_{drum} \tag{5.15}$$

Equation (5.9) for each species may now be written by introducing equations (5.4), (5.5), (5.15) and the definition (5.13).

For species A:

$$\frac{dN_A}{dt} = -J_s A_m C_A\,(1-R_A) - V\left[k_1\left(C_A C_B - \frac{1}{K_{eq}} C_C C_D\right) + k_2 C_A C_D\right] \tag{5.16}$$

which, via equation (5.13) becomes:

$$C_A \frac{dV}{dt} + V\frac{dC_A}{dt} = -J_s A_m C_A\,(1-R_A) - V\left[k_1\left(C_A C_B - \frac{1}{K_{eq}} C_C C_D\right) + k_2 C_A C_D\right] \tag{5.17}$$

The equations for species B, C, D and E are obtained in a similar manner, starting with the simplified molar balance equation (5.9).

By introducing the following dimensionless variables,

$$A = \frac{C_A}{C_{A0}}\ ;\ B = \frac{C_B}{C_{A0}}\ ;\ C = \frac{C_C}{C_{A0}}\ ;\ D = \frac{C_D}{C_{A0}}\ ;\ E = \frac{C_E}{C_{A0}} \tag{5.18}$$

$$\tau = t\, k_1\, C_{A0} \quad ; \quad v = \frac{V}{V_0} \tag{5.19}$$

and parameters:

$$\alpha = \frac{L_v\, C_B|_{drum}}{k_1\, C_{A0}^2\, V_0}\ ;\ \beta = \frac{J_s\, A_m}{k_1\, C_{A0}\, V_0}\ ;\ \gamma = \frac{C_B|_{drum}}{C_{A0}} \tag{5.20}$$

the conservation equations for the species can be written in dimensionless form as follows:

$$\frac{dA}{d\tau} = \frac{1}{v}\left[-A\,\frac{dv}{d\tau} - v\left[A\,B - \frac{1}{K_{eq}}\,C\,D + \frac{k_2}{k_1}\,A\,D \right] - \beta\,(\,1 - R_A\,)\,A \right] \quad (5.21)$$

$$\frac{dB}{d\tau} = \frac{1}{v}\left[-B\,\frac{dv}{d\tau} - v\left[A\,B - \frac{1}{K_{eq}}\,C\,D \right] + \alpha - \beta\,(\,1 - R_B\,)\,B \right] \quad (5.22)$$

$$\frac{dC}{d\tau} = \frac{1}{v}\left[-C\,\frac{dv}{d\tau} + v\left[A\,B - \frac{1}{K_{eq}}\,C\,D \right] - \beta\,(\,1 - R_C\,)\,C \right] \quad (5.23)$$

$$\frac{dD}{d\tau} = \frac{1}{v}\left[-D\,\frac{dv}{d\tau} + v\left[A\,B - \frac{1}{K_{eq}}\,C\,D - \frac{k_2}{k_1}\,A\,D \right] - \beta\,(\,1 - R_D\,)\,D \right] \quad (5.24)$$

$$\frac{dE}{d\tau} = \frac{1}{v}\left[-E\,\frac{dv}{d\tau} + v\,\frac{k_2}{k_1}\,A\,D - \beta\,(\,1 - R_E\,)\,E \right] \quad (5.25)$$

Furthermore, equation (5.12) can be written in dimensionless form as:

$$\frac{dv}{d\tau} = \frac{\alpha}{\gamma} - \beta \quad (5.26)$$

Equations (5.21) to (5.26) form a set of coupled ordinary differential equations for 6 dependent variables: A, B, C, D, E and v, where the dimensionless time τ is the independent variable.

Using the stoichiometry of the reactions, the progress of the reactions can be determined as follows. For the conversion of species A into C by reaction (5.1), x_{A1}:

$$x_{A1} = \frac{moles\ of\ \mathrm{A}\ converted\ into\ \mathrm{C}}{initial\ moles\ of\ \mathrm{A}} = \frac{moles\ of\ \mathrm{C}\ produced}{initial\ moles\ of\ \mathrm{A}} \tag{5.27}$$

where the numerator can be expressed by a simple mass balance:

$$x_{A1} = \frac{moles\ of\ \mathrm{C}\ |_{reactor} + accum.\ moles\ of\ \mathrm{C}\ |_{permeate} - initial\ moles\ of\ \mathrm{C}}{initial\ moles\ of\ \mathrm{A}} \tag{5.28}$$

or

$$x_{A1} = \frac{N_C + A_m \int_0^t J_C\, dt - \theta_C N_{Ao}}{N_{Ao}} \tag{5.29}$$

where θ_C is the ratio of the initial number of moles of species C relative to species A. The expression can be further simplified using the definitions (5.13), (5.18), (5.19) and (5.20) and assuming that θ_C is zero:

$$x_{A1} = \nu\, C + \beta\,(1 - R_C)\int_0^{\tau} C\, d\tau \qquad (5.30)$$

Under similar assumptions, the conversion of species A into E by reaction (5.2), x_{A2}, is:

$$x_{A2} = \nu\, E + \beta\,(1 - R_E)\int_0^{\tau} E\, d\tau \qquad (5.31)$$

Finally, the selectivity of the production of the target compound C, S_C, is calculated as the ratio of the conversion of A to C, to the overall conversion of A to C and E, i.e.,

$$S_C = \frac{x_{A1}}{x_{A1} + x_{A2}} \qquad (5.32)$$

5.4 Operating Conditions

The equations of the mathematical model were solved for different operating conditions, parametric values of which are given in Tables 5.1 and 5.2. The notation used to identify each operating condition consists of two letters followed by a correlative number. The first letter identifies the reactor operation mode (B = batch or S = semibatch), while the second one identifies whether the reactor is coupled to the NF membrane separator or not (C = coupled or U = uncoupled).

Table 5.1 Operation Modes Illustrated in Figures 5.2 to 5.10

Parameters	Operation Modes								
	BU - 1	SU - 2	SC - 3	SC - 4	SC - 5	SC - 6	SC - 7	SU - 8	SU - 9
k_2 / k_1	10.0	10.0	10.0	10.0	10.0	10.0	10.0	10.0	10.0
K_{eq}	4.0	4.0	4.0	4.0	4.0	4.0	4.0	4.0	4.0
α	0.0	α_0	α_0	$3\,\alpha_0$	$5\,\alpha_0$	α_0	α_0	α_0	α_0
β	0.0	0.0	β_0	$3\,\beta_0$	$5\,\beta_0$	β_0	β_0	0.0	0.0
γ	N.A.	62.5	62.5	62.5	62.5	62.5	62.5	62.5	62.5
θ_B	1.0	1.0	1.0	1.0	1.0	1.0	1.0	1.0	1.0
$\theta_C=\theta_D=\theta_E$	0.0	0.0	0.0	0.0	0.0	0.0	0.0	0.0	0.0
$R_A=R_C=R_E$	N.A.	N.A.	1.0	1.0	1.0	0.95	0.9	N.A.	N.A.
R_B	N.A.	N.A.	0.0	0.0	0.0	0.0	0.0	N.A.	N.A.
R_D	N.A.	N.A.	0.0	0.0	0.0	0.0	0.0	N.A.	N.A.
Max. v	Const.1.0	1.25	Const.1.0	Const.1.0	Const.1.0	Const.1.0	Const.1.0	1.50	No limit

BU : batch reactor uncoupled of a NF unit; SU : semi-batch reactor uncoupled of a NF unit; SC : semi-batch reactor coupled with a NF unit; N.A.: not applicable; $\alpha_0 = 1562.5$; $\beta_0 = 25$.

Table 5.2 Operation Modes Illustrated in Figures 5.11 to 5.13

Parameters	Operation Modes							
	BU-10	BC-11	BC-12	BC-13	BC-14	BC-15	BC-16	BC-17
k_2 / k_1	Negligible	Negligible	Negligible	Negligible	Negligible	Negligible	Negligible	Negligible
K_{eq}	4.0	4.0	4.0	4.0	4.0	4.0	4.0	4.0
α	0.0	0.0	0.0	0.0	0.0	0.0	0.0	0.0
β	0.0	0.0050 β_0	0.0075 β_0	0.0100 β_0	0.0100 β_0	0.0100 β_0	0.0100 β_0	0.0100 β_0
γ	N.A.	N.A.	N.A.	N.A.	N.A.	N.A.	N.A.	N.A.
θ_B	1.0	1.0	1.0	1.0	1.0	1.0	1.0	1.0
$\theta_C=\theta_D$	0.0	0.0	0.0	0.0	0.0	0.0	0.0	0.0
$R_A=R_C$	N.A.	1.0	1.0	1.0	1.0	1.0	1.0	1.0
R_B	N.A.	1.0	1.0	1.0	0.5	0.4	0.3	0.0
R_D	N.A.	0.0	0.0	0.0	0.0	0.0	0.0	0.0

BU : batch reactor uncoupled of a NF unit; BC : batch reactor coupled with a NF unit; N.A.: not applicable; $\beta_0 = 25$.

Some parameters were assumed to be constant for all operating conditions, namely K_{eq} and the initial conditions θ_i. The thermodynamic equilibrium constant for the reversible reaction was set at 4.0; this value leads to an equilibrium conversion, $x_{A1}|_{eq}$, of 0.67. The reactants A and B, at a stoichiometric ratio, are the only species initially present in the reactor.

Values for the kinetic constants for the operating conditions of Table 5.1 were k_1 = 0.00005 L mol^{-1} s^{-1} and k_2 / k_1 = 10.0. In Table 5.2, k_1 = 0.005 L mol^{-1} s^{-1} is higher and the side reaction (5.2) is negligible, so k_2 / k_1 is practically zero.

When the reactor is operated in the batch mode, L_v = 0 and hence the dimensionless parameter α = 0. Discrete values of α for a reactor operated in a semibatch mode have been assumed to be multiples of a basic value α_0 = 1562.5. The latter is a realistic value, assuming that L_v = 0.0001 L s^{-1}, $C_B|_{drum}$ = 2.5 mol L^{-1} (equivalent approximately to a 15 wt % solution of a reacting species of molecular weight of 60 daltons in methanol), V_0 = 2 L, k_1 = 0.00005 L mol^{-1} s^{-1} and C_{A0} = 0.04 mol L^{-1} (equivalent to a 2.0 wt % solution of a solute of molecular weight of 400 daltons in methanol). The variation of the value of α can be related to different rates of addition of reactant B, as long as the other terms remain constant.

Parameter β is used to measure the coupling of the reactor to a NF membrane separator. Hence, in an uncoupled reactor, β = 0. Selected values of the parameter β for a coupled reactor were assumed to be multiples (or submultiples) of a basic value β_0 = 25. This value is also realistic, assuming in addition to the values of k_1, C_{A0} and V_0 already mentioned to determine α_0, a solvent membrane flux J_s of 0.005 L (m^2 s)$^{-1}$ and a basic membrane area A_m of 0.02 m^2. The value of J_s is approximately equivalent to 10 Gal (ft^2 d)$^{-1}$, which is the

manufacturer-provided value for pure methanol flux in a solvent-stable NF membrane like MPF-60 (Kiryat Weizmann, 1996) at the maximum operating pressure of 440 psig (3.04 MPa) and 303 K.

Parameter γ was taken as a constant equal to $C_B|_{drum} / C_{A0} = 62.5$.

In general, the volume v will change whenever the reactor is operated in the semibatch mode and/or is coupled to a membrane unit. The particular case of a constant reaction mixture volume implies that the addition, from the drum into the reactor, of the solution of the reactant in excess, B, is at the same volumetric rate as the solvent permeation rate through the membrane unit. From equation (5.26), $dv / d\tau = 0$ and $\alpha / \beta|_{\text{constant volume}} = \gamma$.

5.5 Results

The results were obtained by solving numerically the set of differential equations (5.21) to (5.26) using the ODE solver in Mathematica™ 2.2. Sections 5.5.1 to 5.5.10 show the results for the operating conditions summarized in Table 5.1. The interval for the dimensionless time τ, from 0 to 0.1152, is equivalent to a 16-hour period for a value of $k_1 = 0.00005$ L mol^{-1} s^{-1} and $C_{A0} = 0.04$ mol L^{-1}. Sections 5.5.11 to 5.5.13 show the results for the operating conditions summarized in Table 5.2. In this case, the analysis is restricted to a batch operation mode and assumes that the side reaction (5.2) is negligible. The time interval for τ, from 0 to 3.60, is equivalent to a 5-hour period, considering now a value of $k_1 = 0.005$ L mol^{-1} s^{-1}, and the same C_{A0}. As a sample calculation, computer codes for the operation mode SC-6 are shown in Appendix C.

5.5.1 Effect of Membrane Area on Conversion x_{Al} for Complete Rejection of the Large Species

Figure 5.2 compares the conversion of A to the desired product C (yield, x_{Al}) as a function of the dimensionless time τ for different reactor operation modes. The comparison is based on the same initial conditions: concentrations (C_{i0}) and reaction mixture volume (V_0) are fixed, i.e. identical amounts of the limiting reactant A are involved in each case.

Curve BU-1 (see Table 5.1) represents the batch mode operation, uncoupled of the NF membrane unit, hence $\alpha = \beta = 0$. The conversion x_{Al} is observed to increase slowly due to a competitive side reaction.

Curve SU-2 shows the results for a semibatch reactor, uncoupled of the membrane unit, i.e. $\beta = 0$. Therefore, the reaction mixture volume increases as long as the solution of B is added from the drum into the reactor. A preset maximum or volume cap was fixed at 125% of the initial volume V_0, thus maximum $v = 1.25$. Afterwards, the addition of B is suspended, the volume stays constant and the reactor is operated in the batch mode. For curve SU-2, $\alpha = \alpha_0$ till the maximum volume is reached and $\alpha = 0$ for the rest of the time.

Curves SC-3 ($\alpha=\alpha_0$, $\beta=\beta_0$), SC-4 ($\alpha=3\alpha_0$, $\beta=3\beta_0$) and SC-5 ($\alpha=5\alpha_0$, $\beta=5\beta_0$) represent the semibatch mode operation coupled with the NF membrane unit at constant reaction mixture volume. Ratios α / β for the three curves are $\alpha / \beta = \alpha_0 / \beta_0 = 1562.5/25 = 62.5 = \gamma$ which is the condition stated in section 5.4 for constant volume systems. The membrane rejects the large species (A, C and E) completely and does not reject the small species (B and D). The coupling helps to prevent the dilution that accompanies the addition of the solution of B. This is done by removing the solvent along with the solutes which are

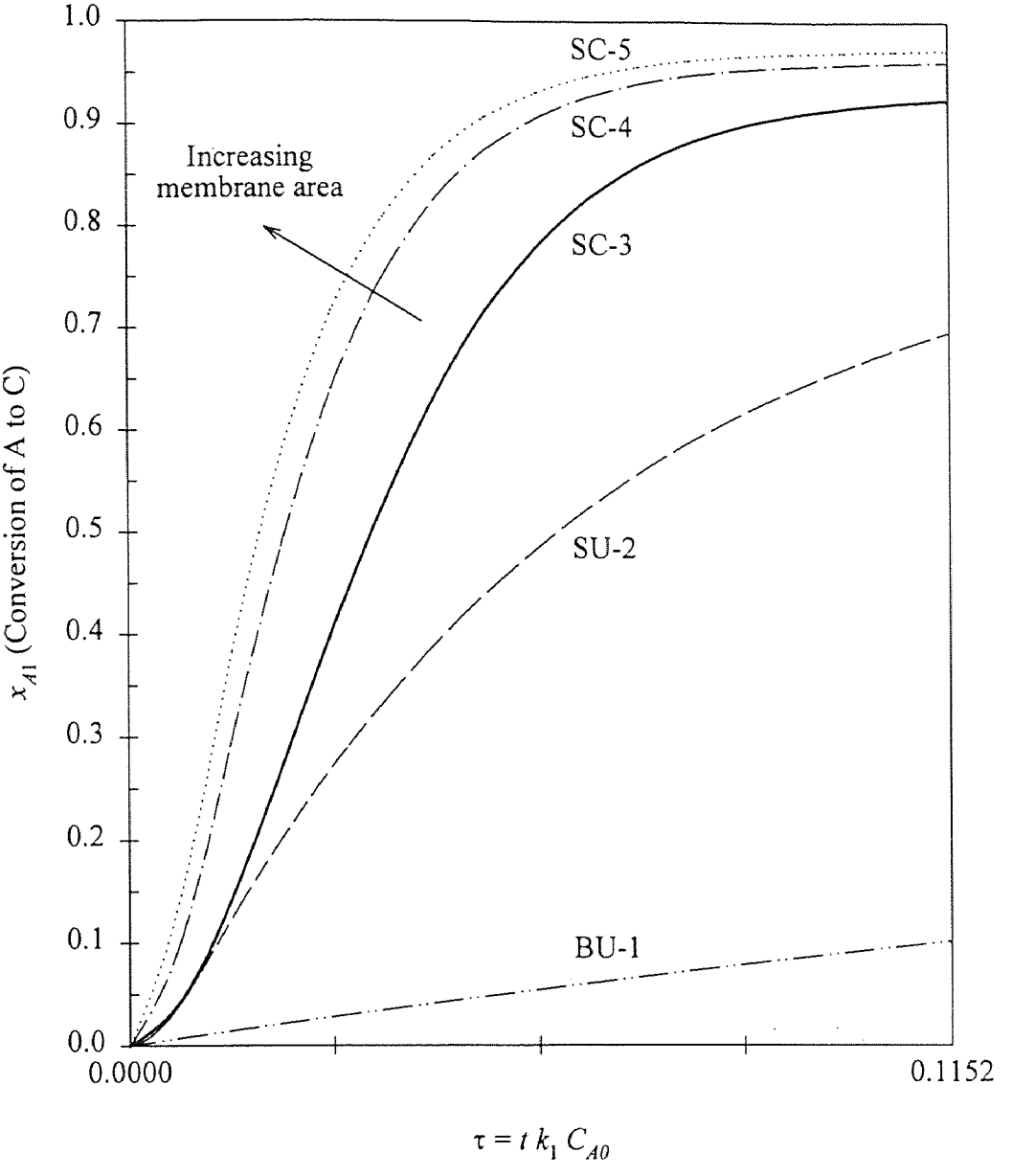

Figure 5.2 Effect of Membrane Area on Conversion x_{A1} for Complete Rejection of the Large Species

not rejected, namely B and D, through the NF membrane. It can be observed that the conversion of A to C increases rapidly over an uncoupled reactor, especially as the membrane area and hence β, increases.

5.5.2 Effect of Membrane Area on Time Required for a Given Conversion x_{Al} for Complete Rejection of the Large Species

Table 5.3 compares the values of τ for a given conversion of the target product C (x_{Al}), for the operation modes discussed in section 5.5.1.

Table 5.3 Comparison of the Time Required for a Given Conversion of the Target Product C (x_{Al}) for Complete Rejection of the Large Species

	Operation Modes				
	BU-1	SU-2	SC-3	SC-4	SC-5
$\tau \mid x_{Al} = 0.33$	0.6065	0.0353	0.0247	0.0155	0.0128
$\tau \mid x_{Al} = 0.67$	----	0.1042	0.0460	0.0302	0.0259
$\tau \mid x_{Al} = 0.90$	----	----	0.0874	0.0558	0.0487
$\tau \mid x_{Al} = 0.95$	----	----	----	0.0816	0.0670
Max. x_{Al}	0.51	0.80	0.93	0.96	0.97

Coupling a semibatch reactor with a NF unit would allow for significant reduction in the reaction time for a given conversion. For instance, the time required to achieve a conversion of 0.67 in the operation mode SU-2 (τ = 0.1042), could be reduced to less than a half of that time by coupling the reactor under the operating conditions SC-3 (τ = 0.0460), SC-4 (τ = 0.0302) or SC-5 (τ = 0.0259); the reduction effect increases as the membrane area

increases. The maximum attainable conversion simultaneously increases with the membrane area. While the maximum conversion x_{A1} in the operation mode BU-1 is only 0.51, it can increase to more than 0.9, provided the reactor is coupled to a membrane separator having sufficient membrane area.

5.5.3 Effect of Membrane Area on the Selectivity S_C for Complete Rejection of the Large Species

Figure 5.3 shows the selectivity S_C with respect to the desired product C as a function of the dimensionless time τ for the reactor operation modes discussed in section 5.5.1. Initially, the selectivity is high, S_C close to 1, since there is no species D available for the side reaction (5.2). The curves show a distinctive decreasing trend, especially when the reactor is not coupled to a NF membrane unit.

Operation of the reactor in the batch mode, represented by curve BU-1 leads to a poor selectivity for C, which becomes even lower as the reaction proceeds. In the semibatch mode, curve SU-2, selectivity is also poor, even though in this case the excess of species B which is being added to the reactor favors the forward reaction (5.1) over the reaction (5.2). However, the coupling of the semibatch reactor with a NF membrane unit, represented by curves SC-3 to SC-5, helps to prevent to a large extent the occurrence of the side reaction, since species D is removed continuously along with the solvent via the NF membrane. In these coupled operation modes, the selectivity is kept at values close to 1 and higher membrane area leads to a much better selectivity.

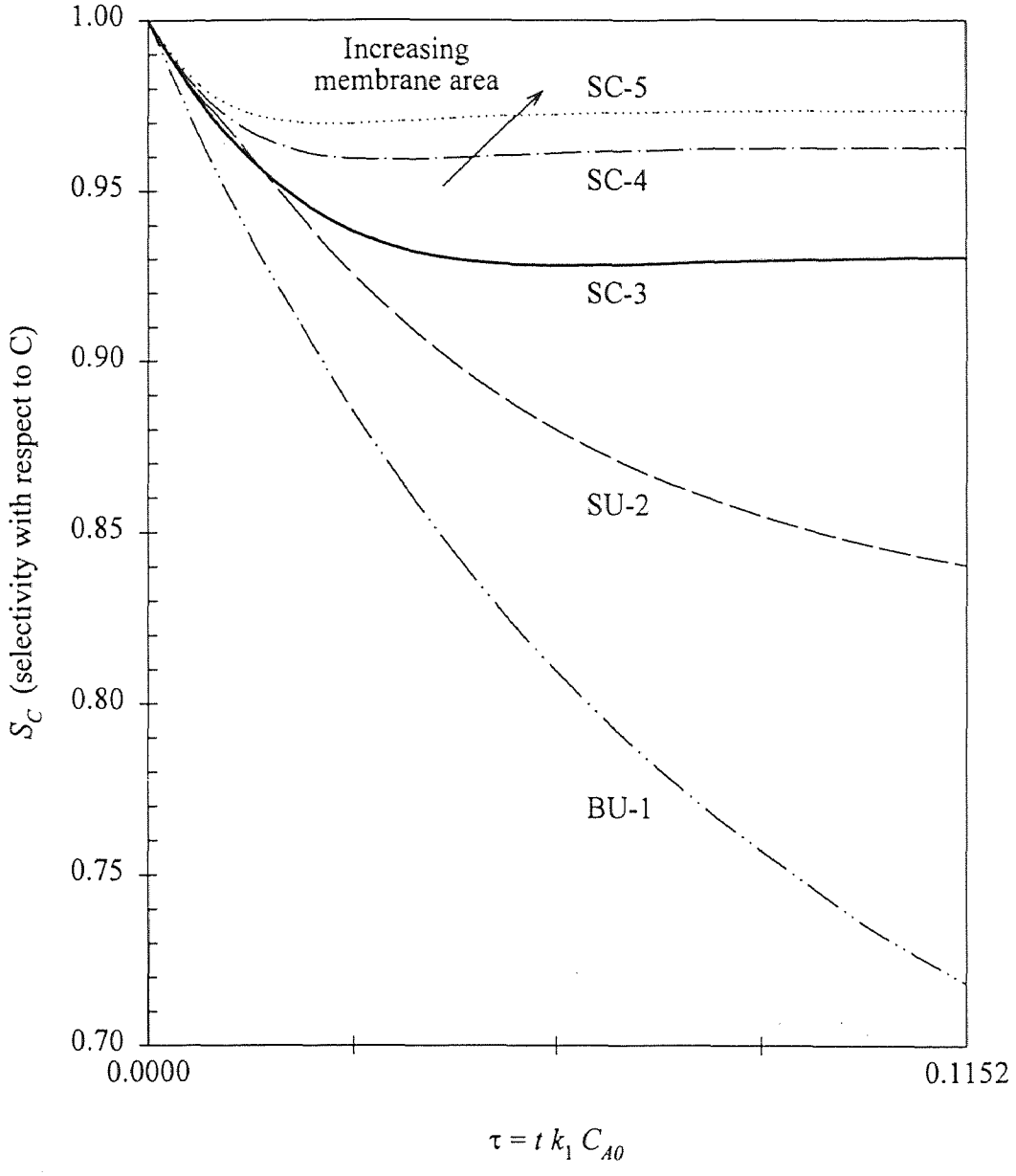

Figure 5.3 Effect of Membrane Area on the Selectivity S_C for Complete Rejection of the Large Species

5.5.4 Effect of Membrane Area on the Reactor Concentration of the Target Product, *C*, for Complete Rejection of the Large Species

Figure 5.4 shows the concentration of species C ($C = C_C / C_{A0}$) as a function of the dimensionless time τ for the operation modes discussed in section 5.5.1. This figure shows the impact of the dilution effect in a semibatch reactor, as in curve SU-2, on the concentration of the desired product C, that leads to considerable needs for downstream separation processes. This figure also indicates the higher concentrations that can be achieved by coupling the semibatch reactor with a NF membrane unit, as in curves SC-3, SC-4 and SC-5.

There are many similarities between Figures 5.2 and 5.4. In fact, the curves for the concentration C corresponding to the operation modes BU-1, SC-3, SC-4 and SC-5 are identical to those shown for the conversion x_{A1}. From expression (5.30), for a constant reaction volume ($v = 1$), $x_{A1} = C$ if one of the following conditions is valid: the reactor is not coupled ($\beta = 0$) or it is coupled but species C is completely rejected ($R_C = 1$).

5.5.5 Effect of Membrane Area on the Reactor Concentration of the Byproduct, *D*, for Complete Rejection of the Large Species

Achievement of a high concentration of C is not the only effect of the reactor-NF membrane unit coupling. This arrangement allows simultaneously for the removal of the byproduct D, the presence of which is deleterious to the reacting system considered and defined by equations (5.1) and (5.2). Figure 5.5 shows the concentration of species D ($D = C_D / C_{A0}$) as a function of the dimensionless time τ for the operation modes discussed in section 5.5.1. In the operation mode BU-1, the concentration is low commensurate with the low conversion

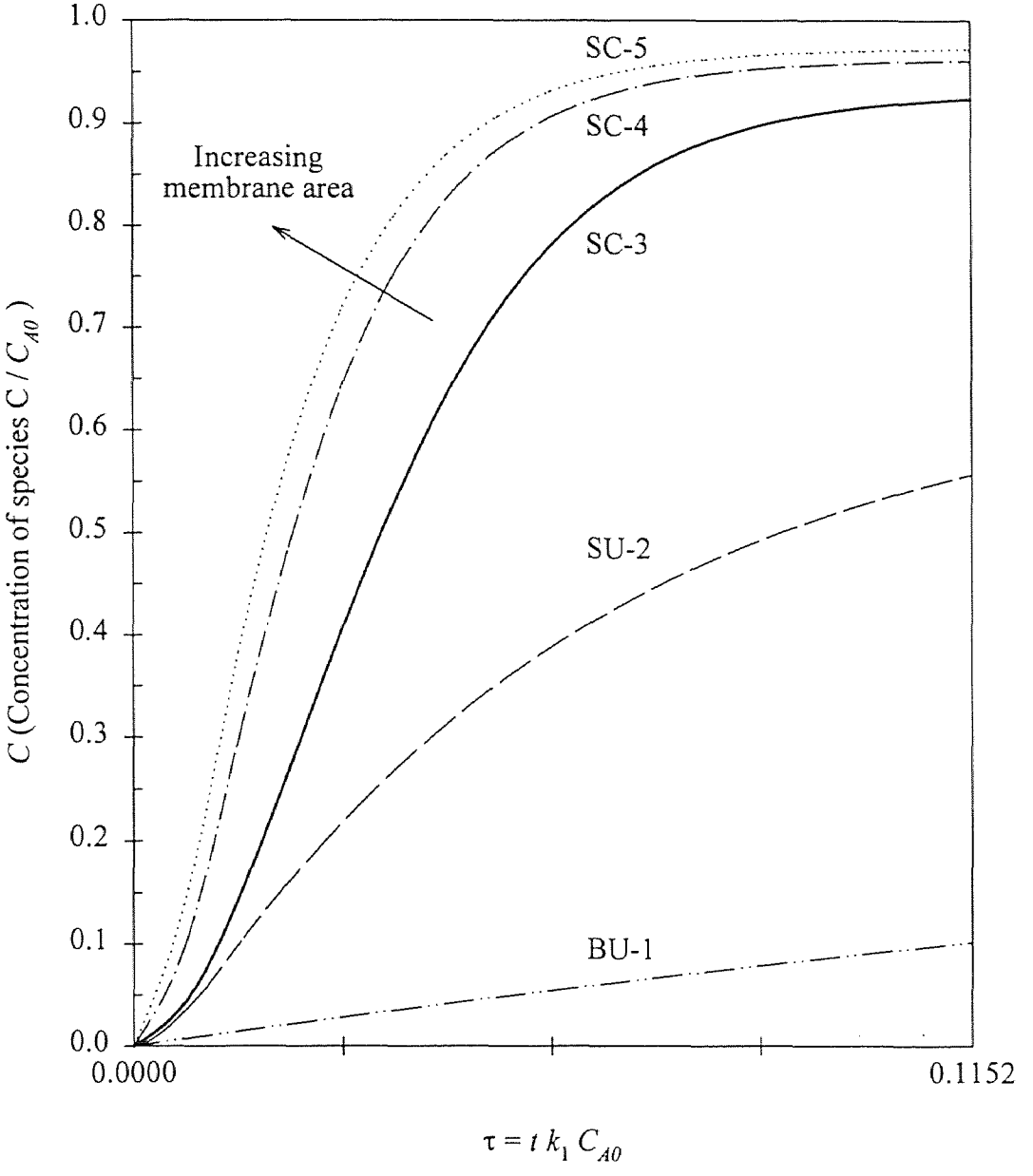

Figure 5.4 Effect of Membrane Area on the Reactor Concentration of the Target Product, *C*, for Complete Rejection of the Large Species

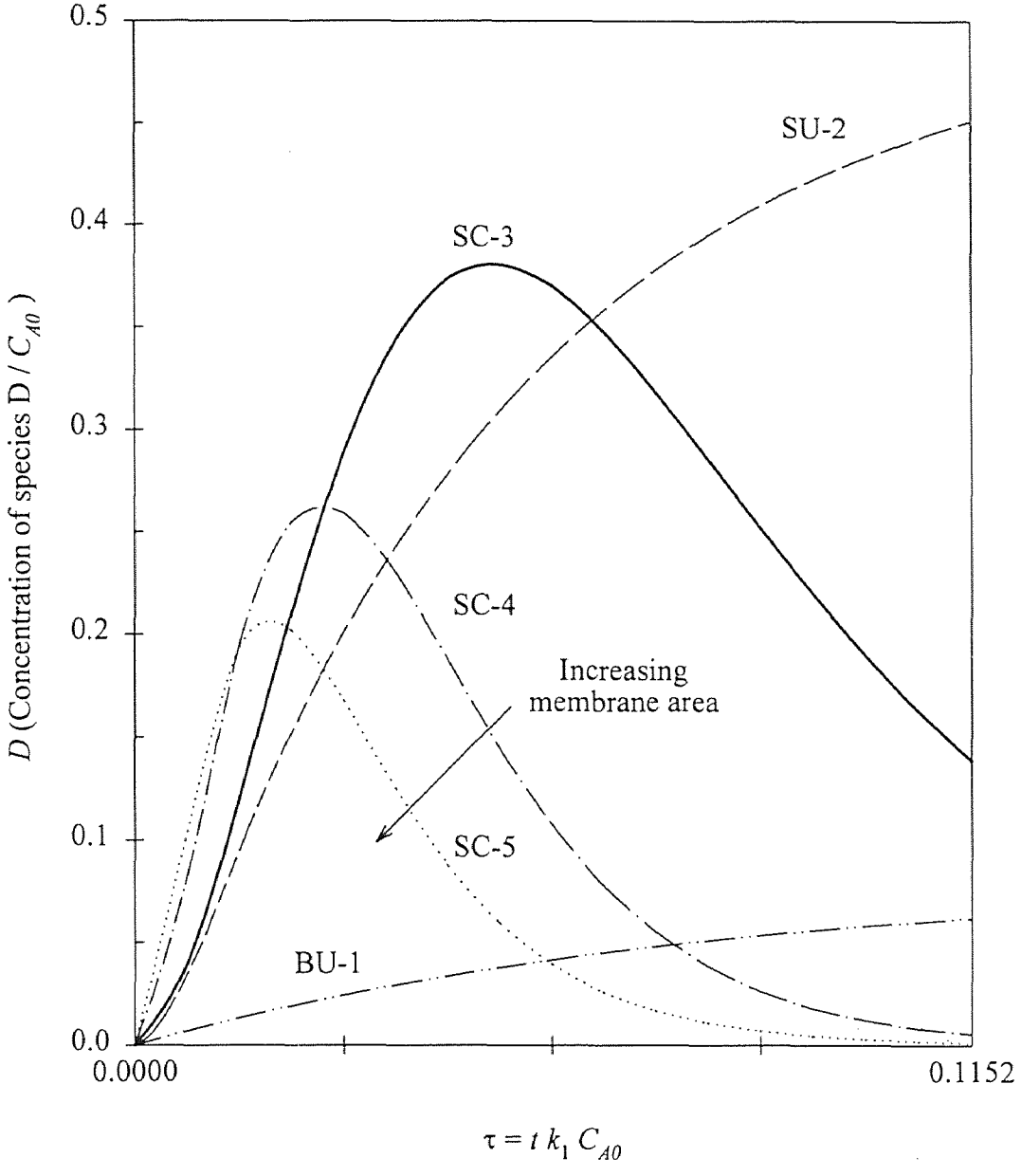

Figure 5.5 Effect of Membrane Area on the Reactor Concentration of the Byproduct, *D*, for Complete Rejection of the Large Species

of the limiting reactant A. In the uncoupled semibatch mode, SU-2, the concentration of D increases with time and leads to low values of the selectivity S_C as was discussed in section 5.5.3. Curves SC-3, SC-4 and SC-5 go through a maximum as reaction proceeds and each has therefore two well-defined zones. Initially, the curve slopes are positive, meaning that the net rate of production of D (from reactions (5.1) and (5.2)) is higher than the rate of removal through the membrane and consequently, D accumulates till a maximum is reached where the rates are equal. Thereafter, the rate of removal is higher and the reaction mixture can be made, for practical purposes, free from D as long as sufficient membrane area is provided and solubility limits are not exceeded. This fact is particularly useful for the planning of downstream separation processes.

5.5.6 Effect of Imperfect Rejection of the Large Species on the Conversion x_{Al}

In Figures 5.2 to 5.5, it was assumed that the large species were completely rejected in the membrane unit. While this is highly desirable, commercial membranes available at this time (Chapter 4) often do not exhibit such a perfect retention. In order to assess the effect of imperfect rejection of the large species on the performance of the reaction, two operation modes were considered, namely SC-6 and SC-7, having a solute retention of 0.95 and 0.90, respectively. All large species were considered to have the same solute retention, whereas the small species were not rejected at all. Figure 5.6 compares the conversion x_{Al} under the operation modes SC-6 and SC-7 with the conversions that would have been attained with the same membrane area, assuming full solute rejection, namely SC-3. Conversion curves for the operation modes BU-1 and SU-2 complete the figure.

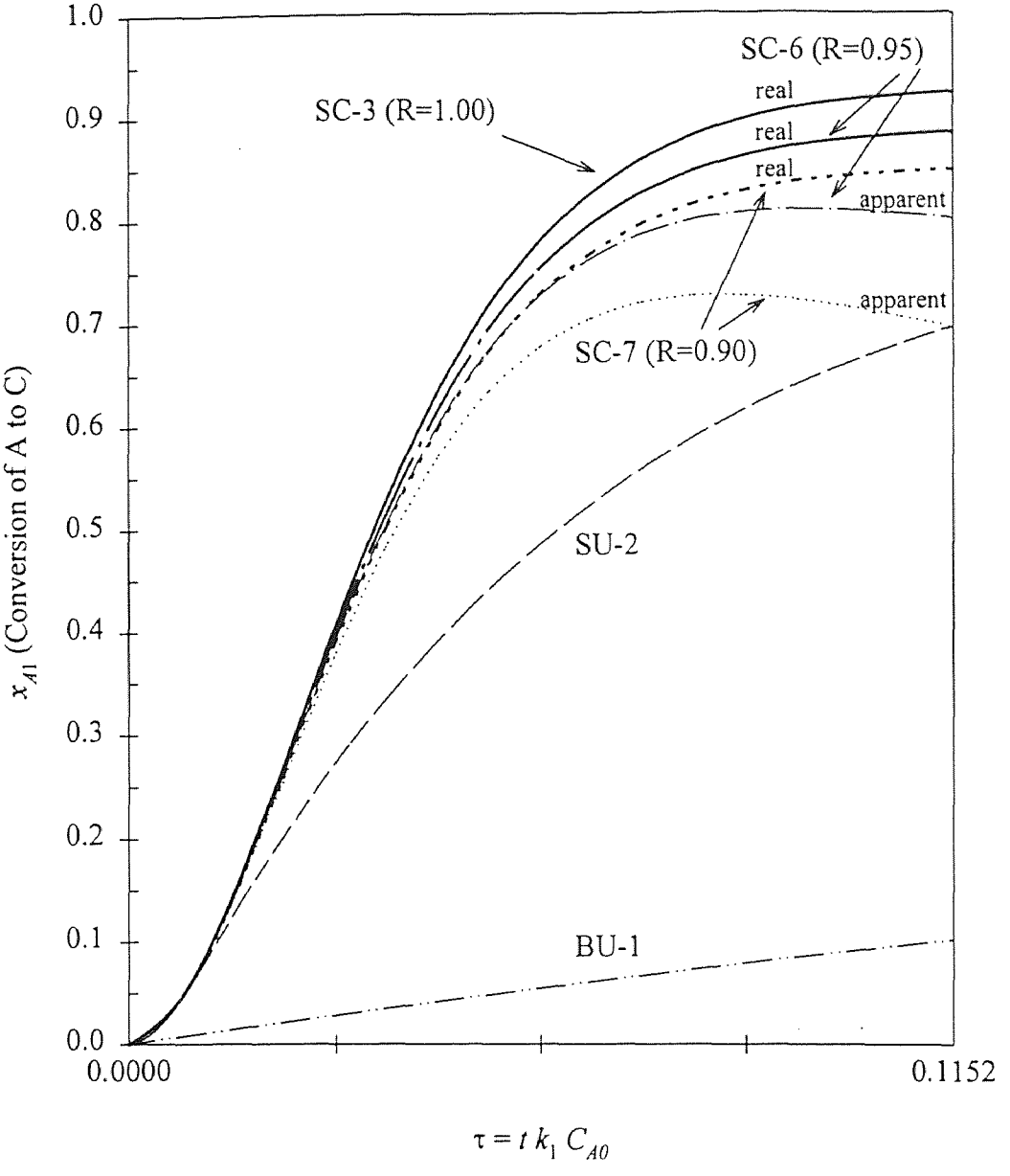

Figure 5.6 Effect of Imperfect Rejection of the Large Species on the Conversion x_{A1}. Comparison of Real Conversion Values with Apparent Values (Calculated with Reactor Concentrations)

Expression (5.30) used to calculate x_{A1} has two terms. The first term is a function of the number of moles of C present in the reactor at any time τ and represents the amount of C that is available in the reaction mixture. The second term is a function of the accumulated number of moles of C that have left in the permeate from $\tau = 0$ to $\tau = \tau$ and its availability will depend on its subsequent recovery from this stream. In Figure 5.6, the "real" conversion is calculated with the expression (5.30) and represents the maximum conversion that could be attained with a membrane of a given solute rejection, if 100% of the moles of C present in the permeate is recovered. In practical terms, this "real" conversion is the limiting value, although it may not be economical because of the capital costs involved in multistep recovery of the species C in the permeate. For this reason, additional curves with "apparent" values of the conversion, calculated using the concentrations in the reactor, have been plotted. As expected, for the same membrane area, the higher the fractional rejection, the higher the conversion x_{A1}. At the end of the time span shown, operation modes SU-2 and SC-7 (R=0.90) give about the same conversion in the reactor, but it would be advantageous, from the conversion point of view, to operate in the uncoupled mode for longer times.

5.5.7 Effect of Imperfect Rejection of the Large Species on the Selectivity S_C

Advantages of coupling the reactor with a membrane separator might not be so evident with imperfect rejection of the large species when the conversion x_{A1} is only examined. Figure 5.7 shows the results for the selectivity S_C for the same operation modes discussed in section 5.5.6. It is observed that, for a given membrane area, the selectivity is not very sensitive to

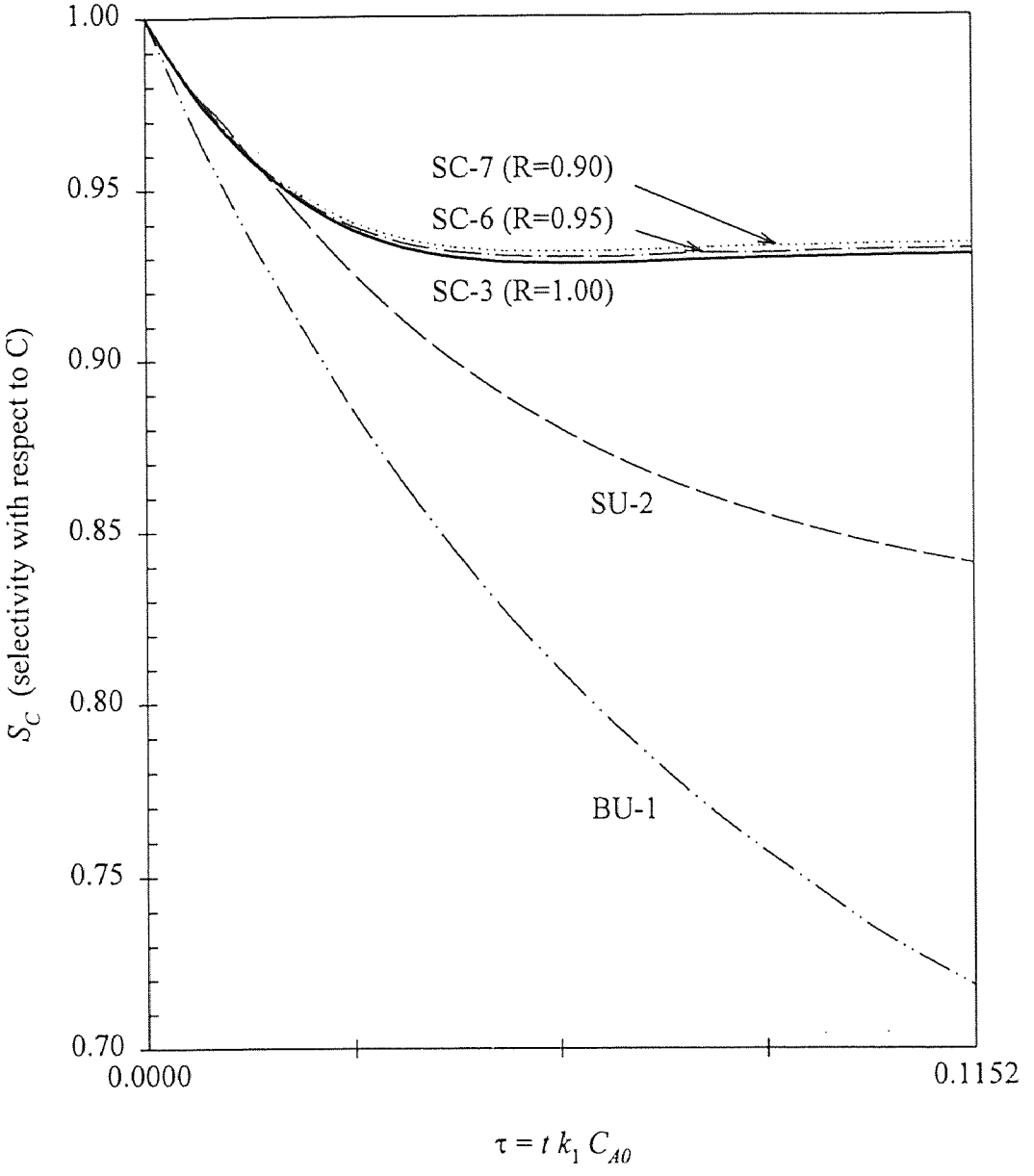

Figure 5.7 Effect of Imperfect Rejection of the Large Species on the Selectivity S_C

changes in the fractional rejection of the large species. Therefore, the selectivity is benefited by the coupling of the reactor to the membrane separator.

5.5.8 Effect of Imperfect Rejection of the Large Species on the Reactor Concentration of the Target Product, *C*

Figure 5.8 shows the effect of imperfect rejection of the large species on the concentration of C in the reactor for the operation modes discussed in section 5.5.6. The concentration of C increases as long as its rate of production is higher than its rate of removal through the permeate. Therefore, once the reaction system is depleted of the limiting reactant A, the losses through the permeate outweighs the production and the concentration will start decreasing, making reactor-membrane separator coupling unattractive for longer times.

5.5.9 Effect of Imperfect Rejection of the Large Species on the Reactor Concentration of the Byproduct, *D*

For the same operating conditions discussed in section 5.5.6, Figure 5.9 shows that, for a given membrane area, the removal of the byproduct D is not affected significantly by the imperfect rejection of the large species. Thus, the coupling of the reactor contributes to the objective of reducing the concentration of D and hence, the extent of the deleterious side reaction.

5.5.10 Effect of Volume Cap in a Semibatch Reactor on the Conversion x_{Af} for Complete Rejection of the Large Species

In Figure 5.10, different schemes of operation of semibatch reactors are compared on the basis of the reactor volumetric capacity. Curves corresponding to the operating conditions

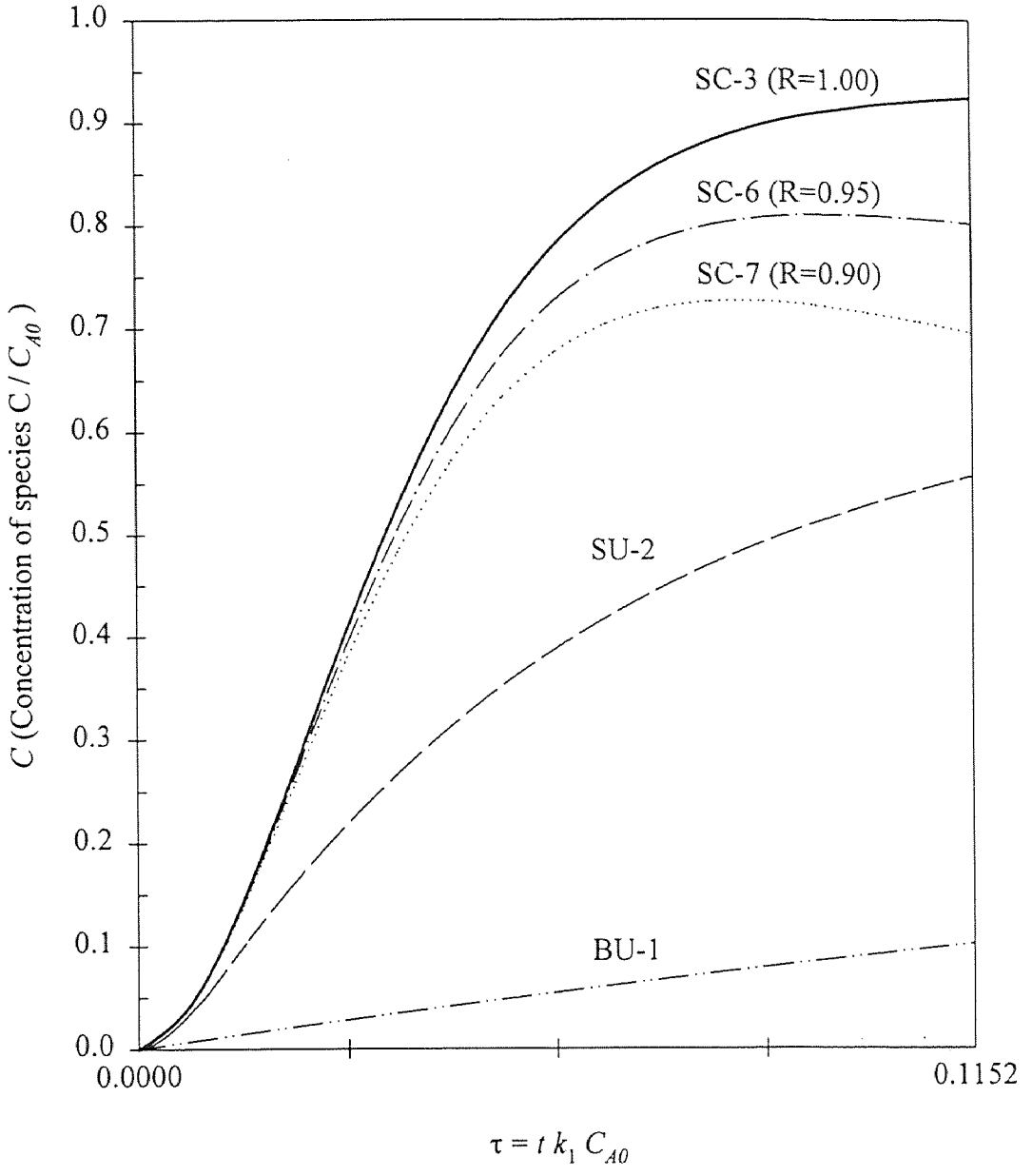

Figure 5.8 Effect of Imperfect Rejection of the Large Species on the Reactor Concentration of the Target Product, *C*

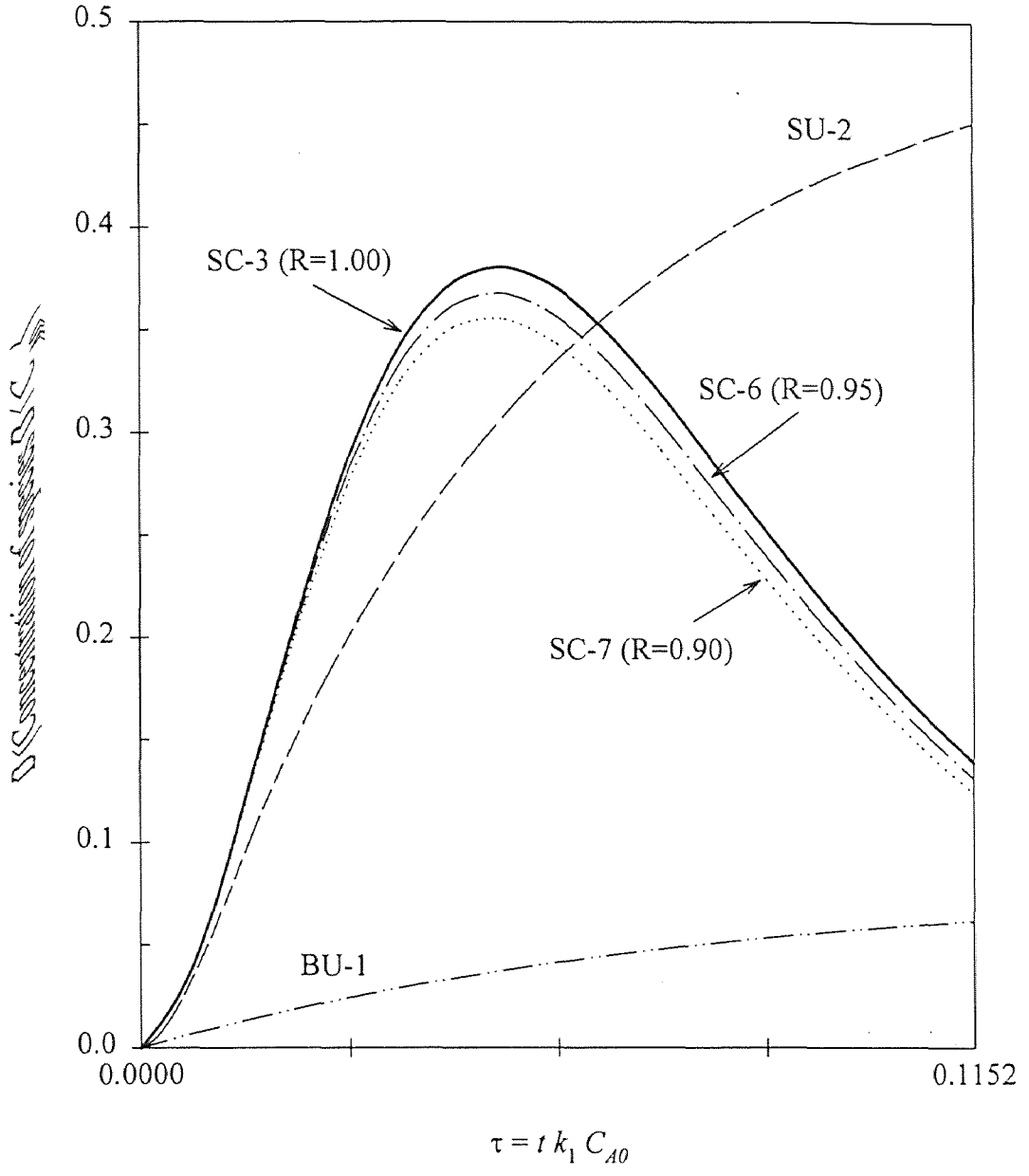

Figure 5.9 Effect of Imperfect Rejection of the Large Species on the Reactor Concentration of the Byproduct, *D*

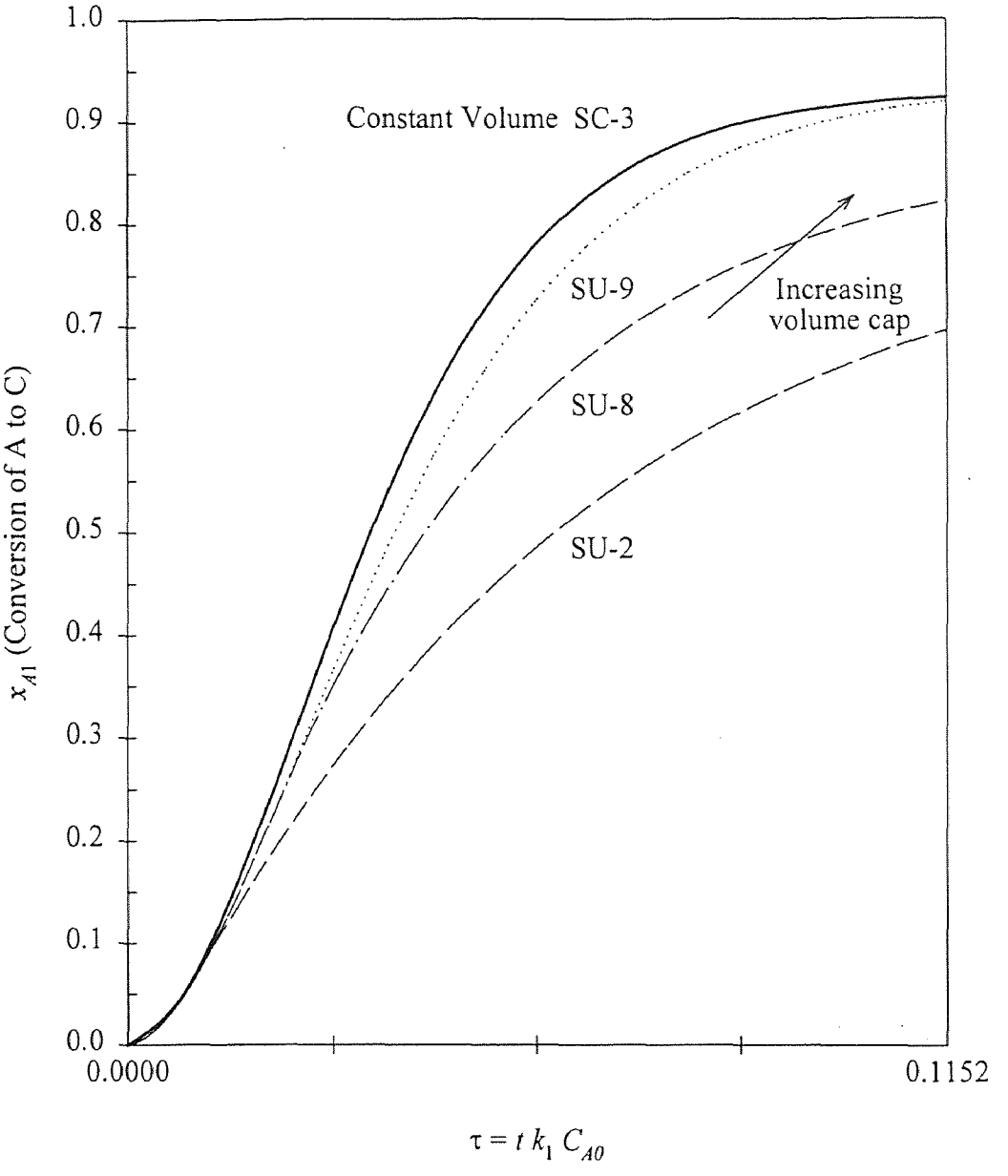

Figure 5.10 Effect of the Volume Cap in a Semibatch Reactor on the Conversion x_{A1} for Complete Rejection of the Large Species

SU-2 and SC-3 have been previously shown in Figure 5.2. The coupled operation SC-3 has constant volume ($v = 1$). The volumes in the other three uncoupled modes, SU-2, SU-8 and SU-9, increase with time. A preset maximum or volume cap of 125% of the initial volume V_0 (maximum $v = 1.25$) was fixed for SU-2, 150% (maximum $v = 1.50$) for SU-8 and no volume constraints (maximum v = No limit) for SU-9. The value of the parameter α is the same for all the curves, as the solution of the reactant B is added. In the uncoupled modes SU-2 and SU-8, $\alpha = 0$ after the maximum volume is reached. It is interesting to note that the conversion x_{Al} increases, for the same τ , as long as the reaction mixture volume cap increases. For the limiting and highly hypothetical case of no volume constraints of curve SU-9, the results are close to, but not better than, those which could be obtained by coupling the reactor as in the operation mode SC-3.

5.5.11 Effect of Membrane Area on the Conversion, x_{Al}, in the Absence of the Side Reaction

While the reaction system of interest in Figures 5.2 to 5.10 consisted of two parallel reactions as described in section 5.2, Figure 5.11 describes results obtained when the side reaction (5.2) is assumed to be negligible. Additionally, a higher kinetic constant $k_1 = 0.005$ L mol^{-1} s^{-1} was selected to emphasize the fact that the reaction (5.1) is equilibrium-limited. Operation modes studied were restricted to the batch mode and hence, $\alpha = 0$ and are summarized in Table 5.2. The base curve BU-10 is typical of a equilibrium-limited reaction. The equilibrium conversion depends on K_{eq} and the initial conditions θ_i; for $K_{eq} = 4.0$ and equimolar feed, it is 0.67.

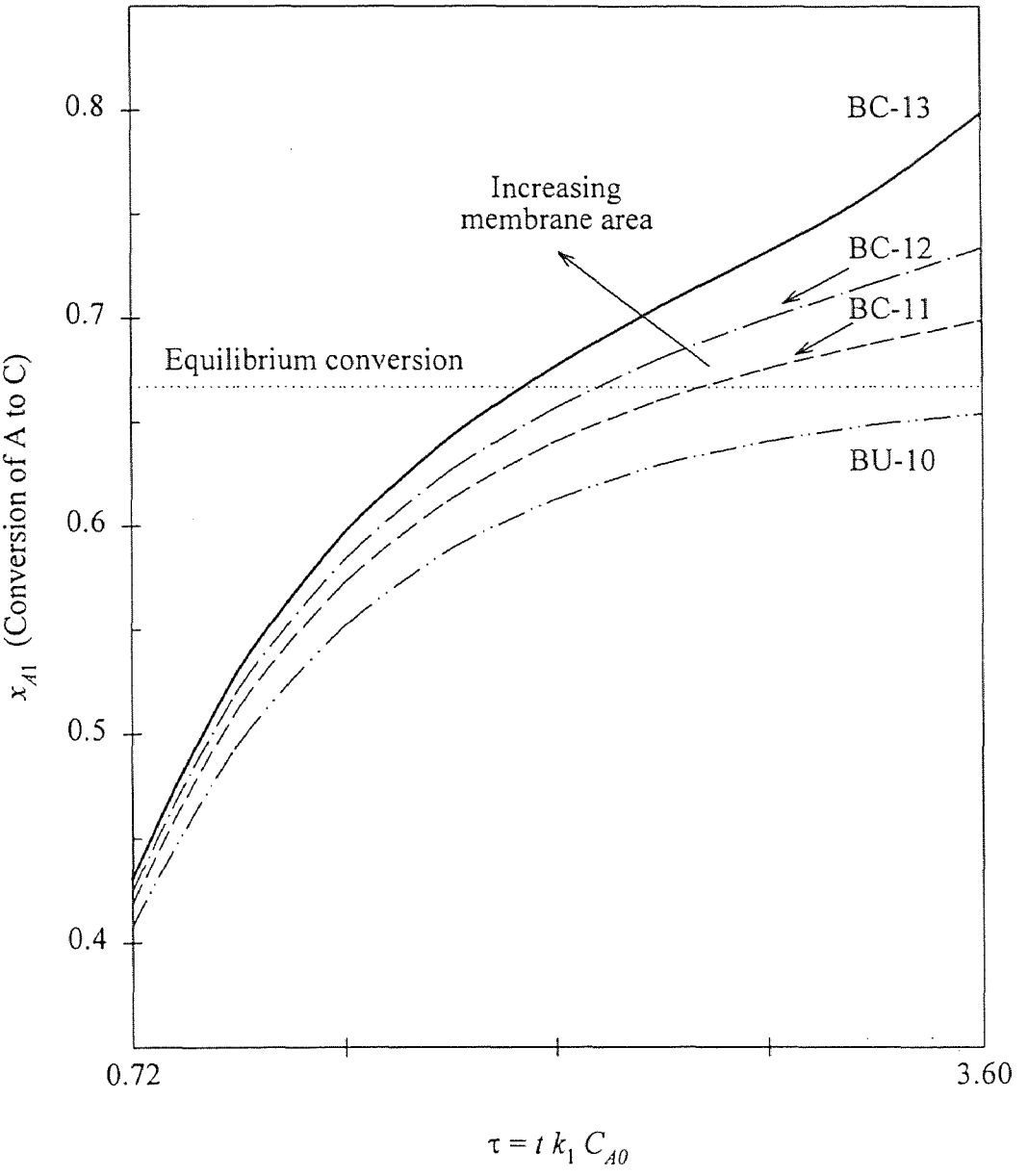

Figure 5.11 Effect of Membrane Area on the Conversion, x_{A1}, in the Absence of the Side Reaction

Three coupled operation modes, namely BC-11, BC-12 and BC-13 of increasing membrane area were considered. Species A, B and C are assumed to be completely rejected by the membrane ($R_A = R_B = R_C = 1.0$), whereas species D is not rejected at all ($R_D = 0.0$). The use of a value of $R_B \neq 0$, as opposed to the assumption used in Figures 5.2 to 5.10 of $R_B = 0$, presupposes that one deals with different chemical species or a different membrane. It is shown in Figure 5.11 that the conversion in coupled operation modes can exceed the value of the equilibrium conversion, due to the simultaneous removal of solvent and product D. Two factors contribute to the higher conversions, the decreasing reaction mixture volume which translates into higher concentrations of all the species and hence, higher rates of reaction, and the removal of D, which shifts the equilibrium to the products side. The effect is more important for higher membrane area, but the operation of the coupled system is limited by the solubility of the different species due to the concentration factor inside the reactor.

5.5.12 Effect of Partial Rejection of Species B on the Conversion, x_{A1} , in the Absence of the Side Reaction

The results shown in Figure 5.11 are restricted to the limiting case where species B is completely rejected ($R_B = 1.0$). Figure 5.12 illustrates the effect on the conversion x_{A1} of a partial rejection of B, so that B and D are removed simultaneously (but not necessarily at the same rate) through the NF membrane unit. For this objective, four operating modes were considered, namely BC-14, BC-15, BC-16 and BC-17, with the same value of the parameter β (i.e. same membrane area) as in the operation mode BC-13 previously discussed in section

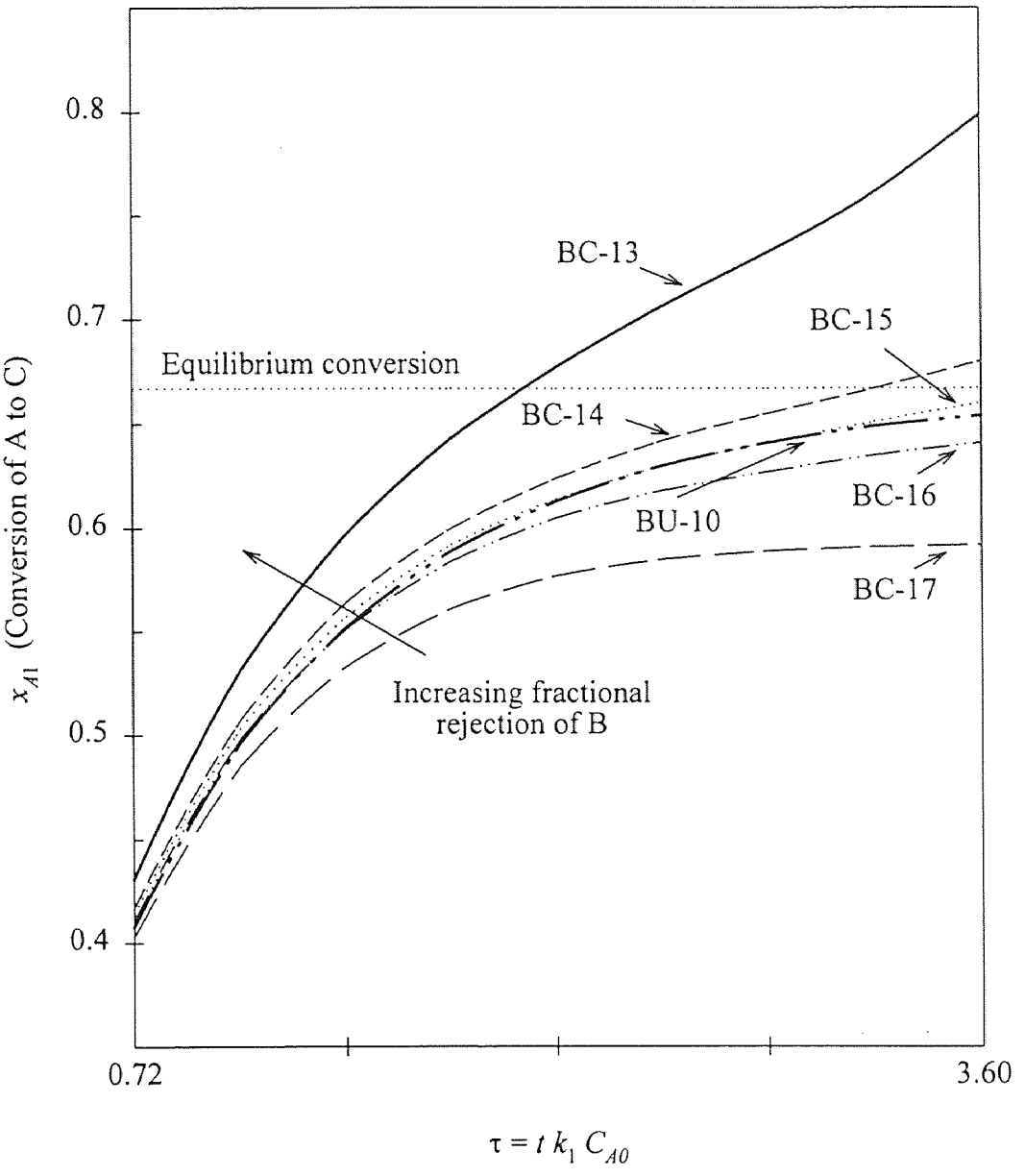

Figure 5.12 Effect of Partial Rejection of Species B on the Conversion, x_{A1}, in the Absence of the Side Reaction. Coupled Modes with the Same Membrane Area

5.5.11, but with a different value of R_B. The conversion curves for optimum rejection of B, BC-13, and for the base uncoupled mode BU-10 complete the figure.

As expected, partial rejection of B (BC-14 to BC-17) gives lower conversion values than those obtained with a membrane that rejects B completely. This effect is more important when R_B approaches zero and B is not rejected at all (BC-17), with conversions even lower than for BU-10. For the particular reaction system studied, it was found that coupling the reactor with a NF membrane unit with an observed fractional rejection of B of 0.40 (curve BC-15) would give a conversion equivalent to that of a batch reactor (curve BU-10).

5.5.13 Effect of Partial Rejection of Species B on the Reactor Concentration of the Target Product, *C*, in the Absence of the Side Reaction

An important advantage of coupling the batch reactor with a NF membrane unit is the possibility of concentration of the target product in the reactor, due to the removal of the solvent. Figure 5.13 illustrates this effect for the operation modes discussed in the section 5.5.12, for different fractional rejections of B. For a given operation time, the concentration increases as R_B is closer to 1.00. This fact can be exploited either to reduce downstream separation processes, provided that the concentrations of the reacting species do not exceed a level beyond which solids will start forming slurries in the system, or to replace subsequent steps of the synthesis, such as solvent exchange.

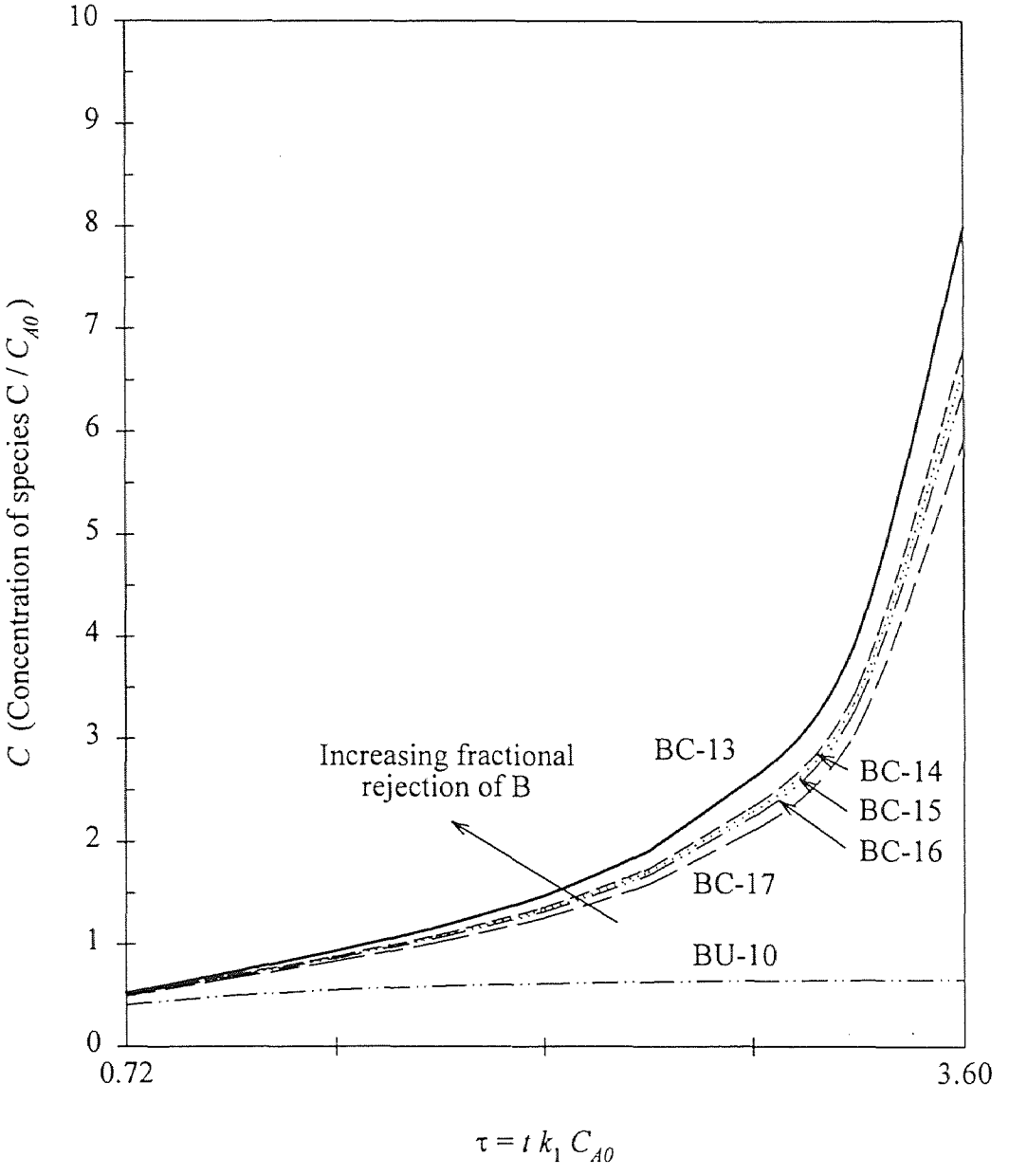

Figure 5.13 Effect of Partial Rejection of Species B on the Reactor Concentration of the Target Product, *C*, in the Absence of the Side Reaction. Coupled modes with the Same Membrane Area

CHAPTER 6

CONCLUSIONS AND RECOMMENDATIONS

6.1 Conclusions

The experimental study of the separation performance of selected solvent-compatible NF membranes using model solutes having a MW in the range of 351 to 1355 has provided valuable information about their applicability and limitations. The benefits of potential applications of these membranes in the separation of mid-sized solutes (such as those active components, with a MW in the range of 300 to 1000, commonly found in organic pharmaceutical syntheses) have been determined quantitatively. From these results, the following conclusions can be extracted:

1) The performances of NF membranes exhibited considerable time-dependence. Two stages were observed:
   - An initial transient stage, which lasted about 12 hours, in which the membrane was undergoing compaction. Both permeate flux and solute rejection were time dependent. The permeate flux decreased as the test progressed, whereas the solute rejection increased. Besides, initially the compaction was not permanent, as the membranes exhibited partial reversibility.
   - A steady-state stage, after about 12 hours, in which no further permeate flux and solute rejection change was observed over the next 4-6 hours, beyond which no experiments were carried out.

2) Membranes have to be compacted to achieve steady-state results. This is of particular importance in industrial applications, involving the need for extended periods of membrane preconditioning and the provision of facilities to recirculate initially the permeate to the feed solution.

3) Steady-state results for a given pair of membrane and solute are functions of the initial solute concentration in the feed and the applied pressure. In general, the permeate flux was found to decrease with increasing concentration, while the solute rejection increased. Both the permeate flux and solute rejection were higher as the applied pressure difference increased.

4) Manufacturer-specified MWCO is an insufficient indicator of the separation capabilities of the membranes. Solute rejection values were somewhat lower than expected for the three membranes studied, even in the cases where the solute MW was several times the MWCO of the membrane.

5) Reaction systems involving species of diverse MW and hence, dimensions, can be significantly enhanced through the external coupling of the reactor with a NF membrane separator. This coupling can increase the conversion of the reaction, lower reaction times, improve the selectivity and reduce downstream separation and purification processes.

6) The mathematical model developed can be used to predict the progress of the reactions with time for different arrangements (batch reactor, semibatch reactor, uncoupled of or coupled to a membrane separator) and conditions (initial concentrations, kinetic and thermodynamic constants, concentration and rate of addition of reactants, membrane area, permeate flux and solute rejection).

7) The model can be extended to any reaction system, provided the basic kinetic data are available.

6.2 Recommendations for Further Research

1) Solvent-compatible NF membranes have been recently introduced commercially; therefore, they are not yet well characterized. Further tests to determine intrinsic properties of the membranes such as the effective membrane thickness, charge density and porosity are necessary to develop a useful predictive model. Besides, adsorption tests to measure the affinity between the solutes and the membranes should be performed.
2) Long-term performance (more than 24 hours) tests should be conducted to confirm the current observations of steady-state results.
3) A continuous NF setup should be implemented to allow for constant operating conditions, avoiding pressurization cycles and degassing of the nitrogen, whose effect on the membrane performance is unknown. This continuously-operated setup could also be used for solvent exchange studies.
4) Separation tests with more than one solute in the feed solution can be performed initially with the same model solutes, since there is no interference at λ_{max}.
5) It would be useful to identify a standard reference solute, vis-a-vis the actual MWCO of the membrane.

APPENDIX A

SAMPLE CALCULATIONS FOR AVERAGE PERMEATE FLUX AND PERCENT REJECTION

Sample calculations of a few results shown in Chapter 4 for the average permeate flux and percent rejection are presented here. Data were obtained in two 8-hour runs, using a pre-conditioned membrane sample under the following test run conditions:

Membrane type	MPF - 60
Effective membrane area	15.2 cm^2
Solute	brilliant blue R
Solvent	methanol
Initial concentration in the feed	0.01 wt%
Applied pressure	220 psig
Stirring	Yes
Temperature	293 K

Table A.1 shows a sample calculation of the average permeate flux, corresponding to the run with an applied pressure of 220 psig shown in Figure 4.14 and Table 4.11 of Chapter 4. Collected volume of permeate and the time are experimental measurements. Samples were taken approximately every 30 minutes, except for the first two, which were taken at 10-minute intervals to allow for determination of the initial flux change with time.

Table A.1 Sample Calculation of the Average Permeate Flux

Sample	Volume of Permeate (cm^3)	Time (h:m:s)	Accumulated running time (h:m:s)	Accumulated running time (hours)	Average permeate flux (cm/s) $x10^4$	Average permeate flux (Gal/(ft^2-D))
1	4.15	0:10:15	0:10:15	0.17	4.44	9.41
2	4.00	0:11:01	0:21:16	0.35	3.98	8.44
3	9.40	0:30:00	0:51:16	0.85	3.44	7.29
4	9.00	0:30:19	1:21:35	1.36	3.26	6.90
5	8.60	0:30:02	1:51:37	1.86	3.14	6.66
6	13.50	0:50:45	2:42:22	2.71	2.92	6.18
7	7.80	0:30:01	3:12:23	3.21	2.85	6.04
8	8.00	0:30:00	3:42:23	3.71	2.92	6.20
9	8.00	0:30:01	4:12:24	4.21	2.92	6.20
10	9.20	0:34:46	4:47:10	4.79	2.90	6.15
11	8.00	0:31:00	5:18:10	5.30	2.83	6.00
12	7.80	0:30:48	5:48:58	5.82	2.78	5.89
13	8.00	0:32:16	6:21:14	6.35	2.72	5.76
14	8.00	0:31:51	6:53:05	6.88	2.75	5.84
15	6.40	0:26:01	7:19:06	7.32	2.70	5.72
16	6.10	0:25:10	7:44:16	7.74	2.66	5.64
17	6.00	0:25:00	8:09:16	8.15	2.63	5.58

Test run conditions :

Effective membrane area : 15.2 cm^2
Initial conc. in the feed : 0.01 wt % (approx.)
Applied pressure : 220 psig
Temperature : 293 K

Membrane: MPF - 60
Solute : brilliant blue R
Solvent : methanol
Stirring : yes
Date : April 10 '98
Day 1 of 2

Table A.1 (Cont.) Sample Calculation of the Average Permeate Flux

Sample	Volume of Permeate (cm^3)	Time (h:m:s)	Accumulated running time		Average permeate flux	
			(h:m:s)	(hours)	(cm/s) $x10^4$	(Gal/(ft^2-D))
			8:09:16	8.15		
1	2.80	0:10:04	8:19:20	8.32	3.05	6.47
2	2.65	0:10:10	8:29:30	8.49	2.86	6.06
3	7.30	0:30:15	8:59:45	9.00	2.65	5.61
4	7.25	0:30:53	9:30:38	9.51	2.57	5.46
5	7.20	0:30:01	10:00:39	10.01	2.63	5.58
6	12.50	0:53:48	10:54:27	10.91	2.55	5.40
7	7.40	0:31:40	11:26:07	11.44	2.56	5.43
8	7.40	0:32:08	11:58:15	11.97	2.53	5.35
9	8.20	0:35:35	12:33:50	12.56	2.53	5.36
10	7.25	0:31:26	13:05:16	13.09	2.53	5.36
11	7.35	0:31:42	13:36:58	13.62	2.54	5.39
12	7.25	0:31:24	14:08:22	14.14	2.53	5.37
13	6.95	0:30:05	14:38:27	14.64	2.53	5.37
14	7.00	0:30:10	15:08:37	15.14	2.54	5.40
15	6.00	0:26:00	15:34:37	15.58	2.53	5.37
16	6.00	0:25:57	16:00:34	16.01	2.54	5.38

Test run conditions :

Effective membrane area : 15.2 cm^2
Initial conc. in the feed : 0.01 wt % (approx.)
Applied pressure : 220 psig
Temperature : 293 K

Membrane: MPF - 60
Solute : brilliant blue R
Solvent : methanol
Stirring : yes
Date : April 11 '98
Day 2 of 2

Average permeate flux of each sample was determined directly, dividing the volumetric flow rate by the effective membrane area:

$$Average\ permeate\ flux\ (cm/s)|_i = \frac{Volume_{permeate}\ (cm^3)|_i}{Time(s) * Effect.\ membrane\ area\ (cm^2)} \quad (A.1)$$

Results are shown in the last two columns of Table A.1, in customary units. For example, for sample 1:

$$Average\ permeate\ flux\ (cm/s)|_1 = \frac{4.15}{60\ (\ 10 + \frac{15}{60}\ ) * (\ 15.2\ )} = 4.44 * 10^{-4}$$

Table A.2 shows a sample calculation of the % rejection. Since the pressure cell was operated in a batch mode, the volume and concentration of the solution inside the cell (retentate) changed with running time. Calculations are presented for both the cell and the permeate solutions. The initial volume in the cell was 248.00 cm^3 and its solute concentration was 106.69 ppmw (approximately 0.01 wt%). In addition to the collected volume of permeate, previously used in Table A.1, the permeate solute concentrations are experimentally obtained quantities.

Calculations in the permeate side

$$C_{permeate}(ppmw)|_i = \frac{Solute_{permeate}(mg)|_i * 10^6}{Solute_{permeate}(mg)|_i + Methanol_{permeate}(mg)|_i} \quad (A.2)$$

Table A.2 Sample Calculation of the Percent Rejection

CELL OR RETENTATE					PERMEATE					
Volume	Solute	Solute Concent.				Volume	Solute Concent.		Solute	%
(cm^3)	(mg)	(ppmw)	(mg/L)	(mg/L)avg	Sample	(cm^3)	(ppmw)	(mg/L)	(mg)	Rejection
248.00	21.1	106.7	84.4							
243.85	20.9	108.2	85.6	85.0	1	4.15	70.4	55.7	0.2	34.4
239.85	20.6	108.8	86.0	85.8	2	4.00	72.7	57.5	0.2	33.0
230.45	20.1	110.4	87.3	86.7	3	9.40	68.7	54.4	0.5	37.3
221.45	19.7	112.3	88.8	88.1	4	9.00	64.9	51.3	0.5	41.7
212.85	19.3	114.4	90.5	89.6	5	8.60	59.5	47.1	0.4	47.5
199.35	18.7	118.6	93.8	92.2	6	13.50	52.2	41.3	0.6	55.2
191.55	18.4	121.5	96.2	95.0	7	7.80	46.2	36.5	0.3	61.6
183.55	18.2	125.1	99.0	97.6	8	8.00	40.2	31.8	0.3	67.4
175.55	17.9	129.2	102.2	100.6	9	8.00	35.8	28.3	0.2	71.9
166.35	17.7	134.3	106.2	104.2	10	9.20	36.2	28.6	0.3	72.6
158.35	17.4	139.3	110.2	108.2	11	8.00	36.2	28.7	0.2	73.5
150.55	17.2	144.7	114.5	112.3	12	7.80	33.9	26.8	0.2	76.2
142.55	17.0	150.9	119.4	116.9	13	8.00	35.2	27.9	0.2	76.2
134.55	16.8	157.7	124.8	122.1	14	8.00	36.0	28.4	0.2	76.7
128.15	16.6	163.8	129.5	127.2	15	6.40	36.4	28.8	0.2	77.4
122.05	16.4	170.2	134.7	132.1	16	6.10	34.3	27.1	0.2	79.5
116.05	16.3	177.3	140.2	137.5	17	6.00	33.9	26.8	0.2	80.5

Test run conditions :

Effective membrane area : 15.2 cm^2

Initial conc. in the feed : 0.01 wt % (approx.)

Applied pressure : 220 psig

Temperature : 293 K

Membrane : MPF - 60

Solute : brilliant blue R

Solvent : methanol

Stirring : yes

Date : April 10 '98

Day 1 of 2

Table A.2 (Cont.) Sample Calculation of the Percent Rejection

CELL OR RETENTATE					PERMEATE					
Volume (cm^3)	Solute (mg)	Solute Concent. (ppmw)	Solute Concent. (mg/L)	Solute Concent. (mg/L)avg	Sample	Volume (cm^3)	Solute Concent. (ppmw)	Solute Concent. (mg/L)	Solute (mg)	% Rejection
248.00	21.2	107.2	84.8							
245.20	21.2	109.0	86.3	85.5	1	2.80	21.7	17.2	0.0	79.9
242.55	21.1	110.0	87.0	86.7	2	2.65	18.6	14.7	0.0	83.0
235.25	21.0	112.9	89.3	88.2	3	7.30	18.7	14.8	0.1	83.2
228.00	20.9	115.8	91.6	90.5	4	7.25	19.5	15.4	0.1	82.9
220.80	20.8	119.0	94.1	92.9	5	7.20	19.9	15.8	0.1	83.0
208.30	20.6	124.9	98.8	96.4	6	12.50	20.7	16.4	0.2	83.0
200.90	20.4	128.6	101.8	100.3	7	7.40	22.4	17.7	0.1	82.4
193.50	20.3	132.7	104.9	103.4	8	7.40	23.3	18.5	0.1	82.1
185.30	20.1	137.4	108.7	106.8	9	8.20	24.5	19.4	0.2	81.8
178.05	20.0	142.0	112.4	110.5	10	7.25	25.1	19.8	0.1	82.1
170.70	19.9	147.0	116.3	114.3	11	7.35	26.0	20.5	0.2	82.0
163.45	19.7	152.4	120.6	118.4	12	7.25	25.1	19.9	0.1	83.2
156.50	19.6	158.0	125.0	122.8	13	6.95	26.0	20.5	0.1	83.3
149.50	19.4	164.1	129.9	127.4	14	7.00	27.6	21.8	0.2	82.9
143.50	19.3	169.8	134.3	132.1	15	6.00	28.7	22.7	0.1	82.8
137.50	19.1	175.9	139.2	136.8	16	6.00	30.3	24.0	0.1	82.5

Test run conditions :

Effective membrane area : 15.2 cm^2

Initial conc. in the feed : 0.01 wt % (approx.)

Applied pressure : 220 psig

Temperature : 293 K

Membrane : MPF - 60

Solute : brilliant blue R

Solvent : methanol

Stirring : yes

Date : April 11 '98 Day 2 of 2

from which the following expression was derived:

$$Solute_{permeate}(mg)|_i = \frac{Methanol_{permeate}(mg)|_i * C_{permeate}(ppmw)|_i * 10^{-6}}{1 - C_{permeate}(ppmw)|_i * 10^{-6}} \quad (A.3)$$

Moreover,

$$C_{permeate}(mg/L)|_i = \frac{Solute_{permeate}(mg)|_i * 10^3}{Volume_{permeate}(cm^3)|_i} \quad (A.4)$$

This is an average of the permeate solute concentration between time i - 1 and time i. As an illustration, for sample 1, assuming a specific gravity of 0.791 for methanol and dilute solutions (Table A.2):

$$Solute_{permeate}(mg)|_1 = \frac{4.15 * 791 * 70.4 * 10^{-6}}{1 - 70.4 * 10^{-6}} = 0.23$$

and

$$C_{permeate}(mg/L)|_1 = \frac{0.23 * 10^3}{4.15} = 55.7$$

Calculations in the cell or retentate side

With this information, the amount of solute remaining in the cell after collecting the sample was calculated immediately through a simple mass balance, by substracting the solute carried

in the permeate from the previous inventory of solute in the cell. A similar procedure was used to calculate the remaining volume in the cell:

$$Solute_{cell}(mg)|_{t=i} = Solute_{cell}(mg)|_{t=i-1} - Solute_{permeate}(mg)|_i \quad (A.5)$$

$$Volume_{cell}(cm^3)|_{t=i} = Volume_{cell}(cm^3)|_{t=i-1} - Volume_{permeate}(cm^3)|_i \quad (A.6)$$

The solute concentration in the cell at any time was determined as follows:

$$C_{cell}(mg/L)|_{t=i} = \frac{Solute_{cell}(mg)|_{t=i} * 10^3}{Volume_{cell}(cm^3)|_{t=i}} \quad (A.7)$$

It was of interest to compare $C_{permeate}|_i$ (which was an average of the permeate solute concentration between time i - 1 and time i) with that in the cell for the same interval. Therefore, an additional variable $C_{cell\ avg}|_i$ was defined as follows:

$$C_{cell\ avg}(mg/L)|_i = 0.5 * \left[C_{cell}(mg/L)|_{t=i} + C_{cell}(mg/L)|_{t=i-1} \right] \quad (A.8)$$

Finally, the % rejection of any permeate sample was calculated with the following expression:

$$\%\ rejection|_i = 100 * \left[1 - \frac{C_{permeate}(mg/L)|_i}{C_{cell\ avg}(mg/L)|_i} \right] \quad (A.9)$$

and the results are shown in the last column of Table A.2. Illustrative numerical calculations after the sample 1 was collected are shown below:

$$Solute_{cell}(mg)|_{t=1} = 21.10 - 0.23 = 20.87$$

$$Volume_{cell}(cm^3)|_{t=1} = 248.00 - 4.15 = 243.85$$

$$C_{cell}(mg/L)|_{t=1} = \frac{20.87 * 10^3}{243.85} = 85.6$$

$$C_{cell\ avg}(mg/L)|_1 = 0.5 * [\ 85.6 + 84.4\ ] = 85.0$$

and the rejection in the permeate sample 1 was:

$$\%\ rejection|_1 = 100 * \left[\ 1 - \frac{55.7}{85.0}\ \right] = 34.4$$

By combining Tables A.1 and A.2, the % rejection can be plotted as a function of the accumulated running time.

APPENDIX B

ESTIMATION OF THE MOLECULAR DIMENSIONS OF SOLUTES

Molecular dimensions of the solutes were estimated using two methods: a classical correlation based on the solute molal volume at normal boiling point, and a computerized estimation using a molecule builder.

Many correlations have been suggested to estimate solute dimensions under the assumption that the molecules have a spherical conformation. A characteristic solute radius (r_i) can be determined when these correlations are used in conjunction with a method to determine the solute molal volume at normal boiling point, V_i, such as the Le Bas Additive Method (Reid et al., 1977; Farrell and Babb, 1973).

Le Bas Additive Method estimates V_i by adding up the atomic volumes of the individual atoms and correcting the result for structural factors such as the presence of aromatic or heterocyclic rings. With this information, a characteristic solute radius can be determined using the following expression where N_{avog} is the Avogadro number:

$$r_i = \left[\frac{3\ V_i}{4\ \pi\ N_{avog}} \right]^{1/3} \qquad \text{(B.1)}$$

Estimated values of the solute radii are shown in Table B.1.

Computerized estimations of the distances between selected atom pairs were done using the software package Spartan, version 4.1 (Wavefunction, Inc.) for two solutes: safranin O and brilliant blue R. Molecular geometry was determined with the built-in

empirical SYBYL force field, in order to minimize the final strain energy of the structure. Results are shown in Figures B.1 and B.2. Estimated distances are in the same order of magnitude as those found using equation (B.1) along with the Le Bas Additive Method.

Finally, the reported value of the hydrodynamic (Stokes) radius of the molecule of Vitamin B_{12}, whose molecular structure is shown in Figure B.3, is $r_i = 0.740$ nm (Bowen et al., 1997). This value is close to the calculated value of $r_i = 0.835$ nm using equation (B.1).

Table B.1 Solute Radii and Molal Volume at Normal Boiling Point using Le Bas Method

Solute	V_i ($cm^3\ mol^{-1}$)	r_i (nm)
Safranin O	370.9	0.528
Brilliant blue R	939.0	0.719
Vitamin B_{12}	1469.3	0.835

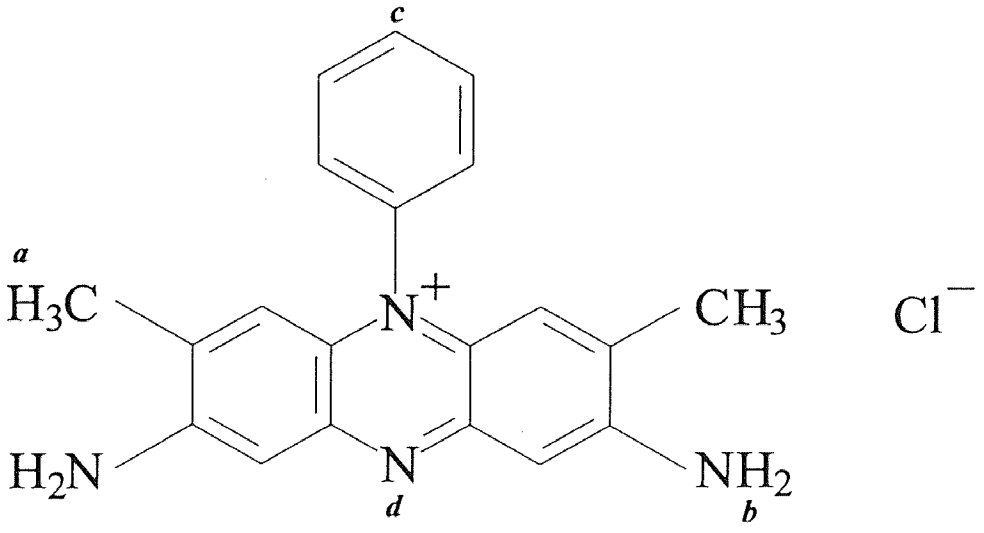

Atom Pair	Distance (nm)*
a - *b*	1.10
c - *d*	0.76
a - *c*	0.99

* Estimated with Spartan, v.4.1

Figure B.1 Molecular Structure and Selected Distances Between Atoms in Safranin O

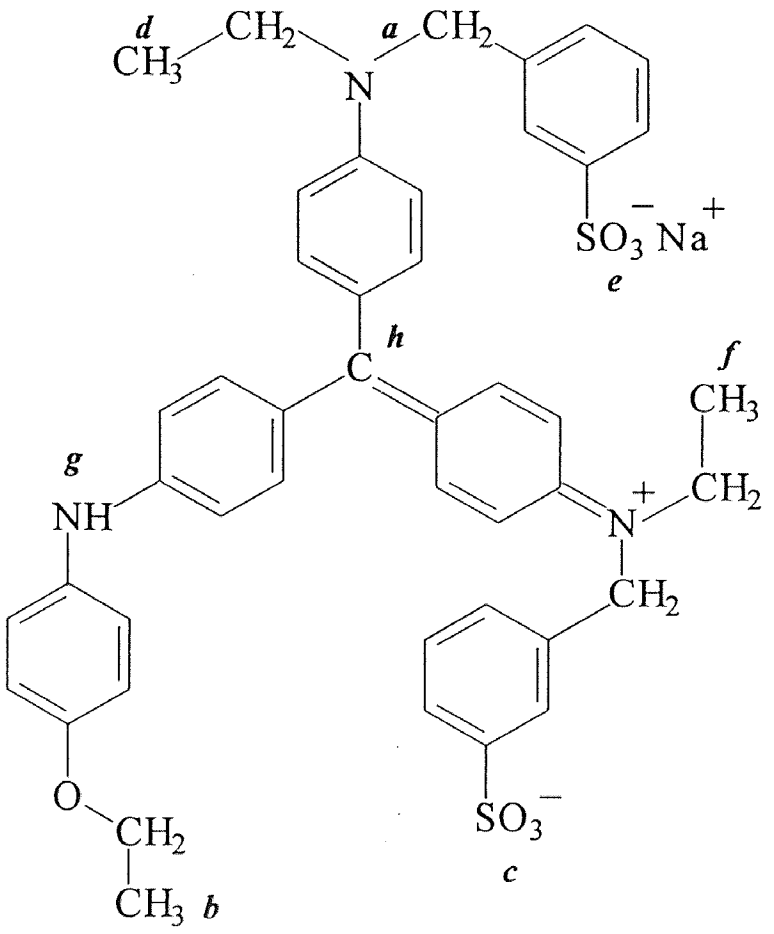

Atom Pair	Distance (nm)*
a - b	1.82
a - c	1.70
c - d	1.74
b - e	1.69
f - g	1.33
a - h	0.75
b - h	1.12
c - h	0.99

* Estimated with Spartan, v.4.1

Figure B.2 Molecular Structure and Selected Distances Between Atoms in Brilliant Blue R

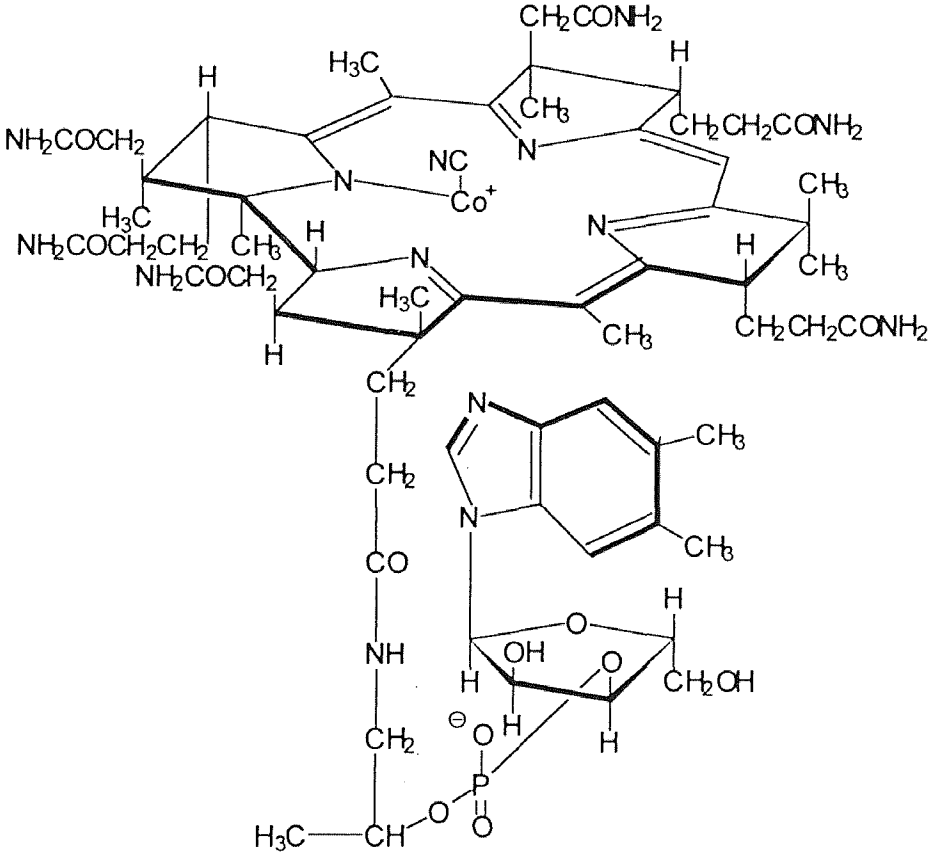

Stokes Radius (nm) *	0.74

*W. R. Bowen et al., JMS, 126, 91 (1997)

Figure B.3 Molecular Structure and Hydrodynamic (Stokes) Radius of Vitamin B_{12}

APPENDIX C

NUMERICAL SOLUTION OF THE MATHEMATICAL MODEL FOR A SEMIBATCH / BATCH REACTOR COUPLED EXTERNALLY WITH A NF MEMBRANE SEPARATOR

The computer codes and the results of the numerical solution of the mathematical model described in Section 5.3 are presented in this appendix. The particular results shown here were obtained using the ODE solver in Mathematica™ 2.2 for the operation mode SC-6 (see Table 5.1 for a complete list of parameter values), which considers an imperfect rejection of 0.95 for the large species, namely A, C and E. Because of the presence of these large species in the permeate, it is of particular importance for this operation mode to assess the contribution of each term in equations (5.30) and (5.31) in the calculation of the conversions x_{A1} and x_{A2}, respectively.

Numerical Solution of the Mathematical Model for the External Coupling of a Reactor with a NF Membrane Separator
Operation Mode SC-6

```
AA          =.
BB          =.
CC          =.
DD          =.
EE          =.
v           =.

k1          = 0.00005       (* L/(mol s) *)
k2          = 0.0005        (* L/(mol s) *)
Keq         = 4
Lv          = 0.0001        (* L/s *)
CBdrum      = 2.5           (* mol/L *)
CAo         = 0.04          (* mol/L *)
Vo          = 2             (* L *)
Am          = 0.02          (* m^2 *)
Js          = 0.005         (* L/(m^2 s) *)

0.00005

0.0005

4

0.0001

2.5

0.04

2

0.02

0.005

alpha       = Lv*CBdrum/(k1*CAo^2*Vo)
beta        = Am*Js/(k1*CAo*Vo)
gamma       = CBdrum/CAo

1562.5

25.

62.5

RA          = 0.95
RB          = 0.00
RC          = 0.95
RD          = 0.00
RE          = 0.95

0.95

0.

0.95

0.

0.95
```

```
Sol = NDSolve[{ AA'[t] == (1/v[t])*(-AA[t]*v'[t]
                        -v[t]*(AA[t]*BB[t]-(1/Keq)*CC[t]*DD[t]
                        +k2/k1*AA[t]*DD[t])
                        -beta*(1-RA)*AA[t]),

                        BB'[t] == (1/v[t])*
                         (-BB[t]*v'[t]
                        -v[t]*(AA[t]*BB[t]-(1/Keq)*CC[t]*DD[t])
                        +alpha
                        -beta*(1-RB)*BB[t]),

                        CC'[t] == (1/v[t])*
                        (-CC[t]*v'[t]
                        +v[t]*(AA[t]*BB[t]-(1/Keq)*CC[t]*DD[t])
                        -beta*(1-RC)*CC[t]),

                        DD'[t] == (1/v[t])*
                        (-DD[t]*v'[t]
                        +v[t]*(AA[t]*BB[t]-(1/Keq)*CC[t]*DD[t]
                        -k2/k1*AA[t]*DD[t])
                        -beta*(1-RD)*DD[t]),

                        EE'[t] ==(1/v[t])*
                        (-EE[t]*v'[t]+v[t]*(k2/k1)*AA[t]*DD[t]
                        -beta*(1-RE)*EE[t]),

                        v'[t]   == alpha/gamma-beta,

                        AA[0] == 1.0,
                        BB[0] == 1.0,
                        CC[0] == 0.0,
                        DD[0] == 0.0,
                        EE[0]  == 0.0,
                        v [0]   == 1.0},

                        {AA[t],BB[t],CC[t],DD[t],EE[t],v[t]},{t,0,0.1152}]
```

```
{{AA[t] -> InterpolatingFunction[{0., 0.1152}, <>][t], BB[t] -> InterpolatingFunction[{0., 0.1152}, <>][t],
  CC[t] -> InterpolatingFunction[{0., 0.1152}, <>][t], DD[t] -> InterpolatingFunction[{0., 0.1152}, <>][t],
  EE[t] -> InterpolatingFunction[{0., 0.1152}, <>][t], v[t] -> InterpolatingFunction[{0., 0.1152}, <>][t]}}
```

```
$DefaultFont = {"Times", 8}
```

```
{Times, 8}
```

```
concA = Table[{t, Evaluate[AA[t]/.Sol] }, {t, 0, 0.1152, 0.0072}];
TableForm[concA]
```

0 1.

0.0072 0.946739

0.0144 0.835063

0.0216 0.692816

0.0288 0.545825

0.036 0.41204

0.0432 0.300479

0.0504 0.21318

0.0576 0.148023

0.0648 0.101088

0.072 0.0681736

0.0792 0.0455556

0.0864 0.0302487

0.0936 0.0200071

0.1008 0.0132116

0.108 0.00872872

0.1152 0.00578211

```
Plot[AA[t]/.Sol, {t, 0, 0.1152}, AxesLabel->{t, A}]
```

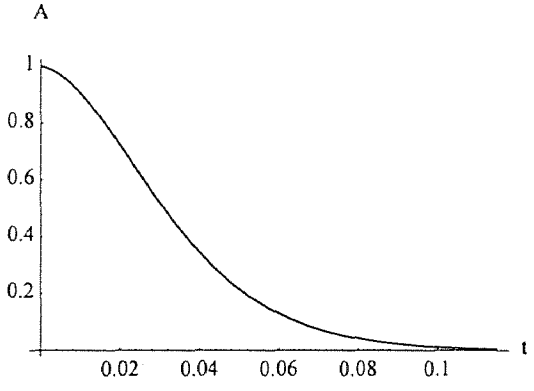

```
concB = Table[{t, Evaluate[BB[t]/.Sol] }, {t, 0, 0.1152, 0.0072}];
TableForm[concB]
```

0 1.

0.0072 11.0902

0.0144 19.4681

0.0216 26.4408

0.0288 32.2615

0.036 37.1341

0.0432 41.2219

0.0504 44.6557

0.0576 47.5416

0.0648 49.9667

0.072 52.0038

0.0792 53.7138

0.0864 55.1482

0.0936 56.3505

0.1008 57.3576

0.108 58.2009

0.1152 58.9065

```
Plot[BB[t]/.Sol, {t, 0, 0.1152}, AxesLabel->{t, B}]
```

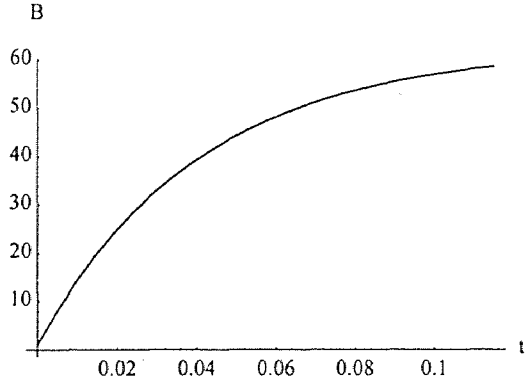

```
concC = Table[{t, Evaluate[CC[t]/.Sol] }, {t, 0, 0.1152, 0.0072}];
TableForm[concC]
```

0 0.

0.0072 0.0432625

0.0144 0.141138

0.0216 0.265728

0.0288 0.393257

0.036 0.508038

0.0432 0.602474

0.0504 0.674988

0.0576 0.727526

0.0648 0.763555

0.072 0.7868

0.0792 0.800592

0.0864 0.807628

0.0936 0.809963

0.1008 0.809093

0.108 0.806078

0.1152 0.801651

```
Plot[CC[t]/.Sol, {t, 0, 0.1152}, PlotRange->{0, 1}, AxesLabel->{t, C}]
```

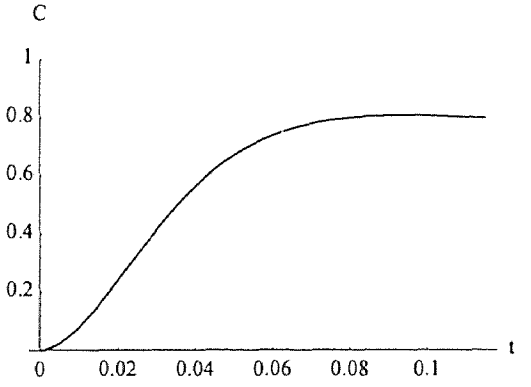

```
concD = Table[{t, Evaluate[DD[t]/.Sol] }, {t, 0, 0.1152, 0.0072}];
TableForm[concD]
```

0 0.

0.0072 0.0396723

0.0144 0.119416

0.0216 0.207398

0.0288 0.282583

0.036 0.334848

0.0432 0.362275

0.0504 0.367826

0.0576 0.356595

0.0648 0.333984

0.072 0.30473

0.0792 0.272525

0.0864 0.239993

0.0936 0.208842

0.1008 0.180069

0.108 0.154157

0.1152 0.13125

```
Plot[DD[t]/.Sol, {t, 0, 0.1152}, PlotRange->{0, 0.5}, AxesLabel->{t, D}]
```

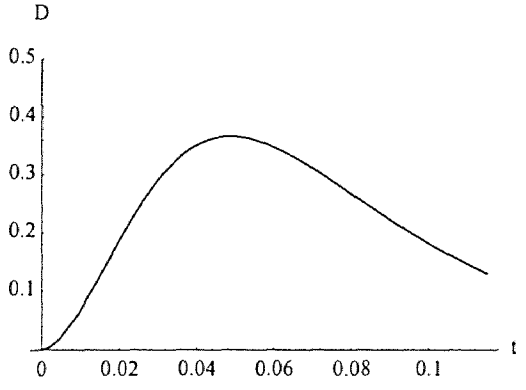

```
concE = Table[{t, Evaluate[EE[t]/.Sol] }, {t, 0, 0.1152, 0.0072}];
TableForm[concE]
```

0 0.

0.0072 0.00103865

0.0144 0.00595988

0.0216 0.0148176

0.0288 0.0255584

0.036 0.0359204

0.0432 0.0444797

0.0504 0.0507748

0.0576 0.0549827

0.0648 0.0575514

0.072 0.0589574

0.0792 0.059595

0.0864 0.0597505

0.0936 0.0596152

0.1008 0.0593101

0.108 0.0589087

0.1152 0.0584543

```
Plot[EE[t]/.Sol, {t, 0, 0.1152}, PlotRange->{0, 0.1}, AxesLabel->{t, E}]
```

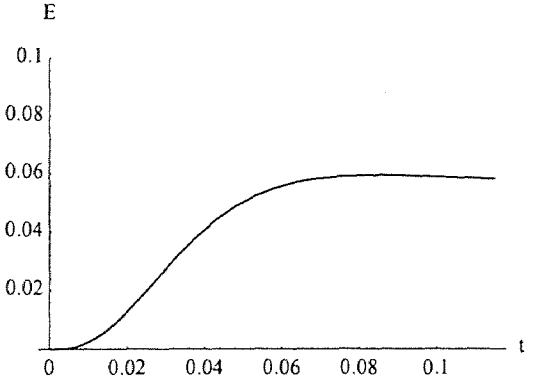

```
volume = Table[{t, Evaluate[v[t]/.Sol] }, {t, 0, 0.1152, 0.0072}];
TableForm[volume]
```

0 1.

0.0072 1.

0.0144 1.

0.0216 1.

0.0288 1.

0.036 1.

0.0432 1.

0.0504 1.

0.0576 1.

0.0648 1.

0.072 1.

0.0792 1.

0.0864 1.

0.0936 1.

0.1008 1.

0.108 1.

0.1152 1.

```
Plot[v[t]/.Sol, {t, 0, 0.1152}, AxesLabel->{t, v}]
```

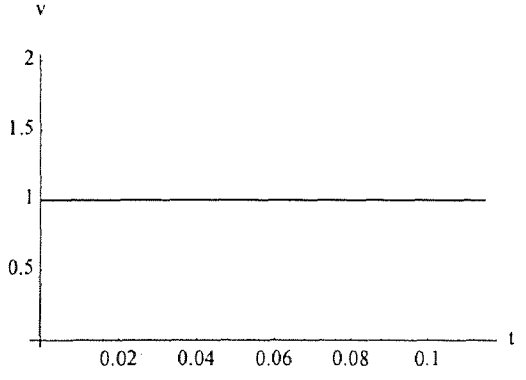

```
conv1reactor = Table[{t, Evaluate[v[t]*CC[t]/.Sol]}, {t, 0, 0.1152, 0.0072}];
TableForm[conv1reactor]
```

0 0.

0.0072 0.0432625

0.0144 0.141138

0.0216 0.265728

0.0288 0.393257

0.036 0.508038

0.0432 0.602474

0.0504 0.674988

0.0576 0.727526

0.0648 0.763555

0.072 0.7868

0.0792 0.800592

0.0864 0.807628

0.0936 0.809963

0.1008 0.809093

0.108 0.806078

0.1152 0.801651

```
Clear[permC]
permC[i_] = beta*(1-RC)*NIntegrate[Evaluate[CC[t]/.Sol], {t, 0, i}];
Do[Print[{i, permC[i]}], {i, 0, 0.1152, 0.0072}]
```

```
{0, {0}}
{0.0072, {0.000143557}}
{0.0144, {0.000942964}}
{0.0216, {0.00276371}}
{0.0288, {0.00573402}}
{0.036, {0.00980326}}
{0.0432, {0.0148171}}
{0.0504, {0.0205817}}
{0.0576, {0.0269068}}
{0.0648, {0.0336276}}
{0.072, {0.0406125}}
{0.0792, {0.0477617}}
{0.0864, {0.0550029}}
{0.0936, {0.062285}}
{0.1008, {0.0695727}}
{0.108, {0.0768422}}
{0.1152, {0.0840779}}
```

```
conversion1 = Table[{t, Evaluate[v[t]*CC[t]/.Sol] + permC[t]}, {t, 0, 0.1152, 0.0072}];
TableForm[conversion1]
```

0 0.

0.0072 0.043406

0.0144 0.142081

0.0216 0.268491

0.0288 0.398991

0.036 0.517841

0.0432 0.617291

0.0504 0.69557

0.0576 0.754432

0.0648 0.797182

0.072 0.827413

0.0792 0.848354

0.0864 0.862631

0.0936 0.872248

0.1008 0.878666

0.108 0.882921

0.1152 0.885729

```
Plot[(Evaluate[v[t]*CC[t]/.Sol] + permC[t]), {t, 0, 0.1152},
    PlotRange->{0, 1}, AxesLabel->{t, Conversion xA1}]
```

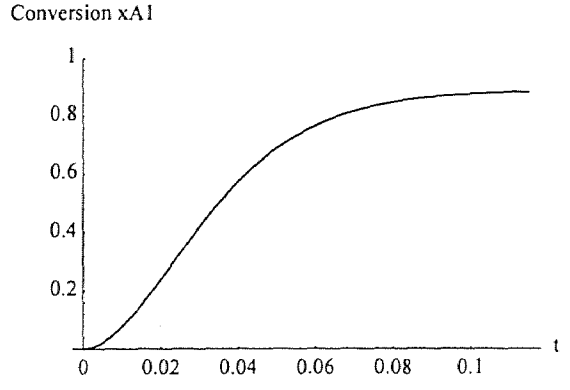

```
conv2reactor = Table[{t, Evaluate[v[t]*EE[t]/.Sol]}, {t, 0, 0.1152, 0.0072}];
TableForm[conv2reactor]
```

```
0       0.

0.0072  0.00103865

0.0144  0.00595988

0.0216  0.0148176

0.0288  0.0255584

0.036   0.0359204

0.0432  0.0444797

0.0504  0.0507748

0.0576  0.0549827

0.0648  0.0575514

0.072   0.0589574

0.0792  0.059595

0.0864  0.0597505

0.0936  0.0596152

0.1008  0.0593101

0.108   0.0589087

0.1152  0.0584543
```

```
Clear[permE]
permE[i_] = beta*(1-RE)*NIntegrate[Evaluate[EE[t]/.Sol], {t, 0, i}];
Do[Print[{i, permE[i]}], {i, 0, 0.1152, 0.0072}]
```

```
{0, {0}}
                -6
{0.0072, {2.60239 10  }}
{0.0144, {0.0000307318}}
{0.0216, {0.000121903}}
{0.0288, {0.000303106}}
{0.036, {0.000580723}}
{0.0432, {0.000944164}}
{0.0504, {0.0013745}}
{0.0576, {0.00185182}}
{0.0648, {0.00235927}}
{0.072, {0.00288427}}
{0.0792, {0.00341821}}
{0.0864, {0.00395554}}
{0.0936, {0.00449285}}
{0.1008, {0.00502811}}
{0.108, {0.00556015}}
{0.1152, {0.00608831}}
```

```
conversion2 = Table[{t, Evaluate[v[t]*EE[t]/.Sol] + permE[t]}, {t, 0, 0.1152, 0.0072}];
TableForm[conversion2]
```

0 0.

0.0072 0.00104125

0.0144 0.00599061

0.0216 0.0149395

0.0288 0.0258615

0.036 0.0365012

0.0432 0.0454238

0.0504 0.0521493

0.0576 0.0568345

0.0648 0.0599107

0.072 0.0618416

0.0792 0.0630132

0.0864 0.063706

0.0936 0.0641081

0.1008 0.0643382

0.108 0.0644689

0.1152 0.0645426

```
Plot[(Evaluate[v[t]*EE[t]/.Sol] + permE[t]), {t, 0, 0.1152},
    PlotRange->{0, 0.1}, AxesLabel->{t, Conversion xA2}]
```

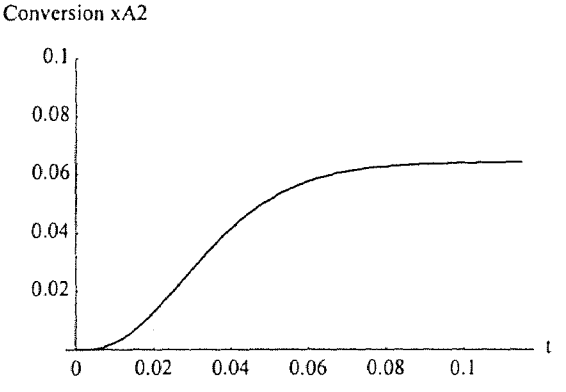

```
selectivity = Table[{t, (Evaluate[v[t]*CC[t]/.Sol] + permC[t])/
((Evaluate[v[t]*CC[t]/.Sol] + permC[t]) + (Evaluate[v[t]*EE[t]/.Sol] + permE[t]) )},
{t, 0, 0.1152, 0.0072}];
TableForm[selectivity]
```

0	Indeterminate
0.0072	0.976573
0.0144	0.959542
0.0216	0.94729
0.0288	0.939128
0.036	0.934154
0.0432	0.931458
0.0504	0.930255
0.0576	0.929943
0.0648	0.9301
0.072	0.930457
0.0792	0.930859
0.0864	0.931228
0.0936	0.931535
0.1008	0.931773
0.108	0.931951
0.1152	0.93208

```
Plot[(Evaluate[v[t]*CC[t]/.Sol] + permC[t])/
    ((Evaluate[v[t]*CC[t]/.Sol] + permC[t]) + (Evaluate[v[t]*EE[t]/.Sol] + permE[t])),
    {t, 0.0001, 0.1152}, PlotRange ->{0.7, 1}, AxesOrigin->{0, 0.7}, AxesLabel->{t, Selectivity}]
```

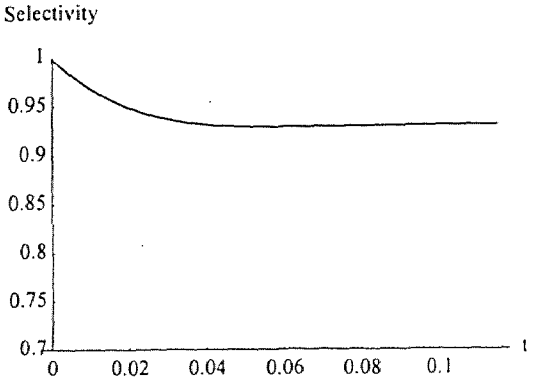

REFERENCES

Afonso, M. D., Geraldes, V., Rosa, M. J. and Pinho, M. N., "Nanofiltration Removal of Chlorinated Organic Compounds from Alkaline Bleaching Effluents in a Pulp and Paper Plant," *Water Res.*, **26**, 1639 (1992).

Aimar, P., Meireles, M. and Sanchez, V., "A Contribution to the Translation of Retention Curves into Pore Size Distributions for Sieving Membranes," *J. Membrane Sci.*, **54**, 321 (1990).

Amy, G. L., Alleman, B. C. and Cluff, C. B., "Removal of Dissolved Organic Matter by Nanofiltration," *J. Environm. Eng.*, **116**, 200 (1990).

Atkins, P. W., Physical Chemistry, W. H. Freeman, New York, Fifth Edition, (1994).

Awadalla, F. T., Striez, C. and Lamb, K., "Removal of Ammonium and Nitrate Ions from Mine Effluents by Membrane Technology," *Sep. Sci. Technol.*, **29**, 483 (1994).

Blau, T. J., "DBP Control by Nanofiltration," *J. AWWA*, **84**, 104 (1992).

Bowen, W. R. and Mukhtar, H., "Characterization and Prediction of Separation Performance of Nanofiltration Membranes," *J. Membrane Sci.*, **112**, 263 (1996).

Bowen, W. R., Mohammad, A. W. and Hilal, N., "Characterization of Nanofiltration Membranes for Predictive Purposes -Use of Salts, Uncharged Solutes and Atomic Force Microscopy," *J. Membrane Sci.*, **126**, 91 (1997).

Deen, W. M., "Hindered Transport of Large Molecules in Liquid-Filled Pores," *AICHE J.*, **33**, 1409 (1987).

Eriksson, P., "Nanofiltration Extends the Range of Membrane Filtration," *Environm. Prog.*, **7**, 58 (1988).

Farrell, P. C. and Babb, A. L., "Estimation of the Permeability of Cellulosic Membranes from Solute Dimensions and Diffusivities," *J. Biom. Mat. Res.*, **7**, 275 (1973).

Fu, P., "Selecting Membranes for Removing NOM and DBP Precursors," *J. AWWA*, **86**, 55 (1994).

Ho, W. H. and Sirkar, K. K. (Editors), Membrane Handbook, Chapman & Hall, New York, (1992).

REFERENCES
(Continued)

Jacangelo, J., "Selected Processes for Removing Nom: an Overview," *J. AWWA*, **87**, 64 (1995).

Kirk-Othmer Encyclopedia of Chemical Technology, John Wiley & Sons, Inc., New York, Third Edition, Volume 24, (1984).

Kiryat Weizmann Ltd., Membrane Products. Technical Data Sheets, (1996).

Levenstein, R., Hasson, D. and Semiat, R., "Utilization of the Donnan Effect for Improving Electrolyte Separation with Nanofiltration Membranes," *J. Membrane Sci.*, **116**, 77 (1996).

Lonsdale, H. K., Merten, U. and Riley, R. L., "Transport Properties of Cellulose Acetate Osmonic Membranes," *J. Appl. Pol. Sci.*, **9**, 1341 (1965).

Meares, P. (Editor), Membrane Separation Processes, Elsevier, New York, (1976).

Merck Index (The), Merck & Co., Whitehouse Station, Twelfth Edition, (1996).

Merten, U. (Editor), Desalination by Reverse Osmosis, The M.I.T. Press, Cambridge, (1966).

Meindersma, G. W. and Kuczynski, M., "Implementing Membrane Technology in the Process Industry: Problems and Opportunities, *J. Membrane Sci.*, **113**, 285 (1996).

Muldowney, G. P. and Punzi, V. L., "A Comparison of Solute Rejection Models in Reverse Osmosis Membranes for the System Water-Sodium Chloride-Cellulose Acetate," *Ind. Eng. Chem. Res.*, **27**, 2341 (1988).

Nabetani, H., Nakajima, M., Watanabe, A., Ikeda, S., Nakao, S. and Kimura, S., "Development of a New Type of Membrane Osmometer," *J. Chem. Eng. Jpn.*, **25**, 269 (1992).

Nidetzky, B., Haltrich, D. and Kulbe, K. D., "Carry out Coenzyme Conversions Economically," *Chemtech*, **20**, 31 (1996).

Nyström, M., Kaipia, L. and Luque, S., "Fouling and Retention of Nanofiltration Membranes," *J. Membrane Sci.*, **98**, 249 (1995).

REFERENCES
(Continued)

Paul, E. L. and Rosas, C. B., "Challenges for Chemical Engineers in the Pharmaceutical Industry," *Chem. Eng. Prog.*, **86**, 17 (1990).

Popovych, O. and Tomkins, R. P. T., Nonaqueous Solution Chemistry, John Wiley & Sons, New York, (1981).

Raman, L. P., Cheryan, M. and Rajagopalan, N., "Consider Nanofiltration for Membrane Separations," *Chem. Eng. Prog.*, **90**, 68 (1994).

Rautenbach, R. and Gröschl, A., "Separation Potential of Nanofiltration Membranes," *Desalination*, **77**, 73 (1990).

Reid, R. C., Prausnitz, J. M. and Sherwood, T. W., The Properties of Gases and Liquids, McGraw-Hill Book Company, New York, Third Edition, (1977).

Sarrade, S., Rios, G. M. and Carlés, M., "Nanofiltration Membrane Behavior in a Supercritical Medium," *J. Membrane Sci.*, **114**, 81 (1996).

Schirg, P. and Widmer, F., "Characterization of Nanofiltration Membranes for the Separation of Aqueous Dye-Salt Solutions," *Desalination*, **89**, 89 (1992).

Soltanieh, M. and Gill, W. N., "Review of Reverse Osmosis Membranes and Transport Models," *Chem. Eng. Commun.*, **12**, 279 (1981).

Tsuru, T., Urairi, M., Nakao, S. and Kimura, S., "Reverse Osmosis of Single and Mixed Electrolytes with Charged Membranes: Experiment and Analysis," *J. Chem. Eng. Jpn.*, **24**, 518 (1991).

Willard, H. H., Merritt, L. L., Dean, J. A. and Settle, F. A., Instrumental Methods of Analysis, D. Van Nostrand Company, New York, Sixth Edition, (1981).